

SPIE. FIELD
GUIDE

Field Guide to
**Digital
Micro-Optics**

Bernard C. Kress

SPIE Terms of Use: This SPIE eBook is DRM-free for your convenience. You may install this eBook on any device you own, but not post it publicly or transmit it to others. SPIE eBooks are for personal use only. For details, see the SPIE [Terms of Use](#). To order a print version, [visit SPIE](#).

SPIE.

Field Guide to

Digital Micro-Optics

Bernard C. Kress

SPIE Field Guides
Volume FG33

John E. Greivenkamp, Series Editor

SPIE PRESS
Bellingham, Washington USA

Library of Congress Cataloging-in-Publication Data

Kress, Bernard C., author.

Digital micro-optics / Bernard C. Kress.

pages cm. – (The field guide series; FG33)

Includes bibliographical references and index.

ISBN 978-1-62841-183-6

1. Optoelectronic devices—Design and construction.

2. Optical MEMS. 3. Integrated optics. 4. Digital electronics. 5. Diffraction gratings. I. Title.

TK8360.O68K74 2014

621.36—dc23

2014016927

Published by

SPIE

P.O. Box 10

Bellingham, Washington 98227-0010 USA

Phone: 360.676.3290

Fax: 360.647.1445

Email: Books@spie.org

www.spie.org

Copyright © 2014 Society of Photo-Optical Instrumentation Engineers (SPIE)

All rights reserved. No part of this publication may be reproduced or distributed in any form or by any means without written permission of the publisher.

The content of this book reflects the thought of the author(s). Every effort has been made to publish reliable and accurate information herein, but the publisher is not responsible for the validity of the information or for any outcomes resulting from reliance thereon.

Printed in the United States of America.

Last updated 11/20/2014.

SPIE.

Introduction to the Series

Welcome to the *SPIE Field Guides*—a series of publications written directly for the practicing engineer or scientist. Many textbooks and professional reference books cover optical principles and techniques in depth. The aim of the *SPIE Field Guides* is to distill this information, providing readers with a handy desk or briefcase reference that provides basic, essential information about optical principles, techniques, or phenomena, including definitions and descriptions, key equations, illustrations, application examples, design considerations, and additional resources. A significant effort will be made to provide a consistent notation and style between volumes in the series.

Each *SPIE Field Guide* addresses a major field of optical science and technology. The concept of these *Field Guides* is a format-intensive presentation based on figures and equations supplemented by concise explanations. In most cases, this modular approach places a single topic on a page, and provides full coverage of that topic on that page. Highlights, insights, and rules of thumb are displayed in sidebars to the main text. The appendices at the end of each *Field Guide* provide additional information such as related material outside the main scope of the volume, key mathematical relationships, and alternative methods. While complete in their coverage, the concise presentation may not be appropriate for those new to the field.

The *SPIE Field Guides* are intended to be living documents. The modular page-based presentation format allows them to be updated and expanded. We are interested in your suggestions for new *Field Guide* topics as well as what material should be added to an individual volume to make these *Field Guides* more useful to you. Please contact us at **fieldguides@SPIE.org**.

John E. Greivenkamp, *Series Editor*
College of Optical Sciences
The University of Arizona

The Field Guide Series

Keep information at your fingertips with all of the titles in the Field Guide Series:

- Adaptive Optics*, Second Edition, Robert Tyson & Benjamin Frazier
Atmospheric Optics, Larry Andrews
Binoculars and Scopes, Paul Yoder, Jr. & Daniel Vukobratovich
Diffraction Optics, Yakov Soskind
Digital Micro-Optics, Bernard Kress
Displacement Measuring Interferometry, Jonathan Ellis
Geometrical Optics, John Greivenkamp
Holography, Pierre-Alexandre Blanche
Illumination, Angelo Arecchi, Tahar Messadi, & John Koshel
Image Processing, Khan M. Iftexharuddin & Abdul Awwal
Infrared Systems, Detectors, and FPAs, Second Edition, Arnold Daniels
Interferometric Optical Testing, Eric Goodwin & Jim Wyant
Laser Pulse Generation, Rüdiger Paschotta
Lasers, Rüdiger Paschotta
Lens Design, Julie Bentley & Craig Olson
Microscopy, Tomasz Tkaczyk
Nonlinear Optics, Peter Powers
Optical Fabrication, Ray Williamson
Optical Fiber Technology, Rüdiger Paschotta
Optical Lithography, Chris Mack
Optical Thin Films, Ronald Willey
Optomechanical Design and Analysis, Katie Schwartz & James Burge
Physical Optics, Daniel Smith
Polarization, Edward Collett
Probability, Random Processes, and Random Data Analysis, Larry Andrews
Radiometry, Barbara Grant
Special Functions for Engineers, Larry Andrews
Spectroscopy, David Ball
Terahertz Sources, Detectors, and Optics, Créidhe O'Sullivan & J. Anthony Murphy
Visual and Ophthalmic Optics, Jim Schwiegerling

Field Guide to Digital Micro-Optics

The term “digital micro-optics” was introduced in the early 1990s to refer to a specific variety of micro-optics. It is now widely accepted by industry and academia. Digital micro-optics can be related to their counterparts in the electronics realm—“digital electronics,” or “integrated electronics” (ICs)—in various ways, from design to modeling, from prototyping to mass fabrication, and eventually system integration. Historically, the term “digital” in digital electronics refers to three aspects:

- their digital functionality (binary logic),
- the way they are designed via a digital computer, and
- the way they are fabricated (through sets of digital or binary masks).

In digital micro-optics, the term primarily refers to how such optics are designed and fabricated, similar to digital electronics, through specific electronic-design-automation (EDA) software packages and sets of digital masks. Traditional macro-optics, such as telescopes, microscopes, and other imaging optics, have been designed without complex design software tools. Digital optics, especially wafer-scale micro-optics, cannot be designed without specific software and tools. Digital layouts for wafer-level fabrication of micro-optics are also often generated by algorithms similar to the ones used in conventional EDA tools (Cadence, Synopsys, Mentor-Graphics, etc.). Because there is often no analytical solution to the micro-optics design problem, complex iterative optimization algorithms may be required to find an adequate solution.

Unlike digital electronics, digital micro-optics can implement either digital or analog functionality, or a combination thereof. A typical digital function may be a fan-out beam splitter, and an analog function may be an imaging task. A hybrid may result in a complex multifocus imaging lens, a function impossible to implement in traditional analog macro-optics.

Bernard C. Kress

Google [X] Labs, Mountain View, CA

Table of Contents

Glossary	xii
Refractive Micro-Optics	1
Digital Micro-Optics	1
Naming Conventions	2
Free-Space and Guided-Wave Micro-Optics	3
Maximizing the Refractive Effect	4
Maximizing the Diffractive Effect	5
Total Internal Reflection	6
Guided-Wave Digital Optics	7
Optical Waveguide Types	8
Modes in Optical Waveguides	9
Coupling Losses in Optical Waveguides	10
Free-Space Micro-Optics	11
Graded-Index Micro-Optics	12
GRIN Lenses	13
Spectral Dispersion in Micro-Optics	14
Imaging with Microlens Arrays	15
Light-Field Cameras	16
Light-Field Displays	17
Beam Steering with MLAs	18
Beam Shaping/Homogenizing with MLAs	19
Diffractive Micro-Optics	20
Digital Diffractive Optics	20
Analytic and Numeric Diffractives	21
Fresnel and Fourier Diffraction Regimes	22
Fourier and Fresnel Diffractive Optics	23
Analytic Diffractive Elements	24
Reflective Gratings	25
Amplitude Gratings	26
Binary Phase Gratings	27
Multilevel Diffractives	28
Diffractive Lens Surface Profiles	29
Diffraction Efficiency	30
Diffractive Fresnel Lens	31
Diffractive Lens Profile Descriptions	32
Microlens Parameters	33
Spectral Bandwidth of Diffractives	34

Table of Contents

Broadband Diffractives	35
Achromatizing Hybrid Lenses	36
Athermalizing Hybrid Lenses	37
Hybrid-Lens Surface Descriptions	38
Hybrid Refractive/Diffractive Lens	39
Aberrations in Micro-Optics	40
Beam-Shaping Lenses	42
Vortex Microlenses	43
Extended Depth of Focus Microlenses	44
Aperture and Wavefront Coding	45
Spatially Multiplexed Planar Optics	46
Diffractive Null Lenses	47
Interferogram Lenses	48
Toroidal and Helicoidal Planar Lenses	49
 Iterative Optimization Process	 50
Numerical Optimization	50
Numeric Diffractives	51
CGH Design Constraints	52
Merit Function Definition	53
IFTA Algorithm	54
Direct Binary Search	55
Simulated Annealing	56
Beam-Shaping CGHs (Numeric)	57
Spot Array Generators	58
MLAs and Multifocus Lenses	59
Dammann Gratings	60
Talbot Self-Imaging	61
 From Micro-Optics to Nano-Optics	 62
Subwavelength Optics	62
Large- and Small-Period Gratings	63
Zero-Order Gratings	64
Rigorous EM Diffraction Theory	65
Effective Medium Theory	66
EMT Encoding Schemes	67
Form Birefringence	68
Antireflection microstructures	69

Table of Contents

Parity-Time Symmetry in Optics	70
PT Grating-Assisted Couplers	71
Nonreciprocal Free-Space PT Gratings	72
Surface Plasmonics	73
Photonic Crystals	74
Metamaterials	75
Metasurfaces and Resonant Antennas	76
Holographic Micro-Optics	77
The Holographic Process	77
Gabor and Leith Holograms	78
Thin and Thick Holograms	79
Reflection and Transmission Holograms	80
Fraunhofer and Fresnel Holograms	81
Holographic Interference	82
The Grating Vector	83
Floquet's Theorem and the Bragg Conditions	84
Grating Strength and Detuning Factor	85
Kogelnik Theory for Volume Holograms	86
Angular and Spectral Bandwidths in Holograms	87
Two-Step Holographic Recording	88
Surface-Relief Holograms	89
Holographic Recording Media: Applications	90
Holographic Recording Media: Advantages and Drawbacks	91
Dynamic Micro-Optics	92
Dynamic Micro-Optics	92
Liquid-Crystal Optics	93
Liquid-Crystal Microdisplays	94
OLED Micro-Displays	95
Quantum-Dot Displays	96
H-PDLC Switchable Hologram	97
H-PDLC Recording and Playback	98
MEMS/MOEMS Micro-Optics	99
MEMS Gratings	100
MEMS Display Panels	101
MEMS Laser Scanners	102

Table of Contents

Holographic Backlights and Displays	103
Tunable Moiré Micro-Optics	104
Liquid Micro-Optics	105
Electroactive Polymer Microlenses	106
Micro-Optics Modeling Techniques	107
Diffraction Modeling Theories	107
Ray Tracing through Diffractives	108
Fresnel and Fourier Approximations	109
Near- and Far-Field Regions	110
FFT-Based Physical Optics Propagators	111
Oversampling Process in CGH Modeling	112
Physical Optics Modeling: Resolution Increase	113
Physical Optics Modeling with FFT Algorithms	114
Replication of CGHs	115
Numerical-Reconstruction Windows	116
Numerical-Reconstruction Window Scaling	117
DFT-Based Propagators	118
Fresnel Propagator Using a DFT	119
Arbitrary-Reconstruction Windows	120
DFT-Based Numerical Propagator	121
Physical Optics versus Ray Tracing	122
Micro-Optics Fabrication	123
Fabrication Timeline of Micro-Optics	123
Holographic Exposure and Etching	124
Multiple Holographic Exposures	125
Refractive Micro-Optics Fabrication	126
Sag Calculations for Microlenses	127
Diamond Ruling/Turning	128
Binary Lithography	129
Multilevel Optical Lithography	130
Etch Depth: Critical Distance and Groove Depth	131
Etch Depth: Single-Step Height and Diffraction Efficiency	132
Multilevel Lithographic Fabrication	133
GDSII Mask Layouts	134
Wafers for Micro-Optics	135

Table of Contents

Optical Lithography	136
Step-and-Repeat Lithography	137
Useful Lithography Parameters	138
Direct-Write Lithography	139
Greyscale Masking Techniques	140
Greyscale Lithography (Binary)	141
Greyscale Lithography (HEBS)	142
Photomask Patterning	143
Optical Proximity Correction	144
Replication Shim	145
Shim Recombination	146
Plastic Replication Technologies	147
Roll-to-Roll UV Embossing	148
Plastics: Acrylic and Polycarbonate	149
Plastics: Polystyrene and Cyclic Olefin Copolymer	150
Plastics: Cyclic Olefin Polymer and Ultem 1010	151
Effects of Fabrication Errors	152
Micro-Optics in Industry	153
Applications of Micro-Optics	154
 Equation Summary	 155
Bibliography	162
Index	173

Glossary

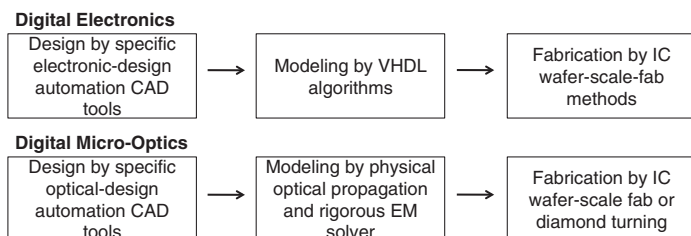
AMOLED	Active-matrix organic light-emitting diode
ARS	Antireflection surface
CD	Critical dimension
CGH	Computer-generated hologram
CIF	Caltech Intermediate Format
DBS	Direct binary search
DEAP	Dielectric electroactive polymer
DFT	Discrete Fourier transform
DOE	Diffraction optical element
DOF	Depth of focus
DTM	Diamond turning machine
DWDM	Dense wavelength division multiplexing
EAP	Electroactive polymer
EDA	Electronic design automation
EDOF	Extended depth of focus
EMT	Effective medium theory
FDTD	Finite-difference time domain
FFT	Fast Fourier transform
FLCOS	Ferroelectric liquid crystal on silicon
FZP	Fresnel zone plate
GDSII	Graphic Data System II
GRIN	Gradient index
HEBS	High-energy beam sensitive
HMD	Head-mounted display
HOE	Holographic optical element
H-PDLC	Holographic-polymer dispersed liquid crystal
IC	Integrated circuit
IFTA	Iterative Fourier transform algorithm
IL	Insertion loss
ITO	Indium tin oxide
LAF	Light-absorbing film
LC	Liquid crystal
LCOS	Liquid crystal on silicon
LGA	Local grating approximation
M-DOE	Moiré diffraction optical element
MEMS	Micro-electro-mechanical system
MLA	Microlens array
MOEMS	Micro-opto-electro-mechanical system
NA	Numerical aperture

Glossary

OLED	Organic light-emitting diode
OPC	Optical proximity correction
OPD	Optical path difference
OPU	Optical pick-up unit
PBS	Polarization beamsplitter
PC	Photonic crystal
PDLC	Polymer dispersed liquid crystal
PDM	Pulse-density modulation
PLC	Planar lightwave circuit
PSF	Point spread function
PSM	Phase-shift mask
PT	Parity time
PWM	Pulsewidth modulation
RCWA	Rigorous coupled-wave analysis
RET	Resolution enhancement technique
RIE	Reactive ion etching
SA	Simulated annealing
SBWP	Space-bandwidth product
SPDT	Single-point diamond turning
TIR	Total internal reflection
VHDL	Very-high-speed-integrated-circuit hardware description language
VLSI	Very-large-scale integration

Digital Micro-Optics

Typical design and fabrication process flows for both **digital electronics** and **digital micro-optics** are depicted in the following figure.



Digital micro-optics share many features for both the design and fabrication steps of digital (micro) electronics, such as in electronic-design-automation (EDA) tools, numerical modeling, and IC fab. Although “analog optics” is a term that is seldom used in industry (unlike analog electronics), analog optical holography and digital optical holography refer to very different technologies:

- “Analog” refers to the analog nature of traditional volume holographic materials and exposure process.
- “Digital” refers to both the digital nature of thin holograms made of surface-relief microstructures or diffractive optics and the way they are designed (by a specific software) and fabricated (by IC wafer fabrication, diamond turning, or other).

Digital optics can also be fabricated through nondigital masks, such as greyscale masks or resist reflow, but are still referred to as digital optics. Diamond-turned or freeform-machined micro-optics are also referred to as digital optics, especially when they are produced in arrays, such as **microlens arrays** (MLAs). The term “digital optics” has been widely used in industry today and is now a de facto name for a wide spectrum of optical elements, ranging from wafer scale micro-optics, diamond-turned optics, waveguide optics, and nano-optics.

Naming Conventions

General elements

- Digital and binary optics
- Wafer-scale micro-optics
- Phase plates, amplitude and phase coding plates
- Micro-opto-electro-mechanical systems (MOEMs)

Refractive or reflective elements

- Micro-optics
- Refractive microlens arrays (MLAs)
- Refractive diffuser arrays (engineered diffusers)

Diffraction elements

- Diffractive optical elements (DOEs)
- Kinoforms
- Phase masks (as grating exposure masks)
- Diffractive microlens arrays (D-MLAs)
- Diffractive Fresnel lenses and Fresnel zone plates (FZPs)

Holographic elements

- Computer-generated holograms (CGHs)
- Holographic optical elements (HOEs)
- Bragg gratings
- Digital holography (how the hologram is recorded on a digital sensor)
- Digital holograms (how the hologram is calculated and fabricated)
- Parity-time (PT) symmetry holograms

Subwavelength elements

- Subwavelength gratings
- Zero-order or nondiffracting gratings
- Elements designed by effective medium theory (EMT)
- Form birefringent elements
- Photonic crystals
- Optical metamaterials
- Surface plasmon gratings
- Micro-antenna flat optics

Hybrid elements

- Waveguide gratings
- Hybrid refractive/reflective/diffractive elements

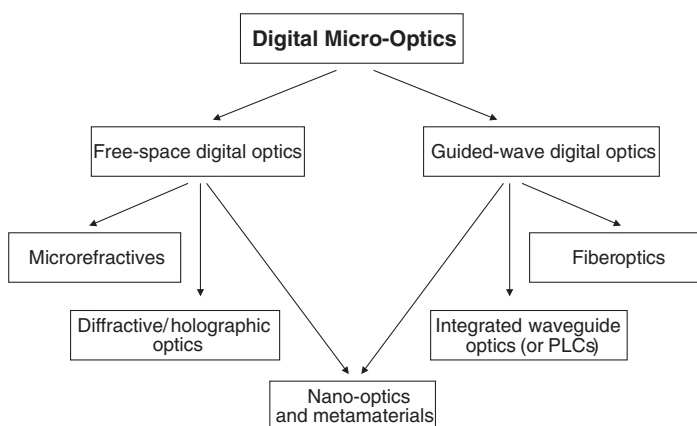
Free-Space and Guided-Wave Micro-Optics

The realm of digital optics includes a wide range of optical elements that all qualify under the term “digital,” as previously defined (i.e., designed by a specific CAD tool, such as EDAs in IC fab and fabricated through sets of binary masks). When fabricated through a lithographical process, these optical elements are also called **wafer-scale micro-optics**. They can be divided into two main categories: free-space and guided-wave optics.

- **Free-space micro-optics** constitute the largest group and combine refractive, reflective, and catadioptric, as well as diffractive and holographic, optics.
- **Guided-wave micro-optics** primarily comprise integrated wave-guided optics or planar light circuits (PLCs).

It is interesting to note that nano-optics are located on the boundary between free-space and guided-wave optics and often have characteristics of both (such as photonic crystals, metamaterials, surface plasmons, etc.).

Hybrid free-space/guided-wave optics can be found, for example, in integrated waveguide optics for DWDM telecom applications, such as echelette-grating and phased-array-grating (PHASARS) demux modules.



Maximizing the Refractive Effect

Similar to prism arrays (or blazed gratings), a **Fresnel lens** can operate either in a refractive mode (in which case it is called a Fresnel lens) or a diffractive mode (in which case it is called a diffractive lens). The diffraction efficiency is tuned by modulating the depth of the grooves; the groove period and orientation dictate the local diffraction angle. When using amplitude elements, such as Fresnel zone plates, the only possible effect is the diffractive effect because there is no refractive surface available to apply Snell's law. The refractive effect can dominate when the diffractive conditions become weak, and vice versa.

For example, the **diffractive phase depth** and **periodicity condition** for a blazed grating can be reduced by designing random prisms with random footprints but the same slopes, so that the **refractive effect** would be the same for all prisms, although each would have a different aspect ratio. The phase condition for diffraction is thus reduced here.

Periodic prism structures (can be tuned for high diffraction)



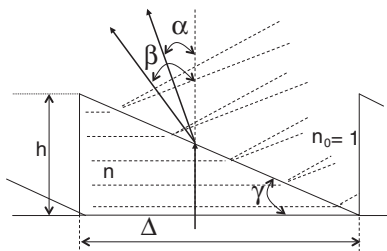
Random prism structures with the same slope (low diffraction, more refraction)



It is possible to increase the diffractive effect by carefully tuning the height (and/or refractive index, if applicable) of the prisms to have a perfect phase condition for maximum efficiency (see the following page). It is generally easier to increase the diffraction effects rather than increase the refraction effects in a microprism array or any other micro-optical element array. Pure refractive effects in micro-optics are very desirable mainly for their broadband operation aspects, but they can be more complex to design and fabricate.

Maximizing the Diffractive Effect

To increase the diffraction efficiency in a specific order, it is intuitively desirable to equate the refractive and diffractive angles to form a single resulting bending angle.



The law of refraction at the prism edge (A) and the grating equation for the fundamental order (B) are given by

$$\begin{cases} \sin(\alpha + \gamma) = n \sin(\gamma) & \text{(A)} \\ \sin(\beta) = \frac{\lambda}{\Delta} & \text{(B)} \end{cases}$$

Maximum efficiency is achieved when both angles α and β are equal, yielding the following condition of the prism optimum height h_{opt} :

$$\alpha = \beta \Rightarrow h = \frac{\lambda}{n_1 - \sqrt{1 - \frac{\lambda}{\Delta}}} \Rightarrow h = \frac{\lambda}{n_1 - 1}$$

$$\alpha = \beta \Rightarrow h_{\text{opt}} = \frac{\lambda}{n - \sqrt{1 - \left(\frac{\lambda}{\Delta}\right)^2}} \approx \frac{\lambda}{n - 1} \text{ for } \lambda \ll \Delta$$

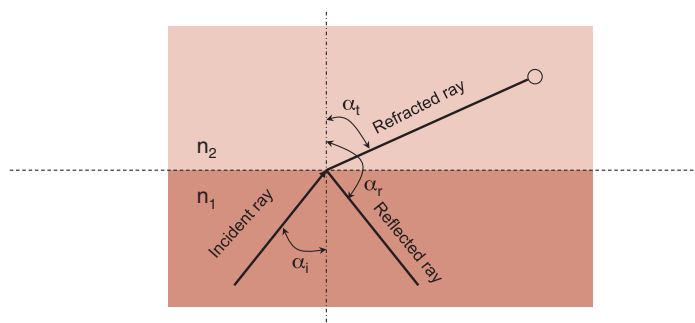
These equations show that the diffraction efficiency is maximal when the phase shift introduced by a microprism is equivalent to λ (or a 2π phase shift for the reconstruction wavelength). The same result can also be derived from **scalar diffraction theory**. Such an optimum depth h_{opt} can be modulated further in order to compensate for an arbitrary incoming beam angle and/or arbitrary number of surface-relief levels in the fabrication of the prism structures (see Multilevel Fabrication), or even for operation over multiple wavelengths (see Harmonic or Multiorder Elements).

Total Internal Reflection

When light hits a smooth, uniform surface, three optical phenomena can happen at the same time:

- Light is refracted by the surface,
- Light is reflected by the surface, and
- Light is absorbed by the surface media.

For rough or structured surfaces, other effects might appear, such as diffraction, scattering, diffusion, etc. In the following figure, $n_2 < n_1$.



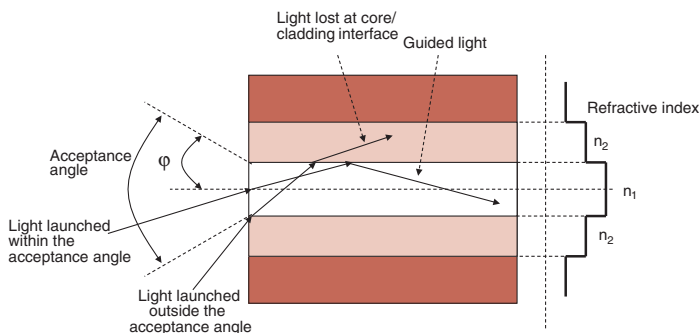
In Snell's equation, n determines the speed of light traveling through the medium ($v = c/n$). If light travels from one medium incident at a specific angle α_i , the refracted angle is a function of n . The reflected angle is independent of n and equal to the incidence angle. As a result, when the refraction angle is greater than 90° , there can no longer be a transmitted ray in the second medium, and therefore all of the light is reflected by **total internal reflection** (TIR). The TIR angle (or critical angle) can therefore be expressed as

$$\alpha_c = \arcsin\left(\frac{n_2}{n_1}\right)$$

The TIR effect cannot happen from lower to higher media (i.e., light can be trapped in glass between air but cannot be trapped in air between glass unless coatings are used).

Guided-Wave Digital Optics

An **optical waveguide** consists of two or more different media (indexes) that confine light in the higher-index core by **TIR**. The region in which the light is trapped is usually referred to as the **core**, and the region producing the TIR effect (lower index) is usually referred to as the **cladding**. The picture below shows a cross-section of a typical waveguide (e.g., a step-profile optical fiber) with a central core and a cladding (other regions around the cladding are usually a protective layer, jackets, etc.).



Prior to guiding light in a waveguide, the light must be injected (or coupled) into the waveguide core. When Snell's law is applied to that interface and the resulting refracted light angle is ensured to have an angle larger or equal to the TIR angle, the acceptance angle or the **numerical aperture** (NA) of such a waveguide (the angle within which the light is coupled and guided in the core) can be derived. The NA of an optical fiber is thus defined as

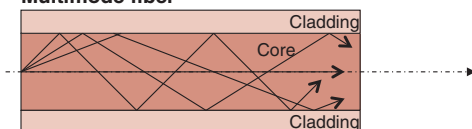
$$NA = \sin(\phi) = \sqrt{n_1^2 - n_2^2}$$

The injection port might be simply butt coupled to a guide with a similar NA, have a lens-shaped-end tip, or use a ball lens, a full-pitch GRIN lens, or diffractive lenses (such as vortex lenses for plastic fiber coupling).

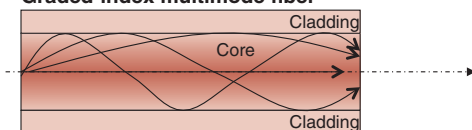
Optical Waveguide Types

There are two main types of **optical waveguide** structures: the step index and the graded index. In a **step-index waveguide**, the interface between the core and cladding is an abrupt change of index, producing the TIR effect. In a **graded-index waveguide**, the change between the core and cladding regions is smooth and continuous, therefore producing a refracted wave rather than a reflected wave. There are two types of step-index waveguides: multimode and monomode (single mode). Only a single mode can propagate in the latter, whereas a multitude of modes (TIR-reflected angles) can propagate in the former.

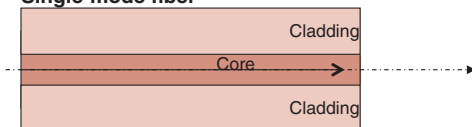
Multimode fiber



Graded-index multimode fiber



Single-mode fiber



When light is confined by coatings rather than by TIR, it may be referred to as a **light pipe** rather than a waveguide. Optical **planar waveguides** come in various types, including buried channel guide (graded index), ridge or strip-loaded channel guide (step index), or even photonic crystal (PC) waveguide (holey fiber).



Buried channel



Ridge channel



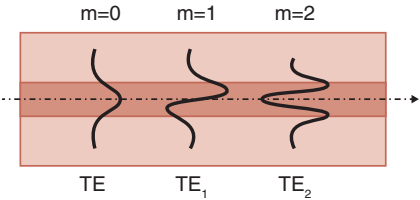
Strip-loaded channel

Modes in Optical Waveguides

The main **parameters** of an optical waveguide are the refractive indexes, the NA, the normalized frequency (V-number), and the cut-off frequency (the frequency under which no further propagation is possible), as well as the number of modes that can propagate down the guide.

Parameter	Step-Index Fiber	Graded-Index Fiber
Refractive index n	$\begin{cases} n_1; r \leq a \\ n_2; r > a \end{cases}$	$\begin{cases} n_1 \sqrt{1 - 2\Delta(r/a)^\alpha}; r \leq a \\ n_2; r > a \end{cases}$
Numerical aperture (NA)	$\sqrt{n_1^2 - n_2^2}$	$\sqrt{n(r)^2 - n_2^2}; r \leq a$
Normalized frequency (V)	$\frac{2\pi a}{\lambda} NA$	$\frac{2\pi a}{\lambda} NA$
Cut-off frequency	2.405	$2.405 \sqrt{1 + 2/\alpha}$
No. of modes	$V^2/2$	$\frac{V^2 \alpha}{2(\alpha + 2)}$

a is the core radius, n_1 and n_2 are the core and cladding indexes, respectively, and λ is the operational wavelength. **Successive-order modes** can propagate down an optical waveguide, referred to by their respective order indexes m . The following figure shows the transverse electric (TE) field for the first three mode orders in a step-index guide.

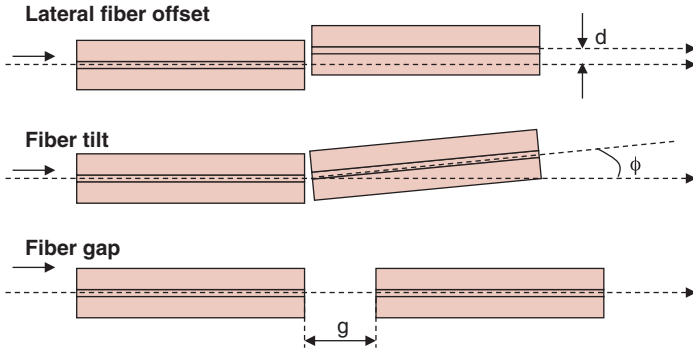


The fundamental-mode size width w of a step-index waveguide (or optical fiber) of normalized frequency V ($0.8 < V < 2.5$) is given by

$$w = 2a \left(0.65 + \frac{1.619}{V^{3/2}} + \frac{2.879}{V^6} \right)$$

Coupling Losses in Optical Waveguides

When considering an integrated optical waveguide system, it is usually required to couple light from one optical waveguide to the other, e.g., from a laser diode to a fiber or waveguide, or from one fiber to another. Losses occur at the coupling region as an effect of alignment errors. These losses are referred to as **insertion losses** (ILs). Typical alignment errors include lateral offset, tilt, and gap, as shown in the following figure.



The resulting ILs are expressed as

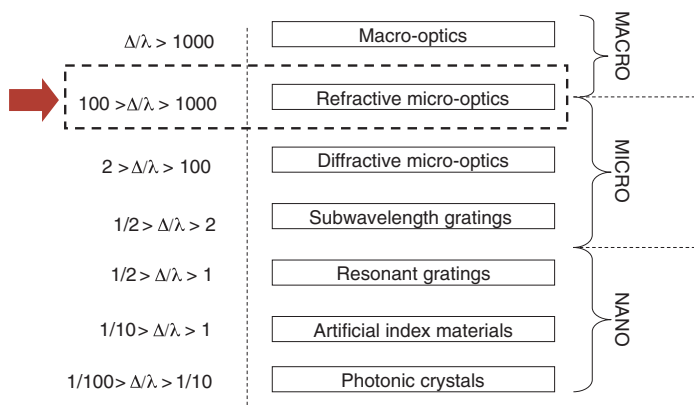
$$\left\{ \begin{array}{l} \text{offset loss} = \left(\frac{2w_1w_2}{w_1^2 + w_2^2} \right)^2 e^{-2 \frac{d^2}{w_1^2 + w_2^2}} \\ \text{tilt loss} = \left(\frac{2w_1w_2}{w_1^2 + w_2^2} \right)^2 e^{-2 \frac{(\pi n_2 w_1 w_2 \phi)^2}{\lambda^2 (w_1^2 + w_2^2)}} \\ \text{gap loss} = \frac{4 \left(4Z^2 + \frac{w_1^2}{w_2^2} \right)}{4Z^2 \left(1 + \frac{w_1^2}{w_2^2} \right) + \frac{w_1^2 + w_2^2}{w_2^2}}, \text{ where } Z = \frac{g\lambda}{2\pi n_2 w_1 w_2} \end{array} \right.$$

where w_1 and w_2 are the mode sizes of the first and second waveguides, respectively.

Free-Space Micro-Optics

Free-space micro-optics are optical elements that do not guide light through their micro- or nano-structures as in guided-wave optics; rather, they refract/reflect/diffract light at media interfaces (free space does not necessarily mean propagation in air and can thus be confined to multiple adjacent materials).

The following figure shows the wide variety of current free-space optics, ranging from macroscopic optics to micro- and nano-optical elements. Note that λ represents the period of the microstructures constituting the optical element.



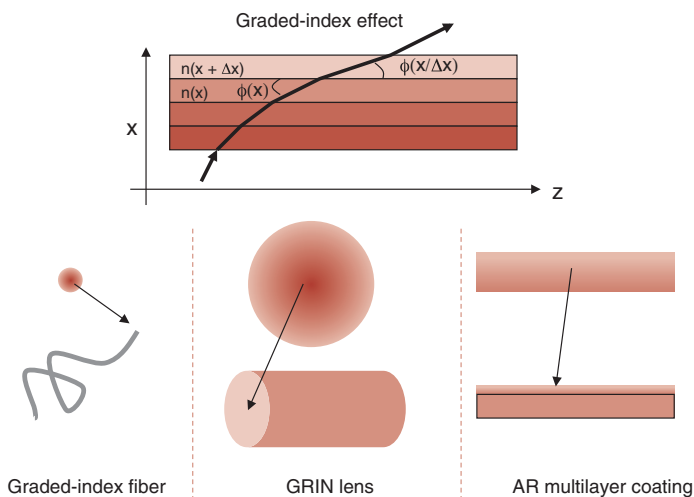
Free-space optics are often used in combination with waveguide optics, such as resonant gratings, artificial index materials, surface plasmons, or PCs.

Guided-wave optics can also be integrated with free-space optics to produce interesting effects, such as slab waveguides and holographic waveguide gratings (Bragg couplers and Bragg reflectors).

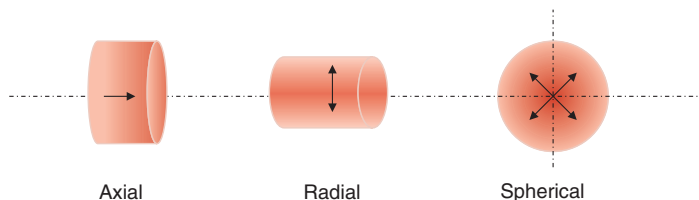
When only a few TIR reflections are used in a large medium (compared to the wavelength), light-guide or light-pipe systems become relevant.

Graded-Index Micro-Optics

A medium in which the refractive index varies gradually may be called **gradient-index (GRIN) micro-optics**. In a multilevel film stack (see below) with successive homogeneous index layers, each with a slightly different index, the stack becomes a 1D GRIN element as the thickness Δx tends to zero. When the film matches both the upper and lower indexes, it becomes an **antireflection (AR)** layer. When the substrate is a rod rather than planar, and the index decreases outward, the element may be a gradient-index fiber (drawn from a GRIN preform rod) or a **GRIN lens**.

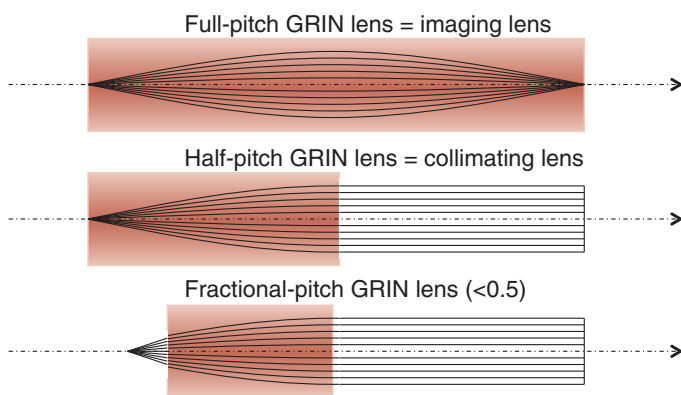


There are three main ways the refractive index may vary inside a rod: axially, radially, and spherically. Gradient-index fibers use a radial distribution, and GRIN lenses may use either radial or axial index distributions.



GRIN Lenses

GRIN lenses are usually cylindrical, can be produced in various ways (either with axial, radial, or spherical index gradients), and can be cut to various lengths to yield a different optical functionality, such as imaging (focusing), collimation, or even fractional imaging.



A similar **GRIN rod** can implement any such functionality by simply cutting the rod at a specific length. This is a unique property of GRIN lenses not achievable with standard refractive lenses, where the optical functionality is dictated by the bulk index and shape of the surface interface rather than the index change.

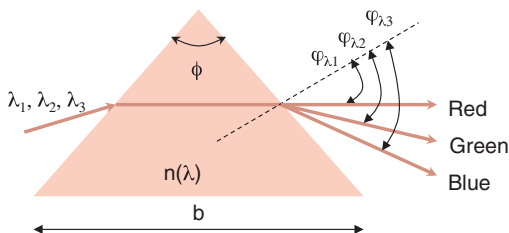
GRIN lenses have numerous advantages over traditional refractive lenses:

- Their aspect ratio is constant and not dependent on the focal length or NA of the equivalent lens.
- They are easily packaged due to their unique form factor (cylindrical rod).
- They are well suited for fiber coupling because the fiber core can be simply butt coupled to the entrance (or exit) GRIN facet without any air gap.

A refractive or diffractive lens may also be formed at the GRIN end facet to correct for specific aberrations. A tilted mirror can be used at the end surface to form a circular fiber (the input fiber is on axis, and the exit fiber is off axis).

Spectral Dispersion in Micro-Optics

Refractive micro-optics can produce **spectral dispersion** due to the wavelength dependence of the refractive index, just like their macroscopic counterparts.



The spectral resolving power of a micropism is defined as

$$R_{\text{prism}} = \frac{\lambda_0}{\delta\lambda} = b \frac{\partial}{\partial\lambda}(n)$$

In comparison, the spectral resolving power of a reflective grating in the m^{th} order is defined as

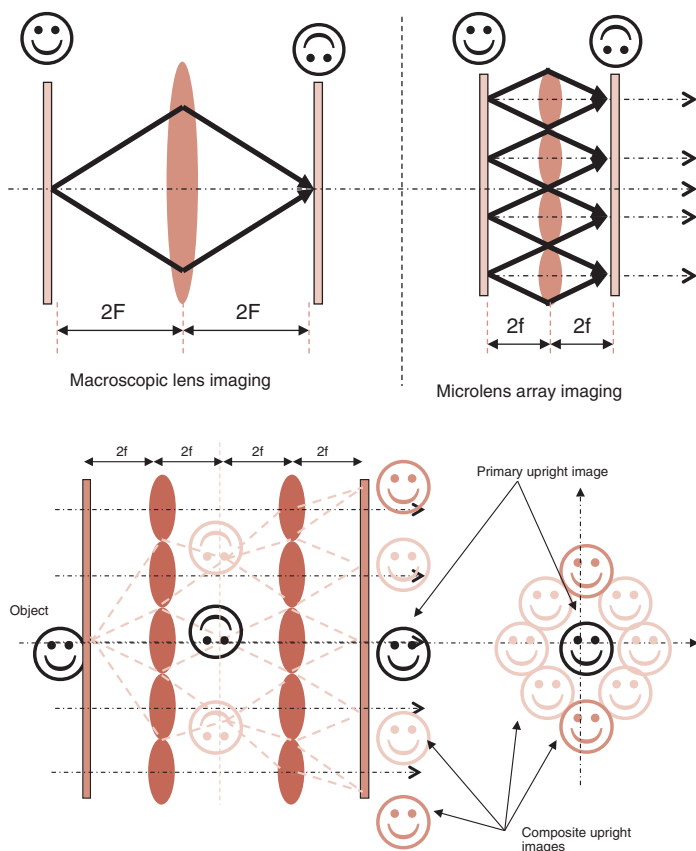
$$R_{\text{grating}} = \frac{\lambda_0}{\delta\lambda} = mN_0$$

where N_0 is the total number of periods considered. When the prisms are replicated and form a prism array, such as a blazed grating, on top of the refractive dispersion, the diffractive dispersion due to the periodicity of the prisms must be considered. Diffraction effects might be predominant for small periods and shallow gratings, and refractive effects may be predominant for large periods and deep gratings, or for random-period prism arrays (see also Maximizing the Refraction/Diffraction Effect).

The dispersion due to material dispersion has a sign opposite that of the dispersion due to the periodicity of the prisms and is usually much weaker (such as in transmission echelette or blazed gratings).

Imaging with Microlens Arrays

Refractive microlens arrays (MLAs) can produce unique imaging or nonimaging effects. Depending on the incoming field, they can produce single images or compound images, as shown below. The first MLA system is a $2f$ system, and the second is a $4f$ system.



Other types of MLA configurations with different focal lengths and signs can yield interesting effects, such as beam steering, afocal arrays for angle enlargers (an array of weak-positive and strong-negative MLAs), or refractive diffuser functions using microlens crosstalk.

Light-Field Cameras

A **light-field camera**, also called a plenoptic camera, is a camera that uses an MLA to capture 4D light-field information about a scene. The first light-field camera was proposed by Gabriel Lipmann in 1908; it used integral photography as the underlying technology. In 1992, Adelson and Wang proposed the design of a plenoptic camera that can be used to significantly reduce the correspondence problem in stereo imaging. To achieve this, an MLA is placed at the focal plane of the camera's main lens. The image sensor is positioned slightly behind the MLA. Using such images, the displacement of image parts that are not in focus can be analyzed, and depth information can be extracted.

This camera system can potentially be used to virtually refocus an image on a computer after the picture has been taken. The drawback of such a system is a lower resolution. Lumsdaine and Georgiev described a new design of a plenoptic camera, called a focused plenoptic camera, where the MLA is positioned before or behind the focal plane of the main lens. This modification samples the light field in a different way that allows for a higher spatial resolution at the expense of a lower angular resolution.

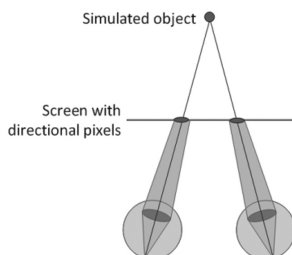
Raytrix (Germany) and Lytro (USA) developed the first commercially available light-field cameras. Shown below are first- and second-generation Lytro cameras.



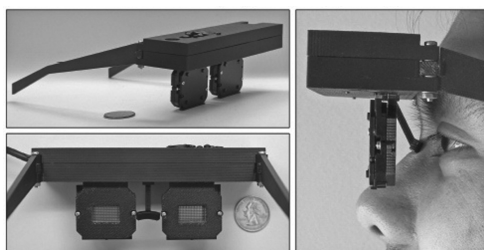
A different design using low-cost printed film instead of MLAs was proposed to overcome chromatic aberrations and allow for a higher spatial resolution. However, a mask-based design reduces light compared to MLAs.

Light-Field Displays

Similar to light-field cameras, **light-field displays** can be implemented in large-scale projectors for numerous viewers to single-user personal displays, such as **head-mounted displays** (HMDs). In light-field displays, multiple fields from various angles are projected on the same exit pupil, thus forming an eye box of light fields.



Light-field displays are usually assimilated into auto-stereoscopic 3D displays, but their 3D functionality is far superior to those of conventional stereo displays. The directionality of the projecting elements can be engineered via MLAs (as in Nvidia's design) or a combination of projectors (or pico-projectors) and a diffusion screen (such as a holographic screen in Holografika's design). Nvidia developed a light-field-occlusion virtual-reality (VR) HMD by adding an MLA over a high-resolution OLED microdisplay, creating a light field in the user's entrance pupil (shown below with a MLA-based design).



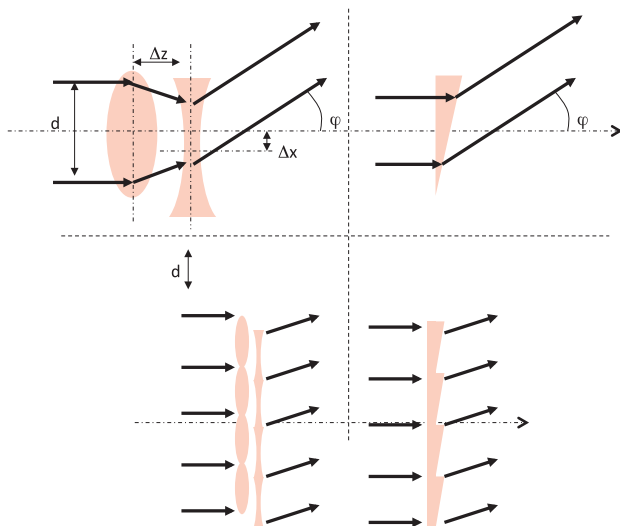
This architecture provides a wide field of view and can also adjust itself to fit most ophthalmic prescription compensations solely by software. Completely transparent light-field displays are currently under investigation for augmented-reality (AR) HMD applications.

Beam Steering with MLAs

Beam steering with MLAs is a useful way to steer an incoming beam by laterally moving one MLA with regard to the other (e.g., an afocal inverted telescope). The following figure shows one such MLA system and its resulting prism counterpart. The same principle can be applied to arrays of such lenses in order to produce a thin but large area to be steered, when thickness is essential. However, care must be taken with parasitic crosstalk between neighboring lenses. The resulting deflection angle for a typical dual-MLA beam-steering system is given by

$$\varphi = -\arctan\left(\frac{\Delta x}{df\#}\right)$$

where $f\#$ is the f -number of the lens, and Δx is the relative lateral MLA displacement.

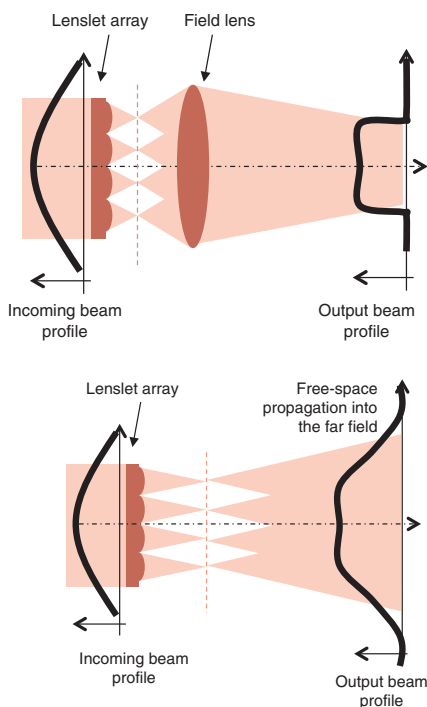


Small lateral offsets can produce large angular deflections. When aligned, such arrays are also known as afocal angle enlargers, enlarging the incoming beam angle by the magnification ratio of the MLA system. If the MLAs are diffractive, spectral dispersion and diffraction efficiency must be addressed. Angular shifts of tens of degrees can be achieved by micrometric lateral shifts.

Beam Shaping/Homogenizing with MLAs

MLAs and fly's-eye arrays are effective beam homogenizers. Such elements are widely used in digital projectors (front and back), located after the light engine to produce uniform illumination on the microdisplay.

MLAs can also be effective beam-shaper systems that shape an incoming beam into a specific far-field pattern defined by the geometry of the aperture of each lens in the array. For example, if the lens aperture is rectangular or hexagonal, the resulting far-field pattern may be rectangular or hexagonal, respectively.



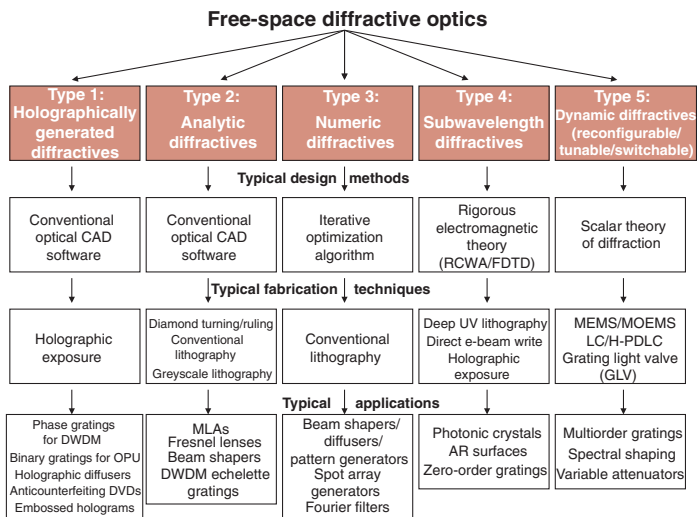
MLAs are used in a multitude of applications: beam shapers and beam homogenizers, light-collection increasers in digital image sensors and LCD projectors, optical fiber array collimators/couplers, stereoscopic displays, plenoptic cameras, etc.

Refractive MLAs are often preferred to diffractive MLAs when using broadband illumination to prevent parasitic spectral dispersion and spectral efficiency modulation. Such beam shapers are insensitive to the incoming beam profile, unlike diffractive beam shapers. Pseudo-random microrefractive element arrays can be arranged in a specific way to yield more-complex near-field or far-field intensity patterns (beam shapers). Such pseudo-lens arrays are usually called **engineered diffusers** and operate over a very wide spectral bandwidth, unlike diffractive beam shapers.

Digital Diffractive Optics

The realm of diffractive optics may be divided into five different categories, chronologically:

1. **Holographic optical elements** (HOEs) are holographically exposed like traditional volume holograms. The object beam can, however, be produced by an optical element, such as a lens, a diffractive element (CGH), or even a spatial light modulator (SLM) rather than by a real amplitude object.
2. **Analytic diffractive elements** (such as DOEs) can be designed or calculated analytically, whereas numeric diffractives require numeric optimization through iterative algorithms because there is no analytical solution to the diffraction problem (see point 3).
3. **Numeric diffractive elements** (such as CGHs).
4. **Subwavelength diffractive elements** can be either analytic or numeric, and they are often nondiffracting due to their subwavelength periods (zero-order gratings).
5. **Dynamic diffractive elements** have three different types: reconfigurable, tunable, and switchable.

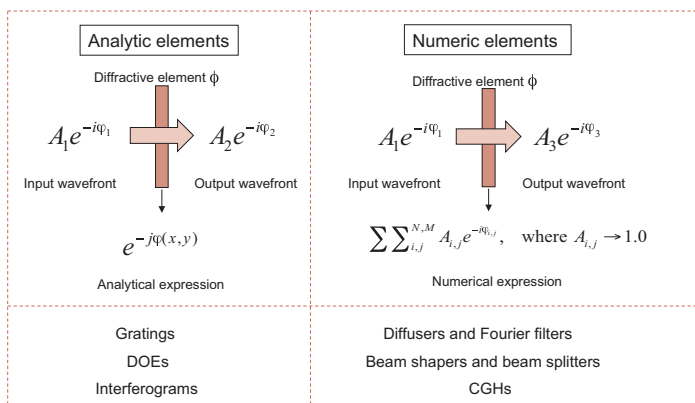


Analytic and Numeric Diffractives

Analytic elements are often designed by external optical-design software based on ray tracing because a phase profile may be defined analytically over an infinitely thin interface (such as a substrate or lens surface). Typical analytic elements are lenses, gratings, and interferograms, which can be single elements or combined with refractive/reflective elements to produce hybrid optics.

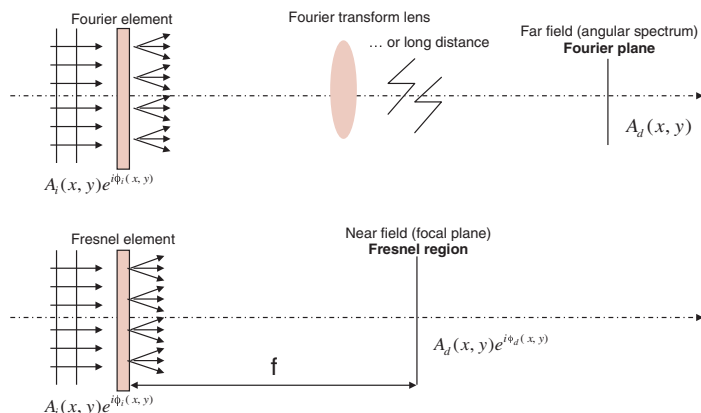
Numeric elements are usually calculated iteratively as a “black-box” element. An incoming wavefront is specified as well as the desired output wavefront. The incoming wavefront is usually a specific amplitude and phase function, and the output field is usually an amplitude-only function, located either in the near or far field. An iterative algorithm aims to reduce a specific cost or merit function that could be the diffraction efficiency in a given order, the uniformity of the reconstruction, the SNR, or the rms error between the desired reconstruction and the actual reconstruction.

Typical numeric elements are a diffuser, beam shapers, beam splitters, spot array generators, CGHs, arbitrary pattern generators, Fourier filters, etc.



Fresnel and Fourier Diffraction Regimes

A **Fourier diffractive element** is an element that reconstructs the desired wavefront in the far field. An example of a simple Fourier element is a grating. The far-field distance is a function of the wavelength, aperture size, and microstructure size. It can range from a few millimeters to a few meters, depending on the parameters. It is usually defined as the Rayleigh distance (see also Near- and Far-Field Regions).



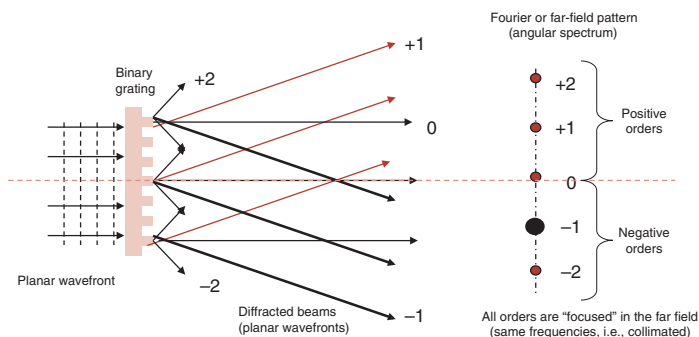
A **Fresnel diffractive optical element** is an element that reconstructs the desired wavefront in the near field. The term “near field” refers to a distance smaller than the Rayleigh distance. A simple example of a Fresnel element is a diffractive lens.

The far-field pattern (Fraunhofer regime or angular spectrum of plane waves) can be brought into the near field by using a Fourier transform lens. For example, if the illumination beam is collimated, the angular spectrum is brought back into the focal plane of the Fourier lens. However, any aberration of such a lens will change the geometry of the original far-field pattern (for example, off-axis beams will yield field curvature and coma when using a spherical lens as a Fourier lens).

Fourier and Fresnel Diffractive Optics

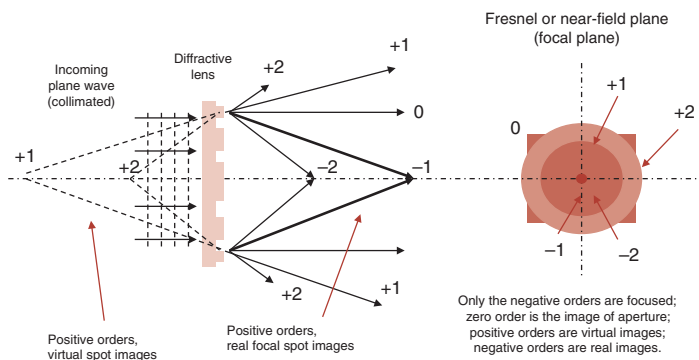
Diffraction through a Fourier element

A linear grating (periodic structures) produces sets of symmetric diffraction spots (with various efficiencies depending on the grating structures) visible in the far field.



Diffraction through a Fresnel element

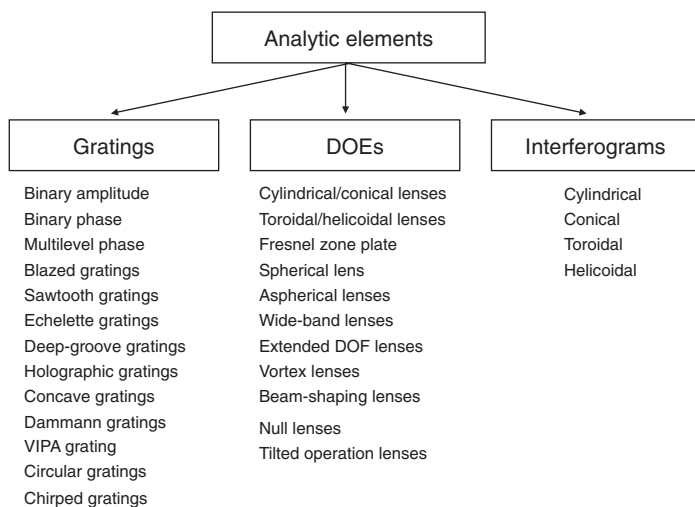
A diffractive lens (nonperiodic structure) produces various spots, located symmetrically on the optical axis, in the near field. For example, a binary diffractive lens can simultaneously be a converging and a diverging lens with the same efficiency.



Analytic Diffractive Elements

Analytic elements are elements that can be expressed in an analytic way, for example, by developing an analytic expression of a phase function (such as a polynomial), solving an integral analytically, or deriving an analytical expression. This is how micro-optics were designed before the advent of computers.

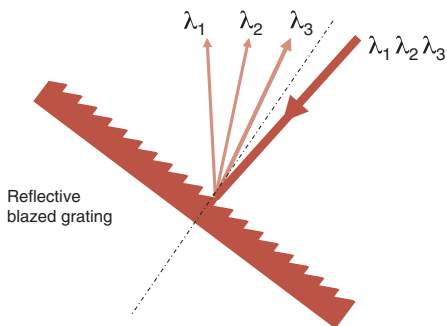
Optimizing an analytic phase function through heavy CPU ray tracing also produces an analytic element. Refractive micro-optics are analytic elements because their surface profile can be described by an equation. Diffractives, on the other hand, can be either analytic or numeric. There are three types of analytic diffractive elements: gratings, DOEs, and interferograms.



Grating-type analytical elements are periodic in one or more dimensions, DOEs are aperiodic elements, such as Fresnel lenses or beam shapers, and interferograms are calculated as sinusoidal interference patterns (see Interferograms).

Reflective Gratings

Reflective gratings were the first analytic elements to be implemented in a product due to their strong spectral dispersion in high diffraction orders (spectroscopy applications or wavelength mux/demux in DWDM systems). This figure depicts the most-common reflective grating: a blazed grating. Depending on the blaze angle and opposite sidewall angle, this grating can also be also considered to be an echelette grating.



Grating equation:

$$m\lambda = \Delta(\sin\alpha + \sin\beta)$$

Angular dispersion D of a reflective grating:

$$D = \frac{\partial\beta}{\partial\lambda} = \frac{m}{\Lambda\cos\beta} = \frac{\sin\alpha + \sin\beta}{\lambda\cos\beta}$$

where Λ is the period of the grating, m is the considered diffraction order (a function of the depth of the grooves), α is the incoming angle, β is the diffracted/reflected angle, and λ is the reconstruction wavelength. The spectral resolution R of a reflective grating is

$$R = \frac{\lambda}{\delta\lambda} = mN_0 = \frac{N_0\Delta(\sin\alpha + \sin\beta)}{\lambda}$$

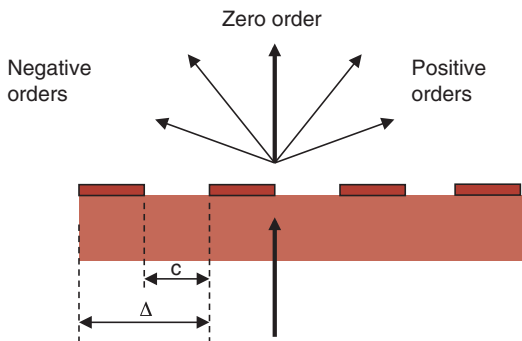
where N_0 is the number of grooves illuminated by the incoming beam. The maximal resolving power of such a grating is $R_{\max} = (2W)/\lambda$.

The free spectral range F of such a grating for a specific wavelength is

$$\begin{cases} F_\lambda = \Delta\lambda = \frac{\lambda_1}{m} \\ \lambda_1 + \Delta\lambda = \frac{m+1}{m}\lambda_1 \end{cases}$$

Amplitude Gratings

A binary **amplitude grating** is a periodic succession of opaque and transparent stripes; each stripe couple forms a single period of the grating. Such a grating can be fabricated as a chrome-on-glass plate with a single lithographical step-and-wet-etching process.



The diffraction efficiency of such a grating is very low: most of the reflected and transmitted light is held in the respective zero orders. Interestingly, this grating has symmetric diffraction configurations in reflection and transmission, which is ideal for a few specific applications.

The Fourier expansion of such a grating can be written as

$$a(x, y) = \begin{cases} 1 & \text{if } m\Lambda \leq x \leq c + m\Lambda \\ 0 & \text{elsewhere} \end{cases} \Rightarrow$$

$$a(x, y) = \frac{c}{\Lambda} \sum_{m=-\infty}^{+\infty} e^{-im\left(\frac{mc}{\Lambda}\right)} \frac{\sin\left(m\pi \frac{c}{\Lambda}\right)}{m\pi \frac{c}{\Lambda}} e^{2i\pi \frac{x}{\Lambda}}$$

The diffraction efficiency of such a grating for a specific duty cycle c can be written as

Duty cycle c

$$\eta_m = \left| \frac{\sin\left(m\pi \frac{c}{\Lambda}\right)}{m\pi} \right|^2$$

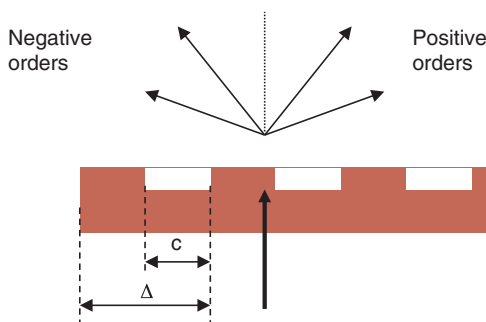
Symmetric

$$\eta_m = \left| \frac{\sin\left(\frac{m\pi}{2}\right)}{m\pi} \right|^2$$

where m is the diffraction order, and Λ is the grating period.

Binary Phase Gratings

A **binary phase grating** is similar to a binary amplitude grating, in which the opaque regions are replaced by etched grooves in either transmissive or reflective media. In amplitude and phase binary elements, the polarity of the structures can be reversed without altering the optical functionality (from Babinet's theorem). Both produce multiple diffraction orders, as shown below.



By decomposing the grating profile in a Fourier coefficient expansion, the efficiency in each order (strength of each Fourier coefficient) can be computed assuming that the optimal groove depth produces a π -phase shift to the incoming normal wavefront.

$$\eta_m^N = \left| \frac{\sin\left(\frac{m\pi}{N}\right)}{\frac{m\pi}{N}} \right|^2$$

By detuning the phase condition (nonoptimal groove depths, operational wavelength drift, incoming beam tilt), the resulting efficiency can be described as follows:

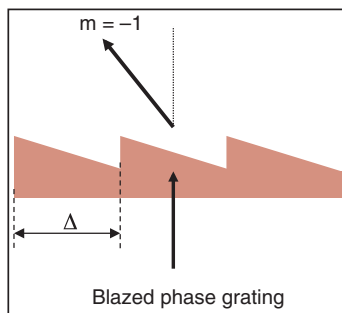
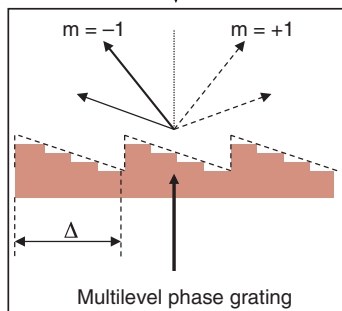
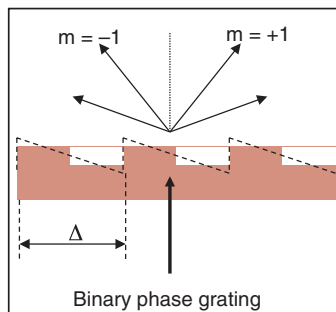
$$\eta_m^N = \left[\frac{\sin(\pi(m - \kappa))}{\sin\left(\frac{\pi(m - \kappa)}{N}\right)} \cdot \frac{\sin\left(\frac{\pi m}{N}\right)}{\pi m} \right]^2$$

where κ is the detuning factor (proportional to the groove-depth change, wavelength drift, or tilt angle). The perfect condition would mean no detuning (i.e., $\kappa = 1$). In many cases, the application calls for a nonmaximum efficiency because the zero order may also be part of the desired signal.

Multilevel Diffractives








Binary diffractives are the simplest to fabricate and replicate. However, they also produce the largest number of diffraction orders. In many applications, it is preferable to increase the efficiency in a specific order; other applications might require many different orders that have the same efficiency. Alternatively, only two orders might be required: symmetric in the far field, such as in on-axis binary Fourier elements, or of opposite vergence in the near field, such as in a binary lens.

Diffraction efficiency is a mathematical description of how much light is coupled into a specific order. This is not usually how application-oriented efficiency is calculated. For example, if the task is to produce a far-field symmetric pattern, the two fundamental orders of a binary Fourier element can be overlapped, thus producing 81% efficiency (the sum of the 40.5% efficiency of both fundamental orders). Diffraction efficiency is not a universal concept; rather, it is an application-oriented concept.



Diffractive Lens Surface Profiles

There are many ways to design and fabricate the same diffractive element (here, for example, a diffractive on-axis spherical lens). Each has its own specificity in terms of diffraction efficiency, number of orders, fabrication costs, etc. A few such examples are listed below. The two values for efficiency correspond to the theoretical and typical experimental values, respectively, that are most commonly achieved by current fabrication technologies.

Element type		Fabrication
Refractive (100% - 100%)		Polishing / Gray scale litho.
Blazed (100% - 90%)		Diamond turning / Gray scale litho.
Saw-tooth (90% - 85%)		Diamond turning
Amplitude (<10% - <8%)		Conv. Litho.
Binary (40.5% - 35%)		Conv. Litho.
Quaternary (81.0% - 70%)		Conv. Litho.
Sinusoidal (33.3% - 25%)		Holographic exposure

Lithographic fabrication techniques—such as binary, multi-level, or direct—and binary grayscale lithography can be used to fabricate low- (binary) to high-efficiency (multilevel or analog surface relief) diffractive lenses. Diamond turning may be used to fabricate diffractives with larger periods, directly as analog surface-relief elements. It is often desirable to produce binary structures rather than multilevel structures, especially if the application calls for multiorder diffraction or high diffraction angles (or subwavelength diffractives). Holographic exposure lithography may be used to produce lenses with (low-efficiency) sinusoidal profiles in resist, which can then be etched down as binary structures through overexposing resist and RIE.

Diffraction Efficiency

The following table summarizes the **diffraction efficiencies** in the main diffraction orders for various fabrication techniques. All numbers are percentages.

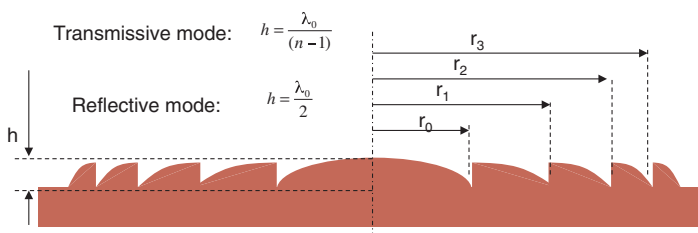
Physical mode	0	+1	-1	+2	-2	+3	-3
Binary amplitude	25	10.1	10.1	0	0	1.1	1.1
Sinusoidal amplitude	35	6	6	0	0	5	5
2 phase levels	0	40.5	40.5	0	0	4.5	4.5
4 phase levels	0	81	0	0	0	0	10
8 phase levels	0	94.9	0	0	0	0	0
16 phase levels	0	98.7	0	0	0	0	0
Blazed phase	0	100	0	0	0	0	0
Sinusoidal phase	32	34	34	0	0	0	0

Amplitude elements have the lowest efficiency. If an amplitude element consists of half absorbing and half transmission patterns (such as an FZP), then only transmission orders are generated. If the amplitude zones are reflective rather than absorbing, the same number of orders (including the zero order) will be diffracted in both directions (transmission and reflection). Such a lens would simultaneously converge, diverge, reflect, and transmit, thus forming a total diffracted field of ~50% (the other 50% is lost in both reflection and transmission zero orders). The conjugate fundamental order continues the fundamental in the opposite direction, e.g., the positive reflective is the conjugate transmission order.

Multilevel elements approximate a continuous analog surface-relief profile, and thus their efficiency converges toward the efficiency of an analog surface-relief element. Sinusoidal phase elements are usually interference patterns in resist, exposed holographically. They yield equal efficiency in the zero and both fundamental orders. An interferogram-type diffractive would have such a profile and such efficiencies.

Diffractive Fresnel Lens

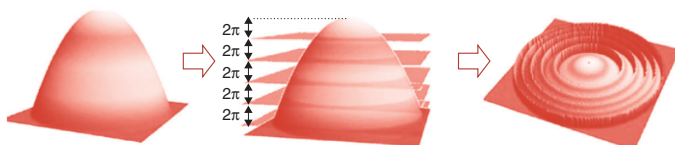
An on-axis **diffractive Fresnel lens** consists of concentric zones that can be either amplitude (FZP) or phase (binary, multilevel, or blazed lens, either reflection or transmission). The location of the zones (for a spherical or aspheric lens) produces local grating structures that diffract light in the direction dictated by the local grating period and orientation. The following figure shows a phase-only blazed diffractive lens with groove depths for reflection or transmission modes.



Different techniques may be used to calculate the position of the successive rings for such a lens:

- The rays at each local grating period can be traced, and the optical path difference (OPD) from one ring to the other can be increased by 2π for the design wavelength.
- The Fresnel rings can also be considered as slices of 2π cut from the continuous phase profile.

The following figure shows how a continuous phase profile is sliced into 2π slices and reset on the same surface to form the Fresnel rings. The phase profile is expressed over a planar or curved surface and is not a refractive profile. The phase profile is imprinted on the wavefront at that surface (at least in the fundamental diffraction order).



Diffractive Lens Profile Descriptions

In a **diffractive lens**, the desired continuous phase profile is imprinted on the wavefront at the desired sur-

face. For a spherical lens, the phase profile $\phi(r, \lambda)$ for each successive Fresnel groove i is shown here (where α is called the detuning coefficient). In many cases, a more-complex phase profile might be required to address specific aberration corrections. A general aspheric phase profile can be described through the sag equation and an astigmatic polynomial series:

$$\theta(r) = \frac{2\pi}{\lambda} \left(\frac{Cr^2}{1 + \sqrt{1 - (A + 1)r^2C^2}} \right) + \sum_{i=1}^N C_i r^{2i}$$

where A is the conic constant, and C is the curvature at the vertex. Note that these phase profiles are described over a target surface that is then converted into a real surface-relief profile as a function of the index and/or the design wavelength.

Fabricating an aspheric diffractive lens, unlike a conventional refractive lens, at the wafer scale has the same cost as fabricating a simple spherical lens. Optical CAD tools based on ray tracing can describe various general phase profiles, such as the rotationally symmetric phase profile (even or odd aspheres):

$$\theta(r) = \sum_{i=2}^n C_i r^i$$

This profile can be fabricated by single-point diamond turning. For off-axis or anamorphic profiles, a nonsymmetric phase profile or even an arbitrary profile described by a polynomial in x and y is often needed:

$$\theta(x, y) = \sum_{j=1}^m \sum_{i=1}^n C_i x^i \cdot C_j y^j$$

Microlithography techniques (binary, multilevel, or grey-scale) can fabricate such profiles, as can diamond-tool CNC machining (or freeform diamond machining), but when the base surface is not planar, e.g., hybrid optics, lithography might be difficult (wafers are usually flat).

Microlens Parameters

- ***f*-number** of a microlens: $f\# = f/D$, where D is the aperture diameter of the lens.
- **Numerical aperture** (NA) of a diffractive microlens:

$$NA = \sin(\alpha_{\max}) = \frac{\lambda}{\Lambda_{\min}} = \sin\left(\arctan\left(\frac{D}{2f}\right)\right) = \frac{D}{2f}$$

where Λ is the smallest period of such lens.

- **Smallest feature** δ in a diffractive lens:

$$\delta = \frac{\lambda}{pNA} = \frac{\Lambda_{\min}}{p}$$

where p is the number of phase levels of the lens.

- **Depth of focus** (DOF) of a microlens:

$$DOF = 2\lambda f\#^2$$

- **Shift in focal length** as a function of wavelength in a diffractive microlens (longitudinal chromatic aberration):

$$\begin{cases} \phi(x) = \exp\left(-i\pi \frac{x^2}{\lambda_0 f_0}\right) \Rightarrow f(\lambda) = \frac{\lambda_0 f_0}{\lambda} \\ \lambda_0 f_0 = \text{constant} \end{cases}$$

- **Abbe V numbers** for refractive and diffractive microlenses:

$$\begin{cases} V_{\text{ref}} = \frac{n_{\lambda_2} - 1}{n_{\lambda_1} - n_{\lambda_3}} \\ V_{\text{dif}} = \frac{\lambda_2}{\lambda_1 - \lambda_3} = -3.452 \end{cases} \quad \begin{cases} \lambda_1 = 486.1 \text{ nm} \\ \lambda_2 = 587.6 \text{ nm} \\ \lambda_3 = 656.3 \text{ nm} \end{cases}$$

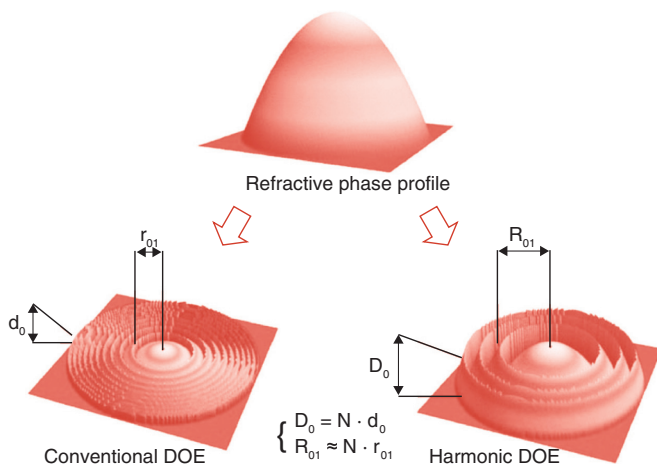
The Abbe numbers (spectral dispersion powers) have opposite signs for refractives and diffractives (50–60 for traditional refractives, and –3.5 for diffractives). A reflective (nondiffractive) microlens yields no dispersion.

Opposite Abbe numbers enable the design of achromatic singlets formed by hybrid refractive/diffractive profiles in which the refractive power is usually much stronger than the diffractive power (related to the spectral dispersion power ratio in both surfaces).

Spectral Bandwidth of Diffractives

A diffractive lens derived from a continuous phase profile over 2π slices can yield high diffraction efficiency at that specific wavelength but rather poor efficiency at all other, larger wavelengths. Diffraction efficiency is maximal for harmonics of that wavelength (shorter wavelengths). By designing derivative diffractives from phase slices that yield different $2\pi[n2\pi]$ phase shifts for various specific wavelengths, the resulting compounded efficiency may become much stronger over a wider spectrum between wavelengths for which the efficiency is maximal.

The following figure shows a same phase profile from which can be derived either a **narrow-band diffractive** lens (left, shallow fringes with a phase shift of $2\pi[0]$) or a multiorder, **broadband diffractive** lens (right, deeper fringes with a phase shift of $2\pi[n2\pi]$). The structures are deeper and wider.



When the design wavelengths are close to each other, the optimal depth may become too deep for fabrication, especially when the lens already has small periods (a fast lens). It is thus wise to choose wavelengths that are wider apart to yield groove depths that are easier to fabricate (litho/etching or diamond turning). Such elements are also referred to as harmonic lenses because they produce a 2π -period phase shift for multiple wavelengths.

Broadband Diffractives

A diffractive lens might be used over more than a single wavelength with high efficiency. Although it is possible to design and fabricate diffractives that yield high efficiency over multiple wavelengths, it is difficult to do so and achieve a uniform efficiency over a wide spectral band, such as the visible. The design phase profile can be sliced to produce multiples of 2π phase shifts for different wavelengths (multiorder or harmonic diffractive lenses). For example, to design a diffractive lens with high efficiency over λ_1 , λ_2 , and λ_3 , the following equations should be solved to find the optimal groove depth:

$$\begin{cases} H_T(\text{mod}_{(2\pi)}(\Delta\phi = 2\pi)) = \frac{N_1\lambda_1}{(n-1)} = \frac{N_2\lambda_2}{(n-1)} = \frac{N_3\lambda_3}{(n-1)} \\ H_R(\text{mod}_{(2\pi)}(\Delta\phi = 2\pi)) = \frac{N_1\lambda_1}{2} = \frac{N_2\lambda_2}{2} = \frac{N_3\lambda_3}{2} \end{cases}$$

where H_T is the groove depth in transmission, and H_R is the groove depth in reflection. A reflective multiorder diffractive lens is more desirable because the depth is much less than the transmissive counterpart and thus easier to fabricate (due to a lower groove-aspect ratio).

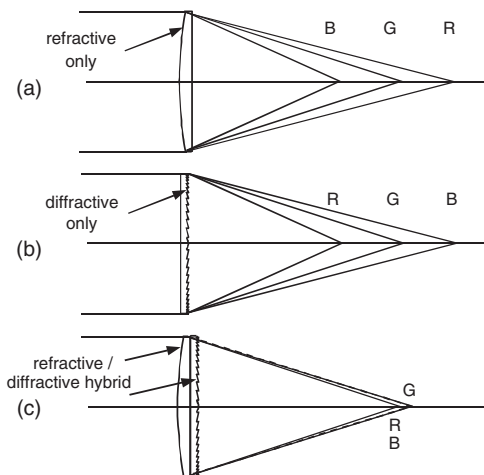
The focal length of the multiorder lens of broadband order p in diffraction order m is $f(\lambda) = (p/m)(\lambda_0 f_0 / \lambda)$. The efficiency in order k for a broadband order p diffractive lens can be written as

$$\begin{cases} \eta = \text{sinc}(\pi(p\psi + k))^2 \\ \psi = \frac{\lambda_0}{n(\lambda_0) - 1} \cdot \frac{n(\lambda) - 1}{\lambda} \Rightarrow \eta \approx \text{sinc}\left(\pi\left(\frac{\lambda_0}{\lambda}p + k\right)\right)^2 \end{cases}$$

p	Design λ_0 (nm)	k	Reconstruction λ (nm)	Efficiency η (%)
10	550	-8	700	99
		-8	650	93
		-9	600	99
		-10	550	100
		-11	500	100
		-12	450	98
		-14	400	98
		-16	350	97

Achromatizing Hybrid Lenses

Because the Abbe numbers of refractive and diffractive lenses have opposite signs, it is possible to achromatize such hybrid singlets (compensate spectral drifts). The following figure shows a (a) refractive and (b) diffractive lens and a (c) hybrid refractive/diffractive singlet reducing chromatic aberrations (i.e., spot shift).



Refractive Abbe number:
$$V_{\text{ref}} = \frac{n_{\text{med}} - 1}{n_{\text{short}} - n_{\text{long}}} \approx 50$$

Diffractive Abbe number:
$$V_{\text{dif}} = \frac{\lambda_{\text{med}}}{\lambda_{\text{short}} - \lambda_{\text{long}}} \approx -3.5$$

By equating both dispersion values, the chromatic aberration can be nulled out, as follows:

$$\frac{C_1}{V_1} + \frac{C_2}{V_2} = 0, \text{ where } C_{\text{total}} = C_1 + C_2$$

Effective focal length of a singlet:
$$\frac{1}{f_{\text{doublet}}} = \frac{1}{f_{\text{ref}}} + \frac{1}{f_{\text{dif}}}$$

Both surface powers have the same sign, unlike traditional achromatic doublets (no power waste).

Athermalizing Hybrid Lenses

Athermalization can be achieved in a hybrid singlet in a way similar to that of achromatic singlets (thermal spectral drifts have opposite signs in refractives and diffractives, similar to spectral dispersion characteristics).

- The **optothermal expansion coefficient** x_{ref} for a refractive lens of focal length f , curvature c , and index n can be written as

$$f = \frac{1}{(n-1)c} \Rightarrow x_{f,\text{ref}} = \left(\frac{1}{f}\right) \frac{\partial f}{\partial T} \approx \left(\frac{1}{n-1}\right) \frac{\partial n}{\partial T}$$

The focal-length variation for a diffractive lens as a function of the temperature is given by

$$f(T) = \frac{n_0 r_m^2}{2m\lambda_0} = \frac{1}{2m\lambda_0} r_m^2 (1 + \alpha_g \Delta T)^2 n_0$$

- The optothermal expansion coefficient x_{dif} for a diffractive lens can be written as

$$x_{f,\text{dif}} = \left(\frac{1}{f}\right) \frac{\partial f}{\partial T} \approx 2\alpha_g + \left(\frac{1}{n_0}\right) \frac{\partial n_0}{\partial T}$$

Inverse to spectral dispersion, the amplitude of the thermal expansion of diffractives is much smaller than the amplitude of the thermal expansion of refractives: $|x_{f,\text{dif}}| \ll |x_{f,\text{ref}}|$.

By equating both values, it is therefore possible to design an athermal lens (a hybrid singlet refractive/diffractive athermal lens) in which the focal length does not vary with temperature as it would for individual refractive or diffractive lenses: $x_{f,\text{doublet}} = x_{f,\text{mount}}$.

Although a typical hybrid achromatic singlet lens would have most of the power on the refractive surface, a typical hybrid athermal singlet will have most of the power on the diffractive surface. This makes it difficult to design and fabricate hybrid refractive/diffractive lenses that are simultaneously achromatic and athermal.

Hybrid-Lens Surface Descriptions

Optical-design CAD tools, such as ZemaxTM, offer various ways to represent a diffractive, holographic, or hybrid refractive/diffractive surface.

Zemax TM Surface Model Index	Description
Binary optic 1	Uses 230-term polynomial to define phase
Binary optic 2	Uses radial polynomial to define phase
Binary optic 3	Dual-zone aspheric and diffractive surface
Cylindrical Fresnel	Polynomial cylindrical Fresnel on a polynomial cylindrical surface
Diffraction grating	Ruled grating on standard surface
Elliptical grating 1	Elliptical grating with aspheric terms and polynomial grooves
Elliptical grating 2	Elliptical grating with aspheric terms and grooves formed by tilted planes
Extended Fresnel	Polynomial Fresnel on a polynomial surface
Extended toroidal grating	Aspheric toroidal grating with extended polynomial terms
Fresnel	Planar surface with refractive power
Generalized Fresnel	XY polynomial Fresnel on an aspheric substrate
Hologram 1	Two-point, optically fabricated transmission hologram
Hologram 2	Two-point, optically fabricated reflection hologram
Lenslet array	Arrays of microlenses
Radial grating	Diffraction grating with radial phase profile
Toroidal grating	Ruled grating on a conic toroid
Toroidal hologram	Toroidal substrate with a two-point, optically fabricated hologram
User defined	General surface that uses an arbitrary, user-defined function to describe the refractive, reflective, diffractive, transmissive, or gradient properties of the surface.
Zone plate	FZP model with annular rings of varying widths

A hybrid *Binary 2* surface can be defined as an underlying refractive or reflective surface with lens sag defined as

$$z = \frac{cr^2}{1 + \sqrt{1 - (1 + k)c^2r^2}} + \alpha_1 r^2 + \alpha_2 r^4 + \alpha_3 r^6 + \alpha_4 r^8 + \alpha_5 r^{10} + \alpha_6 r^{12} + \alpha_7 r^{14} + \alpha_8 r^{16}$$

with a diffractive phase profile on such surface defined as

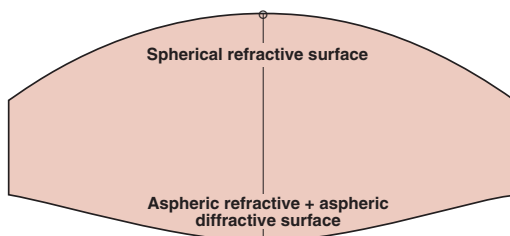
$$\Phi = M \sum_{i=1}^N A_i \rho^{2i}$$

where r and ρ are radial dimensions.

Hybrid Refractive/Diffractive Lens

The following example shows how a **hybrid refractive/diffractive singlet** has a front surface that is a pure refractive (usually spherical) and a second refractive surface (usually aspheric) with an aspheric diffractive profile of weaker power. Such a lens thus has three surfaces: two refractives and one diffractive.

The various aspheric coefficients describing both the second aspheric refractive and aspheric diffractive profiles are listed below, as well as the expression of the first refractive profile.



Description of a hybrid spherical refractive/aspheric refractive + aspheric diffractive lens as a Zemax™ Extended Fresnel surface type

Physical_type:	2
Operation_mode:	1
Design_wavelength_(nm):	587.60
Nb_of_phase_levels:	1
Index_of_refraction:	1.49166657
Hybrid_optical_element	
Nb_of_surfaces:	2
Surface_index:	2
Surface_type:	4
Refractive_profile	
Lens_units:	1000
Paraxial_curvature_(x 106):	-72463.77
Conic_constant_(x 106):	0.00
Phase_units:	1
Nb_of_coefficients:	1
Coefficient_index:	1
Coefficient_order:	4
Coefficient_(x 106):	275.00
Lens_radius_(μm):	8000.0

Surface_index:	1
Surface_type:	3
Refractive_profile	
Lens_units:	1000
Paraxial_curvature_(x 106):	76335.88
Conic_constant_(x 106):	0.00
Phase_units:	1
Nb_of_coefficients:	0
Lens_radius_(μm):	8000.0

Optical designers must be very careful with the dimensions and conventions used to express such aspheric coefficients (waves, radians, microns, millimeters, etc.) and the fact that the lens pupils might be normalized.

Aberrations in Micro-Optics

Refractives and diffractives have very different chromatic dispersions and thermal drift characteristics and can thus be achromatized or athermalized as hybrid singlets. The following tables list some of the aberrations that occur in either pure diffractive or pure refractive lenses.

Parameter	Refractive Lens
Spherical	$S_I = \frac{y^4 \theta^4}{4} \left(\left(\frac{n}{n-1} \right)^2 + \frac{n+2}{n(n-1)} E^2 + 4 \frac{(n+1)}{n(n-1)} ET + \frac{3n+2}{n} T^2 \right)$
Coma	$S_{II} = \frac{-y^2 \theta^2 H}{2} \left(\frac{n+1}{n(n-1)} E + \frac{2n+1}{n} T \right)$
Astigmatism	$S_{III} = H^2 \theta$
Petzval curvature	$S_{IV} = \frac{H^2 \theta}{n}$
Distortion	$S_V = 0$
Bending parameter	$E = \frac{c_1 + c_2}{c_1 - c_2}$
Conjugate parameter	$T = \frac{u + u'}{u - u'} = \frac{m + 1}{m - 1}$

Parameter	Diffractive Lens
Spherical	$S_I = \frac{y^4 \theta^4}{4} (1 + B^2 + 4BT + 3T^2) - 8\lambda B y^4$
Coma	$S_{II} = \frac{-y^2 \theta^2 H}{2} (B + 2T)$
Astigmatism	$S_{III} = H^2 \theta$
Petzval curvature	$S_{IV} = 0$
Distortion	$S_V = 0$
Bending parameter	$B = \frac{2c_{\text{sub}}}{\theta}$
Conjugate parameter	$T = \frac{u + u'}{u - u'} = \frac{m + 1}{m - 1}$

Aberrations in Micro-Optics (cont.)

Although on-axis systems with low NAs may produce decent optical imaging qualities with spherical surfaces, off-axis and higher-NA systems may require more-complex aspheric surfaces. Such surfaces may be described as odd or even aspheres, toroids, anamorphic, or even freeform surfaces. It is usually more complex to fabricate a highly aspheric refractive or reflective surface than a spherical surface. This is not the case for diffractives, at least when they are fabricated via microlithography. For diffractives, a general polynomial (X/Y cross-linked terms) may bear the same lithographic fabrication burden as the fabrication of simpler linear or spherical surfaces.

While designing such aspheric surfaces, care must be taken when unleashing higher-order coefficients in the optimization process (in CAD tools): this may not necessarily yield fewer aberrations if the cost function has not been designed to prevent the divergence of higher aspheric polynomial coefficients. For example, diffractives produce stronger coma aberrations than similar refractives; such coma can be reduced by fabricating the diffractive on a curved surface rather than by optimizing a higher-order aspheric diffractive phase profile.

Although it can be conceived that imprinting the phase profile instantaneously on the incoming wavefront might be an advantage (such as in diffractive optics or HOEs), it is usually an inconvenience that yields more aberrations, which might require fabricating the diffractive or hologram on a curved surface or combining it with refractive elements to form a hybrid optical element.

Beam-Shaping Lenses

Diffractive analytic beam shapers may be designed by deriving a phase profile for a simple geometrical transformation, such as Gaussian-to-top-hat. Such an element can be fabricated as a refractive profile (very difficult to produce refractively due to its arbitrary profile).

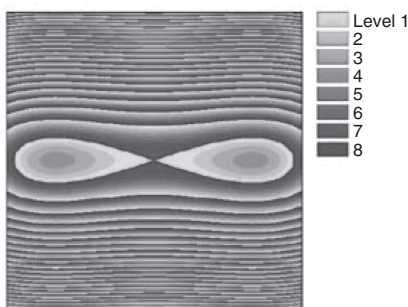
The following expression

$$\begin{cases} \varphi(x_1, y_1) = \varphi_x(x_1) + \varphi_y(y_1) \\ \varphi_x(x_1) = -\frac{\pi}{\lambda f} x_1^2 - \frac{2\pi a}{E_a f} \left[x_1 \operatorname{Erf} \left(\frac{x_1 \sqrt{2}}{\sigma} \right) - \frac{\sigma}{\sqrt{2\pi}} \left[1 - e^{-\frac{2x_1^2}{\sigma^2}} \right] \right] \end{cases}$$

describes such an element as a phase profile that can be implemented either as a refractive or a diffractive element. In this case, it is a Gaussian-to-top-hat beam shaper, where a is the output-square top-hat dimension, σ is the beam waist of the Gaussian incoming beam, and f is the focal length of such a beam-shaper lens).

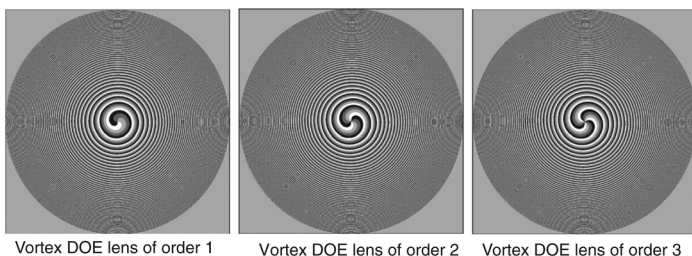
Although this phase expression is separable in the x and y axes, it might be difficult to fabricate such a phase profile as a refractive element but easier as a diffractive (via microlithography). The following image shows such a diffractive beam shaper fabricated over eight phase levels.

Similar to a Fresnel diffractive lens, the fringes have decreasing periods from the optical axis toward the outer regions of the lens. Unlike numeric, diffractive beam-shaper lenses, the phase profile here does not show any phase dislocations (see Beam-Shaping CGHs).

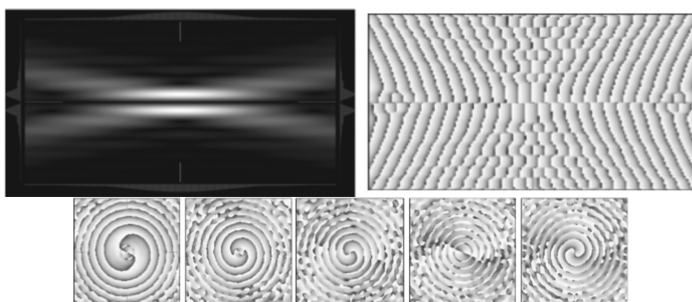


Vortex Microlenses

Vortices are universal and robust states that exist in all realms of physics and, therefore, also optics. Diffractive **vortex lenses** have unique optical functionalities suitable for special applications. Although it is difficult to implement a vortex lens as a refractive or reflective element, it is easy to fabricate one as a planar diffractive. The fringes composing such lenses are not circular but rather helicoidal.



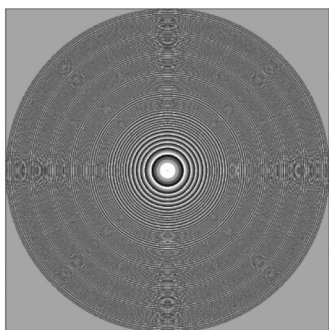
Vortex lenses create a vortex of k vectors propagating within a tore of light around the focus plane. Such a tore is different from the tore produced by conventional toroidal lenses. The following figure shows the longitudinal intensity and phase maps at the vicinity of the focus of a second-order lens and the lateral phase maps (the focus plane is on the fourth reconstruction form from the left). Note the phase vortices.



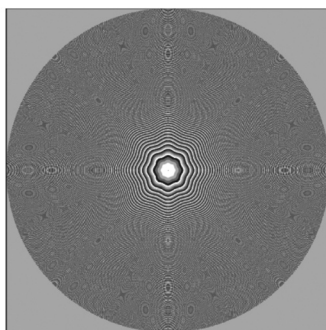
Vortex lenses are currently used in numerous fields, ranging from metrology to interferometry to plastic fiber coupling.

Extended Depth of Focus Microlenses

One of the advantages that diffractive lenses have over their refractive/reflective counterparts is that they can implement complex phase profiles without being more complex to fabricate. An example of the versatility of diffractive lenses is the DOF-modulated lens, a kind of **extended depth of focus** (EDOF) lens. A conventional diffractive lens with a single focus is modulated either radially (left) or circularly (right).



Radial DOF modulation



Circular DOF modulation

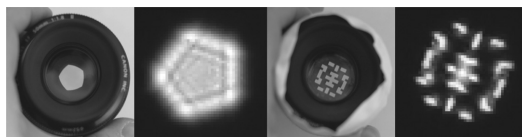
In both cases, a sinusoidal modulation of the focal length (amplitude Δf centered over f_0) has been imprinted on the original circular fringes over N periods. Although radial modulation does not affect the shape of the fringes but rather the periods of the consecutive fringes as they move along from the optical axis, circular modulation affects the shape of the fringes and produces wavy patterns. Such lenses have a spatially localized focal length varying from $f_0 - \Delta f$ to $f_0 + \Delta f$ by N times, either radially or circularly.

Although such modulation will affect the imaging quality of the lens, optimal applications might be found in laser material processing (compensating for work-piece location and/or planarity), optical pick-up units (compensating for disk wobbling), or specific wavefront coding for digital imaging applications (e.g., camera phones, IR missile tracking).

Aperture and Wavefront Coding

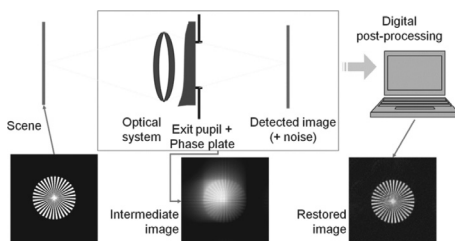
Aperture coding

Traditional cameras use circular apertures and capture blurred images away from the plane of focus. By creating a coded aperture within the objective lens, depth information and all-focus images can be retrieved via signal processing (shown below: (left) conventional and (right) coded apertures and subsequent PSFs).

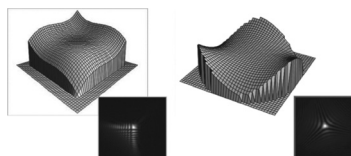


Wavefront coding

Wavefront coding, pioneered by Edward Dowski, Jr. and Thomas Cathey in the 1990s, enhances the depth of field of imaging systems. It is based on codifying the wavefront to replace the ordinary PSF with one featuring invariance properties against defocus. The codification is achieved by adding a phase mask at the exit pupil of the system.

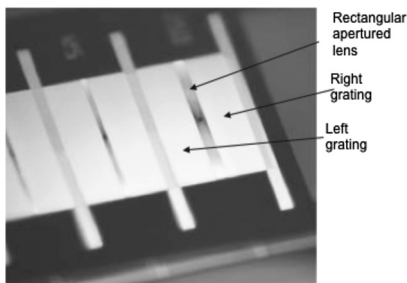


Commonly used phase masks are cubic distributions (shown below with subsequent PSFs). The mask is usually computed using the ambiguity function and stationary phase method. Dynamic range is usually sacrificed to extend the depth of field.

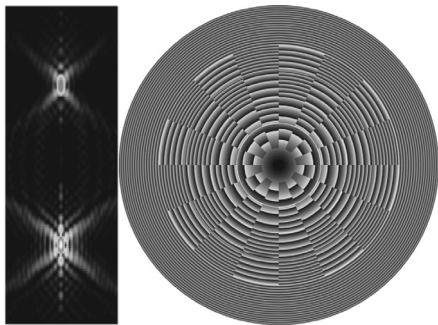


Spatially Multiplexed Planar Optics

Complex apertures can be implemented in diffractive lenses to **spatially multiplex** various lenses or create super-resolution lenses (by blocking the center of the lens). DOE lenses are very versatile elements and can be spatially multiplexed with other elements, such as linear gratings. In this example, a series of diffractive lenses are fabricated over a thin slit area flanked by gratings on each side. Such a transparent element assumes the task of two bulk optical elements, a lens, and an aperture stop (as in optical encoders). A slit is difficult to align to a lens, but a lens with slit functionality already incorporated in its structures has the potential to be easily mass replicated.



Another example is the spatial multiplexing of two lenses with two different prescriptions to be used as a dual-focus lens in **optical pick-up units** (OPUs) to read CDs and DVDs with a single “lens.” The spatial multiplexing architecture chosen here is a complex “dartboard” aperture that maximizes the angular and radial contributions of each lens to produce optimal Strehl ratios in both spots (see the numerical modeling along the optical axis on left side). The smaller spot = DVD @ 650 nm for a higher NA, and the larger spot = CD @ 780 nm for a lower NA).



Diffraction Null Lenses

Diffraction null lenses are used in interferometers to analyze the quality of a refractive or reflective lens profile, usually a highly aspheric surface profile. Such null lenses are also called null CGHs, even though they are analytic diffraction lenses or phase plates designed through ray tracing rather than calculated iteratively as typical numeric CGHs.

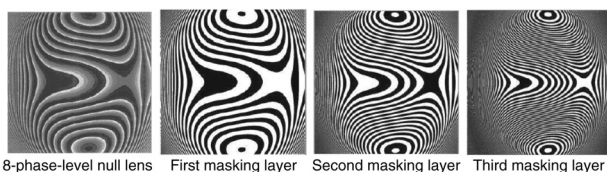
Such lenses may be described through Zernike polynomials (Zernike wavefront description) or any other aspheric phase profile, as listed in “Diffraction Lens Profiles.”

$$\varphi(r, \phi) = \sum a_{m,n} Z_{m,n}(r, \phi)$$

Some of the Zernike orthogonal phase states:

$$\left\{ \begin{array}{ll} Z_{0,0} = 1 & \rightarrow \text{piston} \\ Z_{1,-1} = 2r\sin(\phi) & \rightarrow \text{tip} \\ Z_{1,1} = 2r\cos(\phi) & \rightarrow \text{tilt} \\ Z_{2,-2} = \sqrt{6}r^2\sin(2\phi) & \rightarrow \text{astigmatism} \\ Z_{2,0} = \sqrt{3}(2r^2 - 1) & \rightarrow \text{focus} \\ Z_{2,2} = \sqrt{6}r^2\cos(2\phi) & \rightarrow \text{astigmatism} \end{array} \right.$$

Below is an example of a typical astigmatic null lens corrector (or null CGH) showing the three binary masks used to produce the final 8-level-phase null CGH via lithography.



8-phase-level null lens First masking layer Second masking layer Third masking layer

Although a binary-phase null CGH producing 40.5% diffraction efficiency in the fundamental diffraction order might be sufficient to be used in an interferometer, lower light in the conjugate order as well as in the higher orders will increase the SNR and image contrast in the fringe read-out on the interferometer (achieved through multilevel fabrication).

Interferogram Lenses

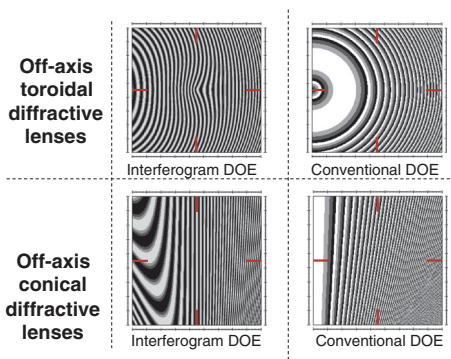
Interferogram diffractive lenses are similar to standard diffractive lenses. However, there are a few important differences. An **interferogram lens** is calculated as an interference pattern formed by a reference and an object wavefront, as in traditional holography. The resulting interference pattern is a sinusoidal profile:

$$t(x, y) = c + 2A_0(x, y)\cos\left[\varphi_0(x, y) + 2\pi\frac{\sin(\alpha)}{\lambda}x\right]$$

where α is the angle between both wavefronts, and c , φ_0 , and A_0 are constants.

An off-axis reference wave is used to produce the off-axis power rather than setting the aperture off-axis, as in a standard diffractive. When setting a toroidal lens in an off-axis position, part of the lens does not

appear in the aperture (top-right image). Only half of the focused ring appears in the focal plane when illuminating such a lens.



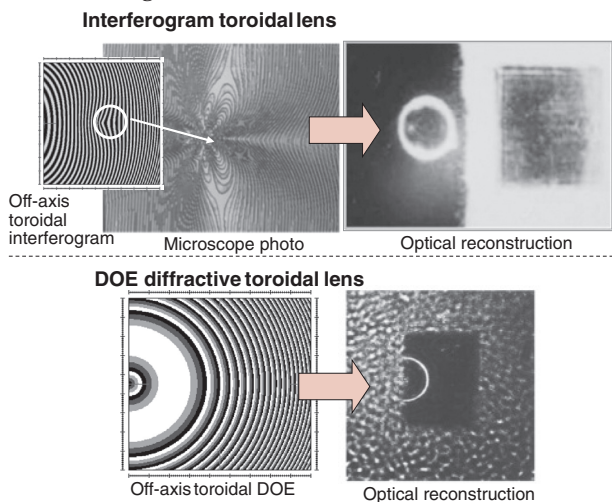
When setting an interferogram toroidal lens off axis, a tilted reference beam is introduced and produces a lens profile (top-left image). When illuminated, the entire light ring still appears in the focal plane. The bottom figures show the same effect with conical diffractive lenses.

Because the phase profile is sinusoidal, it yields a maximum efficiency of only 33%. Such lenses can be used in off-axis modes so that the converging wave (fundamental positive order) does not interfere with either the diverging wave (negative order) or the zero order.

Toroidal and Helicoidal Planar Lenses

When calculating the conventional diffractive lens phase profile, the standard phase-profile description, as given by classical optical design-software tools, is used. When calculating an interferogram lens for the same phase profile, a carrier term (as a grating function) can be included in order to offset the optical reconstruction. The integration of the carrier is not done over the phase profile (which would produce a conventional off-axis lens) but rather in the interferogram fringe pattern (producing the same offset effect without physically setting the aperture offset to the actual lens phase profile).

The following example shows the fringe patterns for a simple toroidal lens and the optically reconstructed pattern off-axis. Only the interferogram fringes reconstruct the entire toro of light.

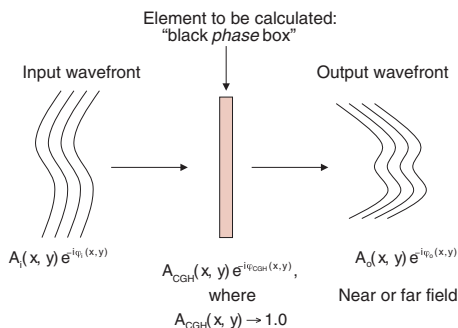


Complex shaped lenses can be effective optics for use in metrology, 3D display, optical telecom, laser material processing, and optical sensing, but very rarely for traditional imaging applications. Such lenses include conical (tilted cylindrical), toroidal, helicoidal, axicon, vortex, etc.

Numerical Optimization

Numeric diffractives are often calculated by iterative optimization algorithms (such as phase retrieval algorithms) because the optical problem usually has no analytical solution. A merit function (or cost function) is defined over n dimensions as well as a set of constraints. The algorithm then tries to find a minimum value of the cost function by modifying various degrees of freedom in the diffractive (typically a sampled phase profile) while addressing the various constraints (typically design, operation, and fabrication constraints).

The following figure illustrates an input and output wavefront (the wavefront constraints). An added constraint is the description of the sampled complex profile, which is usually a phase-only profile with a limited number of phase values for each pixel (or phase levels) and a specific sampling rate (pixel size).



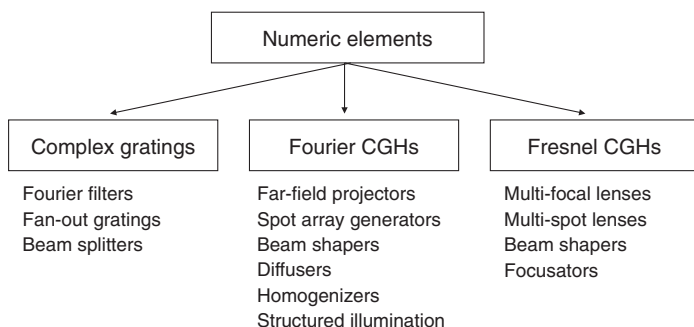
One important indicator of how easily the element might be optimized is its **space-bandwidth product** (SBWP), related to the number of degrees of freedom the algorithm can work on:

$$SBWP = \frac{NM}{C_x C_y} P$$

where N and M are the number of pixels in x and y , C_x and C_y are the size of each pixel, and P is the number of phase levels over each pixel.

Numeric Diffractives

Numeric diffractives designed by an iterative algorithm can produce complex optical functionalities not achievable by analytic diffractives. They are often not used as imaging systems, like their analytic diffractive counterparts, but rather in illumination systems, sensors, and other nonimaging optical systems.



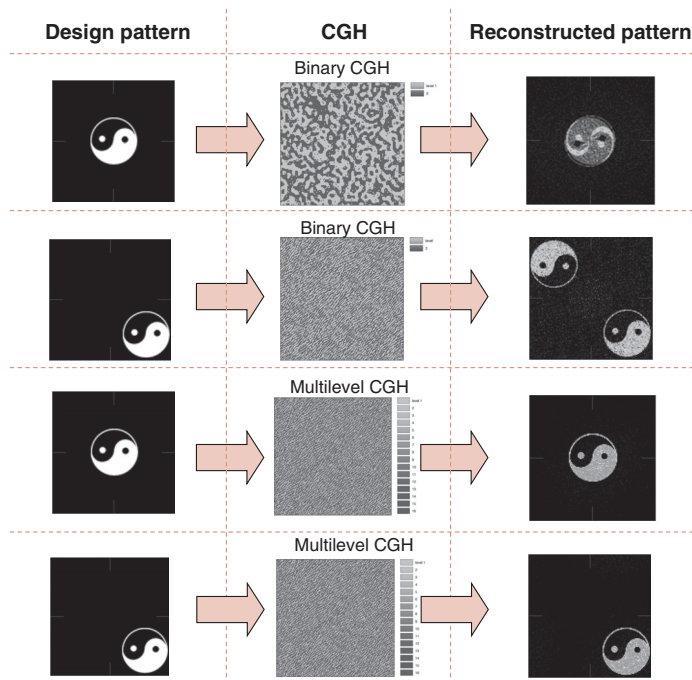
Because the solution to the optical problem (defined as a black box between an input wavefront and an output wavefront) does not need to be analytical, very complex optical functionalities can be produced, such as custom pattern generators in the near and far field, from specific input wavefronts (such as beam shapers, pattern generators, etc.).

Numeric diffractives might reconstruct the desired wavefront in either the near field (Fresnel element) or far field (Fourier element). As opposed to analytic elements, diffractives calculated by iterative algorithms, such as phase retrieval algorithms, can produce phase dislocations for either Fourier or Fresnel elements, which might be a problem in imaging systems.

Fourier diffractives typically yield many more phase dislocations than Fresnel elements. Phase unwrapping algorithms can thus be applied more easily to the latter than the former.

CGH Design Constraints

When defining an object constraint for an iterative optimization algorithm, such as an amplitude (or intensity) constraint, it is important to prevent diffraction pattern overlap or instead force multiple diffraction orders to overlap (e.g., on-axis symmetric Fourier patterns, such as a top-hat beam shaper or spot array generator).

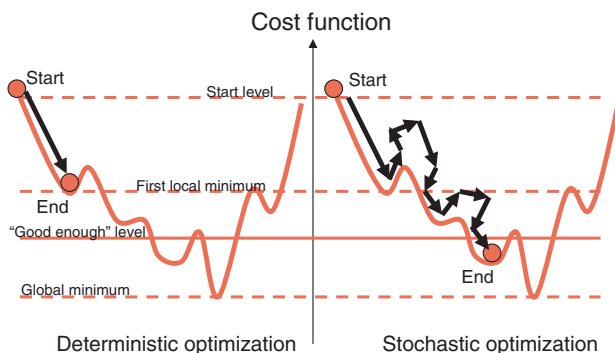


This is particularly true for binary elements, especially in the far field (Fourier binary elements). In this case (first and second example in figure), the object is not symmetric and both orders are overlapping in the binary phase case. For multilevel fabrication (next examples), the energy in the conjugate orders (fundamental and higher) are irrelevant, therefore reducing the burden on object constrains positioning.

Merit Function Definition

In an iterative optimization process for a numeric element, one key issue is to define an appropriate cost function and a set of constraints. The obvious constraint is the reconstruction pattern and the incoming field, but others could be the number of phase levels to be fabricated and the number of pixels in the sampled element. The cost function is usually the diffraction efficiency, but it can assume more-complex roles, such as uniformity in the reconstruction, local SNR levels, RMS error in the reconstruction, etc.

In many cases, the optimal cost function is a linear combination of such criteria, with a weighting factor used for each of them. The choice of iterative algorithm is important: although some would not be able to leave a local minimum (such as direct binary search) over complex **merit functions**, others would converge to a lower global minimum (such as with simulated annealing, shown below).

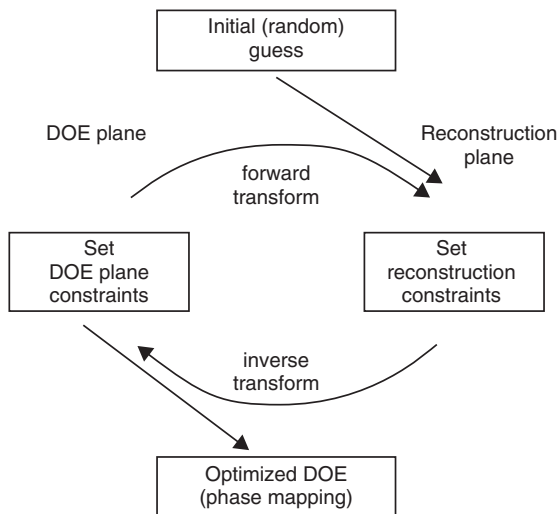


The conditions for termination of the optimization process can vary, such as a specific cost-function limit, specific optical criteria value (such as diffraction efficiency or uniformity), target number of iterations, or evolution rate of the cost function (which is often the most useful because the best achievable cost-function level is usually unknown).

IFTA Algorithm

The **Gerchberg-Saxton algorithm** (also called the **iterative Fourier transform algorithm**, or IFTA) is probably the easiest CGH optimization algorithm to implement and the fastest to converge toward a solution. The iterative algorithm is based on sets of constraints in both the CGH or DOE plane and the reconstruction plane (which can be the far field or the near field). The propagation to and from both planes is performed by either a Fourier transform (far field) or a Fresnel transform (near field). In each plane, the constraints are set (e.g., phase quantization in the CGH plane and amplitude in the reconstruction plane).

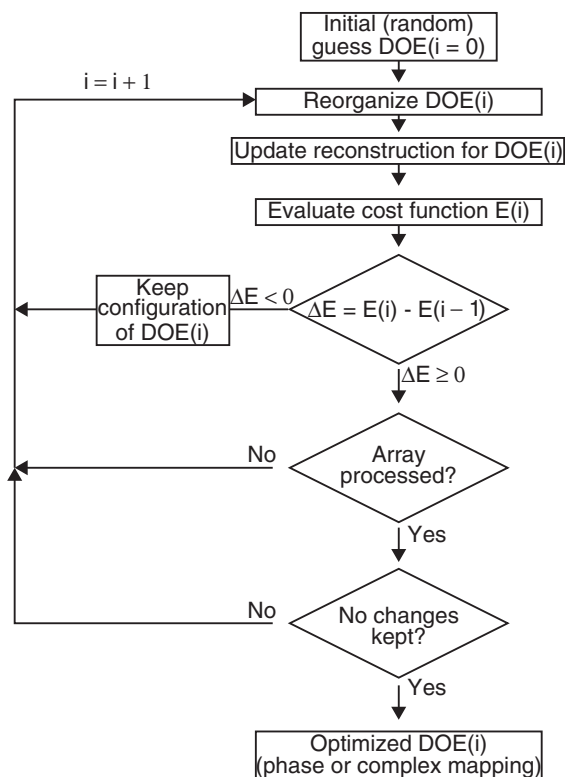
The raw IFTA converges the efficiency very well, but its uniformity and SNR are lacking. Additional features can therefore be implemented, such as simple error reinjection or annealing error reinjection, to improve the convergence of the uniformity in the reconstruction. The initial guess can be random or the output of a previous algorithm or design.



Direct Binary Search

The **direct binary search** (DBS), or steepest-descent algorithm, is a simple, input–output iterative optimization algorithm. It is fast and easy to implement, but it can be trapped in local minima, especially if the cost function is a combination of several criteria, such as efficiency, uniformity, SNR, RMS, etc.

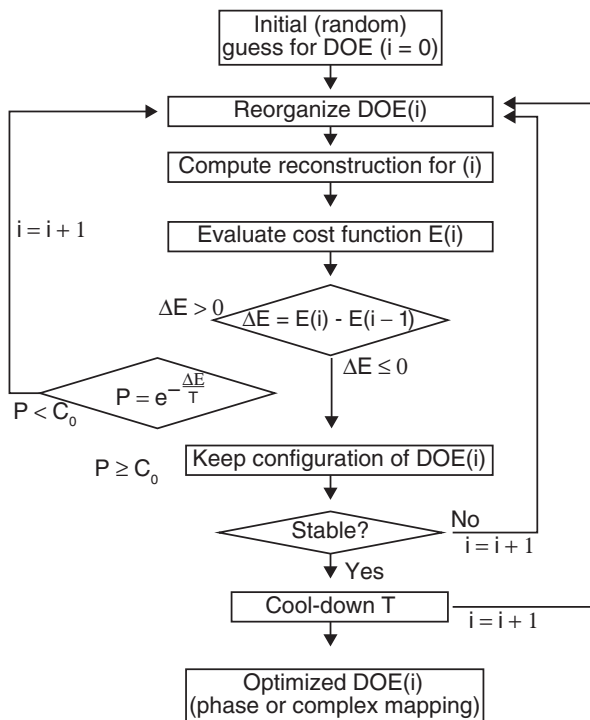
In order to improve the uniformity and SNR in the optical reconstruction, it is useful to run a fast IFTA algorithm and then adjust the phase with a slower DBS algorithm.



Simulated Annealing

The **simulated annealing** (SA) algorithm is a powerful and complex optimization algorithm that, unlike the DBS algorithm (see previous page), can prevent the cost function from being trapped in local minima, especially when this cost function is a linear combination of several criteria. The annealing of the temperature can be set to be fast or slow, depending on the complexity of the cost function to reduce.

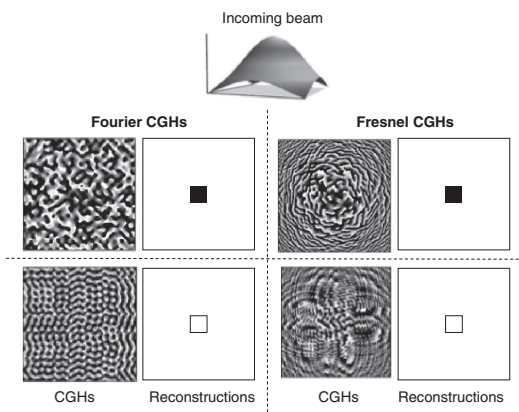
Such an annealing algorithm can be a good addition to an early IFTA optimization task, which would take care of the efficiency at first and then fine-tune the other criteria.



Beam-Shaping CGHs (Numeric)

A typical **beam-shaping CGH**, or top-hat generator, converts a Gaussian incoming field into a uniform-intensity beam profile with a square section in the far field and can be designed by any of the previously described iterative algorithms.

The following figure shows a few such beam shapers transforming an incoming Gaussian beam profile into either a full uniform square (top) or into uniform-edge lines of a square (bottom), for either far-field (left) or near-field operation (right).



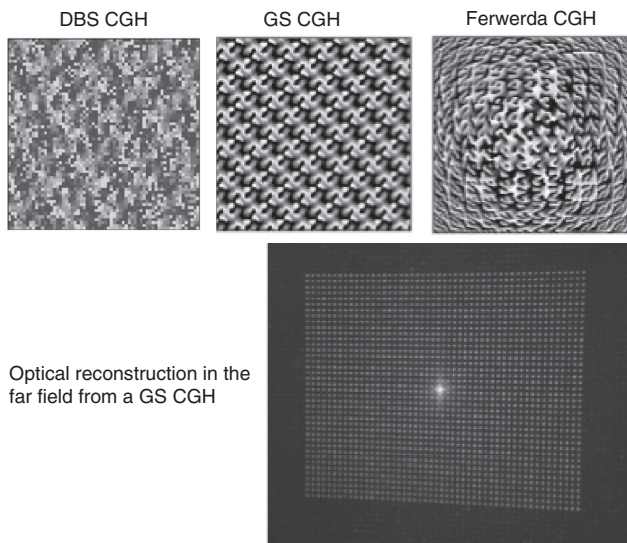
In the case of near-field operation, the beam shaper would be a lens element focusing the desired reconstruction at a unique position after the element. The square edge shapers can be used for laser material processing (such as cutting or welding), whereas the full square shapers can be used as traditional top-hat beam shapers (illumination engines, sensors, etc.).

Although diffractive beam shapers may provide virtually any beam-pattern shaping, the uniformity is usually poor for far-field shapers used with lasers due to pixelation arising from Fourier plane sampling and speckle.

Spot Array Generators

Spot array generators and multifocus lenses can be designed by any of the previously described iterative optimization algorithms. The former produce regular or irregular arrays of spots on the sampling grid of the reconstruction window, and the latter produce similar spot arrangements in the near field (focused spots).

The following figure depicts spot array generators (left and center) and multifocus lenses (right) designed by DBS, GS, and Ferwerda algorithms (a Ferwerda algorithm is basically an IFTA working in the near field).

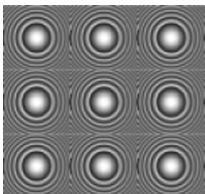
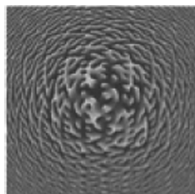
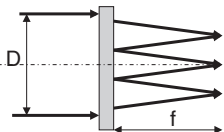
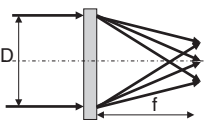


A spot array generator (Fourier element) can be easily distinguished from a multifocus lens (Fresnel element) by the typical periodic structures in such elements. Previously described effects of sampling rates and speckle are not an issue in such elements.

A multifocus lens can also modulate the focus of each spot rather than the off-axis of each spot, or it can generate a combination of off-axis and focus distance for each spot by using an adapted iterative algorithm.

MLAs and Multifocus Lenses

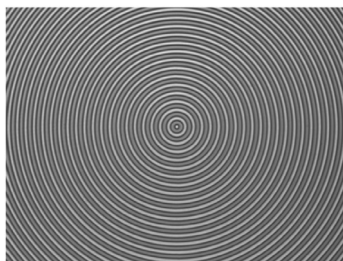
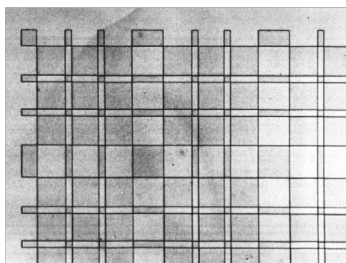
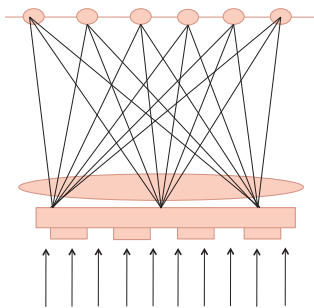
The optical reconstructions from an **MLA** or a **multifocus lens** might be similar, but the optical characteristics can be very different. This table summarizes the NA, f number, and depth of focus for a diffractive MLA and a multifocus Fresnel diffractive lens. Whereas MLAs can be fabricated as refractive or reflective elements (operating over a very large spectrum), fabricating a Fresnel multifocus lens as a refractive or reflective element is quasi-impossible due to the complexity of the surface profile.

	Lens Array	Fresnel CGH
Physical layout		
Lateral view		
Design method	Analytic	Numeric
NA of DOE lens	$NA_A = \sin(\alpha_{\max}) = \frac{\lambda}{\Lambda_{\min}}$ $= \sin\left(\arctan\left(\frac{D/p}{2f}\right)\right) = \frac{D}{2pf}$	$NA_N = \sin(\alpha_{\max}) = \frac{\lambda}{\Lambda_{\min}}$ $= \sin\left(\arctan\left(\frac{D}{2f}\right)\right) = \frac{D}{2pf}$
f -number of DOE lens	$f\#_A = \frac{Nf}{D}$	$f\#_N = \frac{f}{D}$
Depth of focus of DOE lens	$DOF_A = 2\lambda f\#_A^2$	$DOF_N = 2\lambda f\#_N^2$

In many cases, multiple imaging is required by sharing (or dividing) the NA (such as in MLA), and in other cases multiple imaging over the original NA is required (such as in multifocus, Fresnel diffractive lenses).

Dammann Gratings

Dammann gratings are binary phase or amplitude diffractives designed to generate arrays of equal-intensity point sources in the far field. Hans Dammann presented the first binary phase grating to produce equal magnitude orders in the Fourier plane. The figure here shows a 1 to 6 Dammann far-field beam splitter operating in 1D. The far field is produced at the focal length of a conventional Fourier transform lens. Dammann gratings can also be designed as 2D beam splitters (used in optical computing, structured illumination, and even laser material processing). Circular Dammann gratings have also been investigated, yielding circular shape arrays (see below).

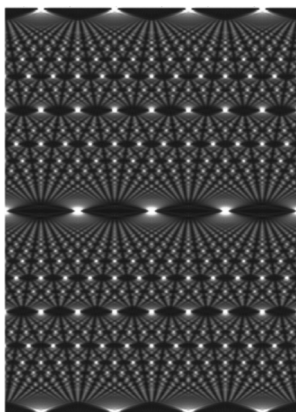


Dammann gratings are analog elements, as opposed to CGHs, which are numeric elements. Both can be used for beam splitting (fan-out elements), but a CGH may implement more complex (nonsymmetric and nonuniform) fan-out architectures. They can also be designed to operate directly in the near field (such as Fresnel diffractives, as opposed to Fourier diffractives). Near-field Dammann gratings have been recently applied to the development of lensless cameras by using a combination of the Talbot self-imaging effect and spatially multiplexed near-field Dammann gratings (as with MLAs).

Talbot Self-Imaging

The **Talbot effect** is a near-field diffraction effect, first observed in 1836 by Henry Fox Talbot. When a plane wave is incident upon a periodic diffraction grating of period Δ , the aerial image of the grating is repeated at regular distances from the grating plane. The regular distance is called the Talbot length, and the repeated images are called self-images or Talbot images.

A self-image occurs at half of the Talbot length, but it is phase-shifted by half a period. At smaller regular fractions of the Talbot length, sub-images can also be observed. At one-fourth of the Talbot length, the self-image appears with half of the period of the grating. At one-eighth of the Talbot length, the period and size of the images is halved again, creating a fractal pattern of sub-images with ever-decreasing size (Talbot carpet).



Lord Rayleigh showed that the Talbot effect was a natural consequence of Fresnel diffraction and that the Talbot length Z_T can be found by the following formula:

$$Z_T = \frac{2\Delta^2}{\lambda}$$

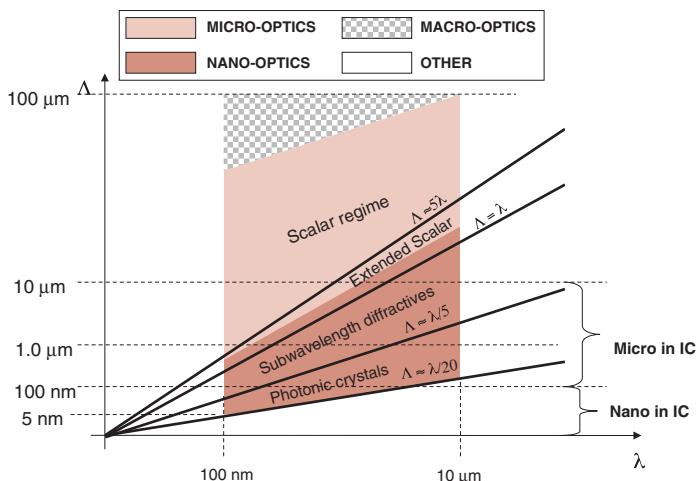
When the wavelength is close to the period, Rayleigh showed that this equation should be used:

$$Z_T = \frac{\lambda}{1 - \sqrt{1 - \left(\frac{\lambda}{\Delta}\right)^2}}$$

In micro-optics fabrication, Talbot self-imaging may be used in proximity lithography (e.g., mask aligner) to form aerial images on the wafer that have periods half of the size of the periods actually printed on the mask. They may also be used in conjunction with physical gratings located at the exact Talbot distance to produce moiré effects for lateral alignment (or front/back wafer alignment).

Subwavelength Optics

Subwavelength micro-optics are micro-optical elements with structures that are smaller than the reconstruction wavelength. Because the reconstruction wavelength can be quite large (a CO₂ laser at 10.6 μm) or quite small (an EUV source at 13 nm), such optical elements cannot be classified solely by the absolute size of the structures constituting them but rather as the ratio between the reconstruction wavelength and their smallest structures (unlike micro-electronics, where only the absolute size of the smallest feature is considered: the critical dimension). The following figure classifies macro-, micro-, and nano-optics along that ratio.

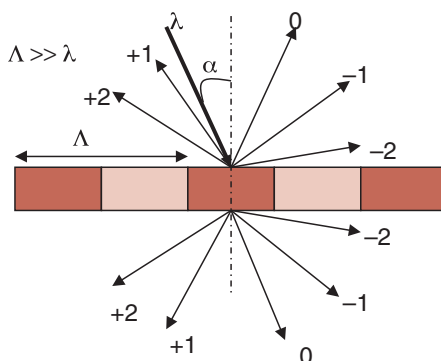


When the ratio between the wavelength and period becomes smaller than unity, major changes occur in the way the structures interact with the incoming light. Diffraction in the fundamental mode (and in higher modes) is no longer present. However, this is only valid for wavelength-to-period ratios, not wavelength-to-smallest-feature ratios (CD). The CD can be much smaller than the wavelength and still produce strong diffraction in the fundamental orders as long as the period is larger than the wavelength.

Large- and Small-Period Gratings

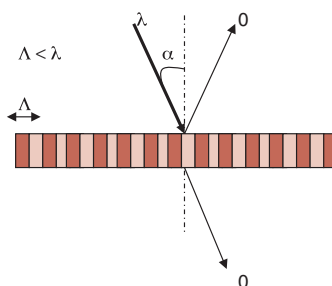
Large-period gratings (periods much larger than the reconstruction wavelength) are considered to operate in the scalar regime of diffraction and may produce multiple diffraction orders of energy (or efficiency) that can be accurately predicted by scalar theory. Both means of polarizing light diffract in a very similar way.

Multiorder grating



Small-period gratings (equal to or smaller than the reconstruction wavelength) are nondiffracting gratings because all higher orders are nonpropagating and therefore produce only a zero order, which can happen in both reflection or transmission modes.

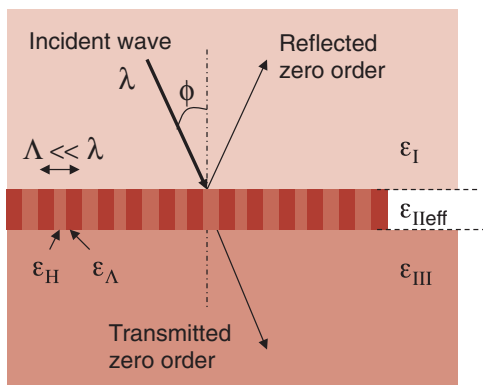
Subwavelength grating



Such gratings are also called **zero-order gratings** and have very interesting polarization characteristics.

Zero-Order Gratings

A **zero-order grating** is a nondiffracting grating that produces only a reflective and transmissive zero order, which is very dependent on the polarization.



The condition for having a zero-order grating operation is

$$\frac{\Lambda}{\lambda} < \frac{1}{\max\{\sqrt{\epsilon_I}, \sqrt{\epsilon_{III}}\} + \sqrt{\epsilon_{II}} \sin \phi_{\max}}$$

where ϵ_I , ϵ_{II} , and ϵ_{III} are the permittivity of the upper medium, the effective grating modulation medium, and the lower medium, respectively; ϕ is the incidence angle on the grating; Δ is the period of the grating; and λ is the reconstruction wavelength.

An obvious application of such a grating is polarization beam splitting: one polarization direction is reflected, the other is transmitted, and both are zero-order diffraction beams.

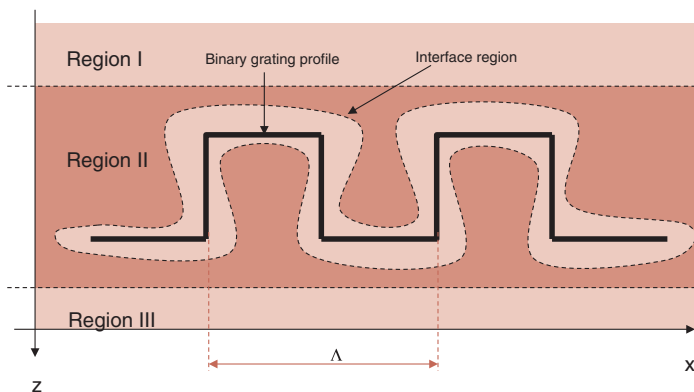
Although the periods of such gratings might be very small (and thus difficult to fabricate), it is very unlikely that multilevel fabrication is needed because it is intended for larger-period gratings to boost efficiency.

Rigorous EM Diffraction Theory

When the ratio between the reconstruction wavelength and the smallest period constituting the optical element approaches unity and below, scalar theory begins to fail, and more-rigorous vector diffraction theories must be applied, solving Maxwell's set of time-harmonic equations:

$$\begin{cases} \text{curl}(\vec{E}) = -\mu \frac{\partial \vec{H}}{\partial t} \\ \text{curl}(\vec{H}) = \epsilon \frac{\partial \vec{E}}{\partial t} \\ \text{div}(\epsilon \vec{E}) = 0 \\ \text{div}(\mu \vec{H}) = 0 \end{cases}$$

The subwavelength structure is no longer considered an infinitely thin surface. The interface boundaries must be precisely defined, as below, for a simple binary grating.



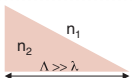
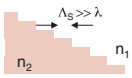
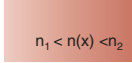
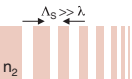
Three regions are considered in this simple example: the first is the region outside the grating (air), the second is the surface-modulation region, and the third is the substrate.

Various techniques can be applied to model the diffraction efficiency of such a grating by solving Maxwell's equations analytically (coupled-wave theories) or numerically (FDTD, etc.).

Effective Medium Theory (EMT)

When the minimum period becomes smaller than the reconstruction wavelength, the incoming light does not reach the structures but rather “sees” an analog effective index modulation that is produced by the subwavelength (usually binary) structures.

The following table shows an example of a blazed grating profile (local phase ramp) that is physically implemented by various techniques (analog or multilevel surface ramp, real index modulation, and effective index ramp through binary subwavelength structures).

Physical aspect	Comments
	A) Continuous profiles
	B) Multi-level approximation -> multi-mask process
	C) Effective medium approach
	D) Single-step planar (binary) technology

In this example, the smooth phase profile producing the blaze is implemented as a **pulsewidth modulation** (PWM) along each period of the grating. The structures are fabricated over a regular grid, and each structure is slightly smaller, producing a linearly varying sub-grating duty cycle. Note that one can also use a **pulse-density-modulation** (PDM) scheme or even an error-diffusion algorithm, such as the one used in greyscale laser printing.

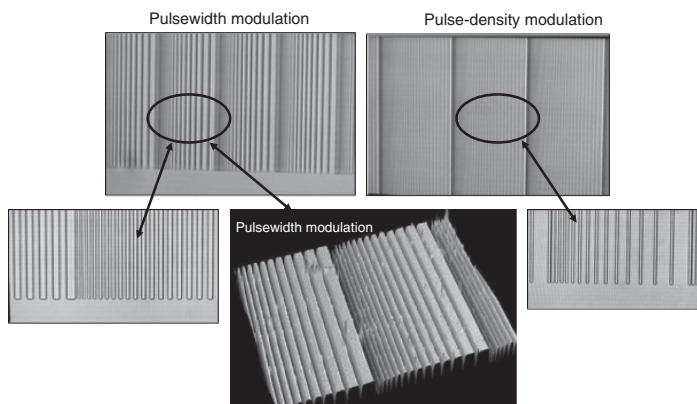
Because there is only a single etch depth for EMT structures, a single lithography and etching step is required. However, the resulting element behaves as a multilevel or quasi-analog surface-relief element. This is thus an efficient fabrication technique when compared to systematic errors (alignment, etch) that occur in multilevel lithography.

EMT Encoding Schemes

In **EMT** elements, an analog phase modulation is produced by subwavelength organization of binary structures, whereas in scalar theory, analog phase modulation is produced by multilevel microstructures (e.g., Fresnel diffractive lenses) or index variation (e.g., volume holographic gratings).

Although the structures are subwavelength and thus defined as rigorous diffraction, the resulting synthetic phase profile can be defined as scalar diffraction (the resulting periods are larger or much larger than the reconstruction wavelength).

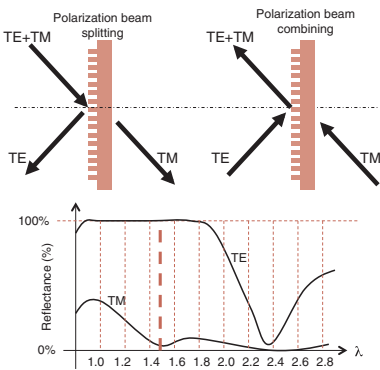
Various means of organizing subwavelength binary structures have been used in the industry to produce highly efficient EMT elements, such as gratings and lenses. The following are examples of blazed grating profiles produced by using either a PDM or PWM scheme.



Note that this technique is very similar to the binary halftone coding used to produce greyscale images (see Halftone Greyscale Lithography). In both analog-phase and amplitude-modulation synthesis through PDM or PWM, the aim is to produce a synthetic analog modulation that is below the resolution of the system (optical imaging resolution for the amplitude and optical diffraction for the phase).

Form Birefringence

Natural birefringence is often a nuisance in optics, but it can also be a desirable tool for the optical engineer. Because EMT is very polarizing, it is thus possible to design and fabricate synthetic birefringent materials by adequately microstructuring an interface. The following example shows polarizing beam splitter/combiner made of a sub-wavelength grating. Such gratings are usually replicated by nano-imprinting and subsequent dry RIE etching.



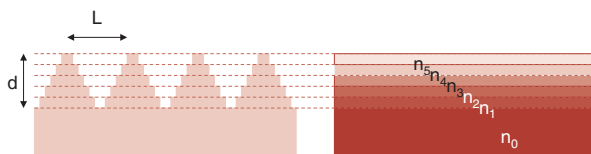
Form Birefringence			
Material	λ_0 (nm)	n	$\Delta n = n_E n_0$
Fused silica	630	1.46	−0.084
Photoresist	630	1.64	−0.151
ZnSe	1.5	2.46	−0.568
GaAs	1.0	3.40	−1.149
Si	1.0	3.50	−1.214
Ge	10.0	4.00	−1.543

Natural Birefringence			
Material	n_0	n_e	$\Delta n = n_E n_0$
Quartz	1.544	1.553	0.009
Rutile	2.616	2.903	0.287
ADP	1.522	1.478	−0.044
KDP	1.507	1.467	−0.040
Calcite	1.658	1.486	−0.172
Proustite	3.019	2.739	−0.280

Antireflection Microstructures

An **antireflection surface** (ARS) is usually made of successive thin films that have slightly varying indexes such that the reflections at each interface are minimized (MgF_2 , etc.).

Because EMT can produce effective indexes as seen by the light, it is thus possible to produce AR structures in the material that act as thin-film AR coatings.



By fabricating subwavelength pyramidal structures, a slightly varying effective index for the incoming light can be produced exactly as if a real stack of thin films were coated on the substrate.

The main advantage of a structured AR surface is that it is part of the same material and cannot be de-laminated. Such structures can be patterned by nano-imprint and transferred via dry RIE etching in the substrate.

The duty cycle of each layer of the 2D pyramid grating slowly increases, going from the top of the pyramid down to the valleys, and is expressed as follows (the current layer index is 2, located between 1 and 3):

$$n_{\text{eff}} = \begin{cases} n_0^{(0)} = \sqrt{n_1^2(1-c) + n_3^2c} & \text{(TE)} \\ n_E^{(0)} = 1/\sqrt{(1-c)/n_1^2 + c/n_3^2} & \text{(TM)} \end{cases}$$

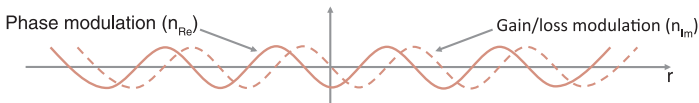
where the optimal grating duty cycles are

$$c = \begin{cases} n_1/(n_1 + n_3) & \text{(TE)} \\ n_3/(n_1 + n_3) & \text{(TM)} \end{cases}$$

Note that a binary grating can already reduce the reflection coefficient at a glass interface by producing an effective intermediate layer between the glass and air, with an effective index between both.

Parity-Time Symmetry in Optics

The concept of **parity-time** (PT) symmetry, borrowed from quantum field theory, has been applied to the design of novel optical structures. In optics, PT symmetry requires that the complex refractive index $n(\vec{r}) = n_{\text{Re}}(\vec{r}) + in_{\text{Im}}(\vec{r})$ obeys the condition $n(\vec{r}) = n^*(-\vec{r})$; in other words, the real index profile (phase) must be an even function of position, whereas the gain/loss must be odd, as shown below.



Long before the PT-symmetry concept was introduced, Poladian theoretically showed that if the imaginary component of the refractive index in a Bragg grating is periodically modulated, the conventional symmetry in the contra-propagating mode interaction in these devices may be altered. This leads to an asymmetrical behavior in the mode-coupling process; specifically, the Bragg grating can induce coupling from the forward-propagating mode into the backward-propagating modes when the light is launched from one end of the grating, but the same is not true when the light is launched from the opposite end.

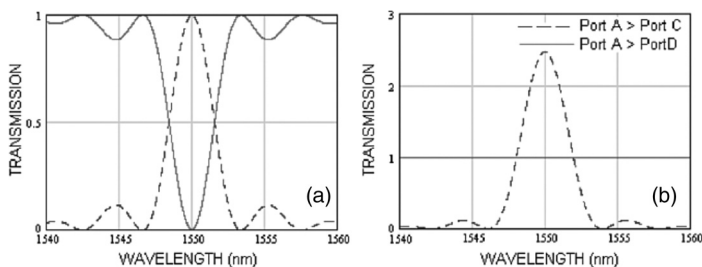
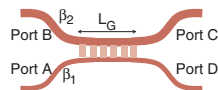
PT-symmetric materials can produce interesting and unusual optical functionalities, such as double refraction and “nonreciprocal” diffraction, or unidirectional Bloch oscillations. In particular, Poladian predicted unidirectional diffraction of reflective-waveguide Bragg gratings when they combine balanced, periodic modulations of the refractive index and loss/gain. This zero reflectivity is combined with an ideal signal transmission thanks to the grating exhibiting no changes to its phase or amplitude, thus forming a unidirectional invisible medium. Probing the same grating from the opposite side produces very strong back diffraction combined again with perfect signal-integrity transmission. The concept of unidirectional diffraction has been experimentally demonstrated.

PT Grating-Assisted Couplers

A **grating-assisted coupler** consists of two single-mode asynchronous waveguides (the propagation constants of both waveguides are different) that interact over a distance L_G via a complex grating coupler that has both index and gain/loss modulations. The complex grating introduces a perturbation to the complex refractive index, as follows:

$$\Delta n = \Delta n_1 \cos(kz) - i\Delta\alpha \sin(kz)$$

Results for traditional gratings (phase modulation only, left side) and for PT-symmetry gratings (phase and gain/loss modulations shifted by a quarter period, right side) are shown below.



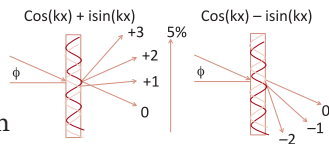
The most noticeable distinction between the two structures (left: conventional coupler; right: PT coupler) is that the PT-symmetry design allows coupling the signal into the neighboring waveguide without depletion. Furthermore, it is worth noting that the power transferred from Port A and Port C is wavelength-dependent. At the same time, the transmission in the excited channel between Port A and Port D remains unaffected by the grating. The power conservation law is not violated because the complex grating is an active structure, and power is supplied to maintain optical gain.

Nonreciprocal Free-Space PT Gratings

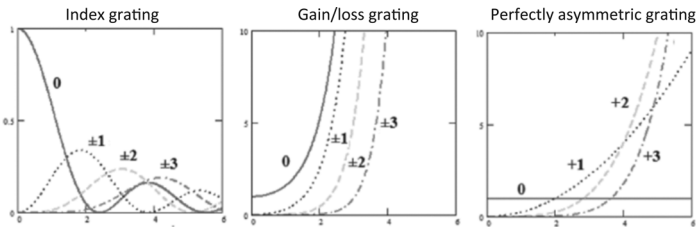
Diffraction asymmetry (also called nonreciprocity or unidirectionality) is achieved by a phase shift between the index and the gain/loss in waveguide gratings. The same effect can be observed in a free-space log period grating (Raman–Nhat regime). The grating is assumed here to be composed of the dielectric constant modulation and modulation of the gain/loss with the same periods but shifted by a quarter period $\Lambda/4$ in either direction:

$$n(x) = n_0 + n_1 \cos(Kx)$$

$$\alpha(x) = \alpha_0 \pm \alpha_1 \sin(Kx)$$



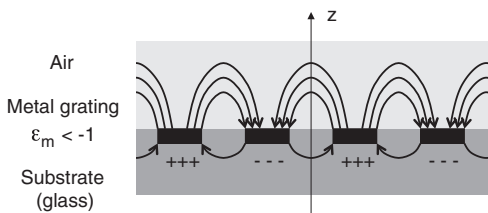
When $n_1 = \alpha_1$, only diffraction into nonnegative or nonpositive orders occurs, depending on the shift between the gratings (see below: diffraction efficiencies in the zero and higher orders for index, gain/loss, and PT gratings as a function of the grating strength).



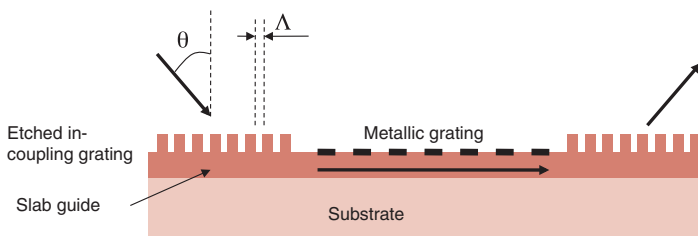
The results for PT symmetric gratings are very different from traditional index modulation gratings. In addition to full diffraction asymmetry, the incident wave is unaffected (light in the zero order = solid horizontal line). The diffraction efficiency in the first order dominates for small values of the grating strength before being diffracted into higher orders. This was obtained for zero average loss/gain ($\alpha_0 = 0$); however, α_0 can be modulated and used to design particular diffraction patterns of the perfectly asymmetric gratings. This amplification produces a very convenient tuning mechanism.

Surface Plasmonics

Surface plasmon polaritrons (SPPs) are collective oscillations of free electrons at the surface between a metal and a dielectric material. Such an oscillation occurs at resonant frequencies. The SPPs are confined to the interface between materials with dielectric constants of opposite signs (e.g., at a metal/glass surface).



The surface confinement of the SPP field to the interface makes it possible to overcome the diffraction limit encountered in classical optics. Such a patterned metallic surface can be excited by an evanescent wave and coupled to the waveguide through an optical coupling mechanism (prism, hologram, grating, etc.).



The coupled SPP propagation vector k_{SPP} can thus be written as

$$k_{\text{SPP}} = \frac{2\pi}{\lambda} \sin \theta + n \frac{2\pi}{\Lambda}$$

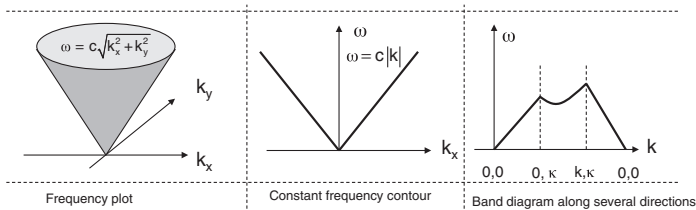
Nanoscale holes etched into thin metallic films can induce SPP effects and act as point source arrays. This is a unique feature that can be used to implement various optical functionalities in planar waveguides, lensing, grating effects, or even beam splitting.

Photonic Crystals

The term “**photonic crystal**” (PC) is a recent creation, but it is based on predictions formulated in 1987 by Eli Yablonovitch at Bell Communications Research (NJ) and Sajeev John at the University of Toronto. Photonic crystals are periodic nano-structures that have singularity geometries wherein light may propagate. The light propagates in a PC similar to the wave function of electrons in crystals.

Another way to describe the light behavior in such structures is to use the density of optical modes compared with the density of modes for electrons in solids. The PC lattice $U_k(r)$ produces a periodic dielectric distribution, which can be written as $U_k(r + a) = U_k(r)$. Bragg scattering through this periodic structure provides strong and coherent reflections at particular wavelengths, and it is the origin of the photonic bandgap. Traditional volume holograms (such as fiber Bragg gratings or 2D holograms) can therefore also be considered as partial bandgap PCs.

Light can be localized in a PC at defects (singularities), which are due to multiple scattering (interferences). The band structure, or dispersion relation, defines the relation between the frequency ω and the wave vector $\omega = c|k|$.



A plane wave will only scatter to plane waves whose wave vectors differ by a reciprocal lattice vector. The reflection is maximal if the Bragg condition is satisfied (as in a traditional volume hologram):

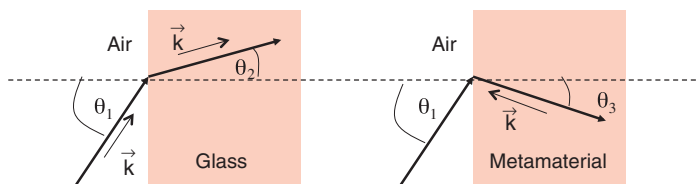
$$e^{2ika} = 1 \Leftrightarrow k = \pi/\Delta$$

Photonic crystals can assume various geometries (1D, 2D, and 3D structures, and PC “holey” fiber/waveguide).

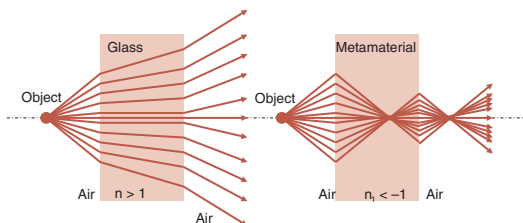
Metamaterials

Richard Feynman predicted in the 1960s that “there is plenty of space at the bottom” (referring to subwavelength structures and photonic crystals). It could also be said that “there is plenty of space below the bottom” when considering **metamaterials**. A metamaterial is a composite or structured material that exhibits properties not found in naturally occurring materials. Left-handed (negative refractive index) materials have electromagnetic properties that are distinct from any known material and are thus metamaterials.

The metallic nanostructures composing a metamaterial have an active effect on the incident light, rather than the passive effect they have in photonic crystals, diffractives, and holograms. The oscillation of the field created by the light interacting with the material changes how the light propagates in that same material. Snell's law is thus reversed in left-handed materials.



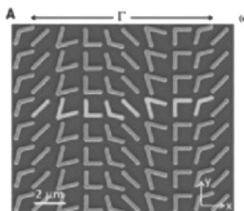
Therefore, the ray paths can be drawn at the interface of conventional materials and at the interface of conventional and metamaterials (left-handed).



Perfectly flat lenses and optical cloaks (using SPPs) are among the notable implementations of metamaterials.

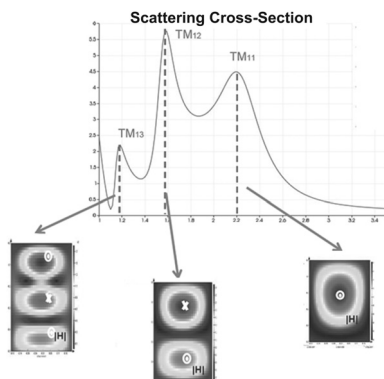
Metasurfaces and Resonant Antennas

Metamaterials remove dependence on the propagation effect by introducing abrupt changes of optical properties. Abrupt and controllable changes of optical properties are achieved by engineering the interaction between light and optical scatterers (or optical antennas), which can take a variety of forms, such as metallic or dielectric micro-/nanoparticles and apertures opened in metallic films.



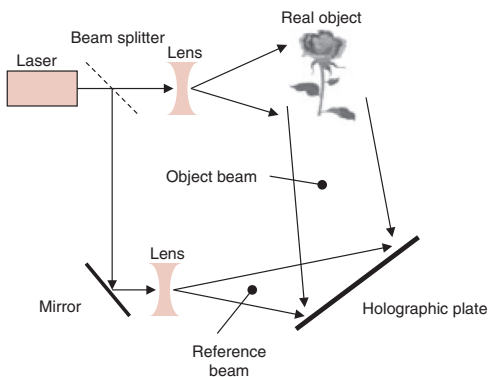
Arrays of antennas are used with subwavelength separation and spatially varying geometric parameters (e.g., antenna shape, size, orientation) to form a spatially varying optical response, thus shaping incoming optical wavefronts into phase profiles designed at will. Such an optical wavefront can be engineered through the nano-antennas to produce an effective lens, prism, beam shaper, beam splitter, DOE, or even CGH or hologram.

Two features distinguish such **metasurfaces** from conventional optical components. First, wavefront shaping is accomplished within a distance much smaller than the wavelength from the interface. Second, metasurfaces based on optical scatterers enable engineering of the spatial distribution of the amplitude, phase, and polarization, all with sub-wavelength resolution. Multiple wavelength-resonance nano-antennas can be used to yield broadband elements; they can then be used to produce arbitrary wavefront surfaces, such as dispersionless flat lenses or color-triggered functionality.

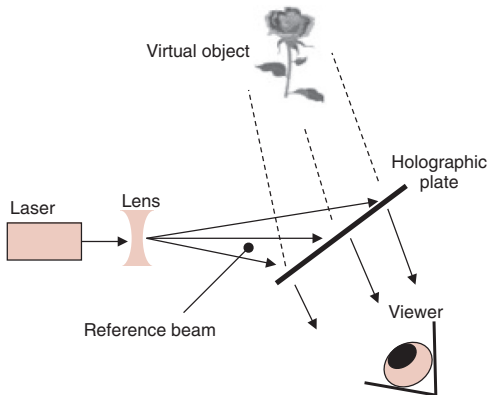


The Holographic Process

Conventional **recording** is the analog process of recording an interference pattern, whether it is an index profile (volume holograms using emulsions, such as silver halide, dichromated gelatin, or photopolymers) or a surface-relief profile (photoresist). The interference pattern is created by an object beam and a reference beam; both are coherent and from the same source. The object can be real or a display (light valve), or it can be another analog hologram (or CGH).



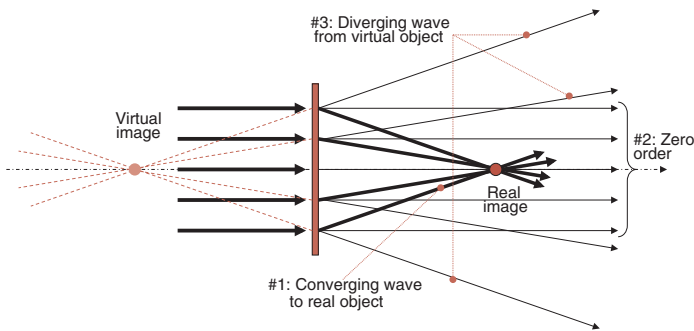
Playback of the hologram is done by illuminating the hologram with the same reference beam used for the recording. This triggers the fundamental Bragg mode and produces the object wavefront by diffraction.



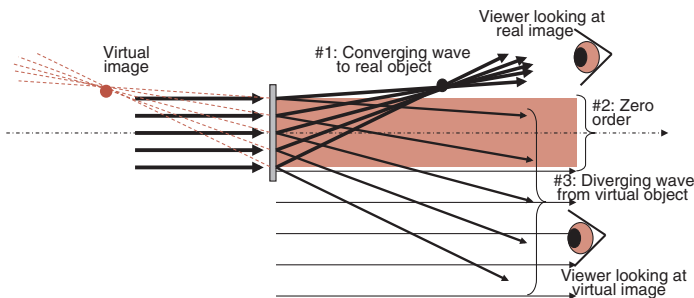
The hologram can also be illuminated with other colors and/or under other angles and still produce a full reconstruction, provided that such a combination of spectral and angular bandwidth satisfies at least one of the Bragg conditions of that hologram.

Gabor and Leith Holograms

Denis Gabor received the Nobel Prize in 1948 for inventing the principle of holographic recording and playback. By using an on-axis reference wave, his recording technique produced on-axis holograms in which multiple orders are superimposed, as shown below (this figure shows the reconstruction of a single spot in the near field, as in an on-axis Fresnel holographic lens). This technique was thus adapted only to transparent objects, such as phase objects.



Emmett Leith and **Juris Upatnieks** later proposed an off-axis holographic recording technique (using an off-axis reference wave) that spatially separates the diffraction orders one from each other as well as from the zero order. Most current holograms are recorded this way.



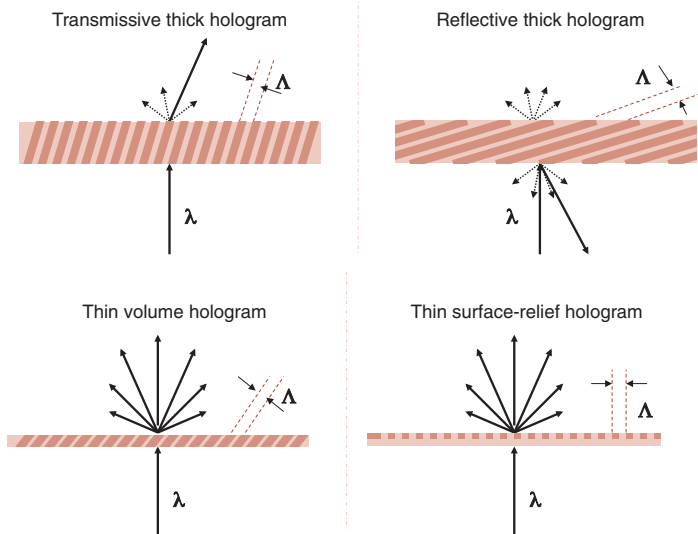
Thin and Thick Holograms

The notion of “thin” and “thick” holograms is related to the physical thickness of the holographic emulsion. A **thick hologram** may incorporate the full Bragg selectivity (both angular and spectral), whereas a **thin hologram** would act more like a surface-relief diffractive element, producing multiple diffraction orders and being unable to work in reflection mode without a proper reflective coating.

The quality factor Q of a hologram is expressed as follows:

$$Q = \frac{2\pi\lambda d}{n\Delta^2 \cos \alpha}$$

A hologram is considered thin when $Q \leq 1$, thick when $Q \geq 10$, and in an intermediate regime in between.



Thin holograms operate in the Raman-Nath regime (similar to the scalar regime for surface-relief diffractives), whereas thick holograms operate in the Bragg regime. However, it has been shown that even for thin holograms, for a weak index modulation, there might only be a single order diffracting. When the index modulation is stronger, higher orders might be diffracted, such as in surface-relief holograms (where the index modulation is $n - 1$, with n being the index of the etched material).

Reflection and Transmission Holograms

The recording geometries to produce either a transmission or a reflection hologram are listed below.

Point sources		Optical recording setup	Type	Optical reconstruction setup
s_1	Real		Reflective	
s_2	Real			
s_1	Real		Transmissive	
s_2	Real			
s_1	Real		Transmissive	
s_2	Virtual			
s_1	Virtual		Transmissive	
s_2	Virtual			
s_1	Virtual		Reflective	
s_2	Virtual			

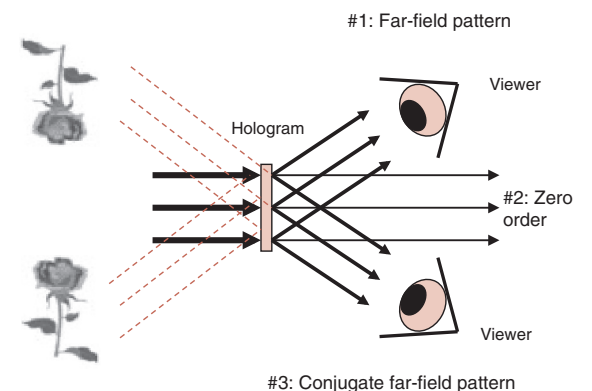
The spectral and angular bandwidth of both reflection or transmission holograms can be modeled with Kogelnik's coupled-wave theory. Kogelnik should be used to determine which hologram thickness and which (Greek capital Delta) n (material index modulation) should be used to achieve the desired efficiency (defining the material before preparing the recording set-up). Although recording holograms with point sources and/or plane waves (such as depicted in this figure) might produce sufficient imaging performance to image such points, it is often helpful to use a CGH to record a more-complex phase map, which would correct aberrations when imaging an extended-size object (real object) or account for using the lens in various off-axis positions. The design and optimization of a CGH phase map is usually done in a traditional optical CAD tool. The phase profile is then etched in a fused silica wafer through optical lithography and dry oxide etching. A CGH can be used to expose a transmissive or reflective hologram.

Note that a reflective hologram might also be transparent to the field, as would a transmissive hologram. Transparent reflection holograms are good candidates to implement HUD or HMD combiners. While silver halide, dichromated gelatin (DCG), or photopolymers can be recorded as either transmissive or reflective holograms, H-PDLC holograms are usually recorded as transmissive elements.

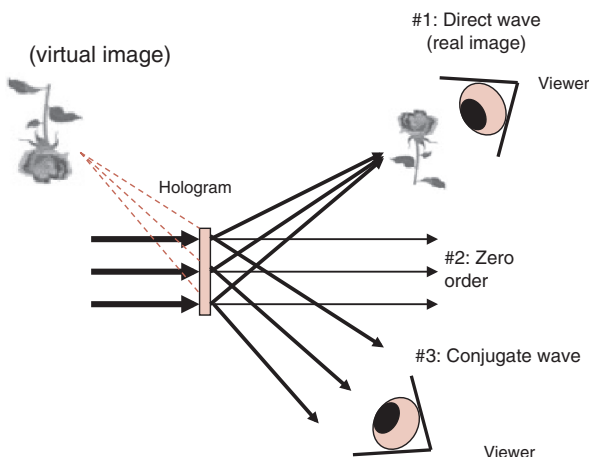
Fraunhofer and Fresnel Holograms

The following figures show the differences between a **Fraunhofer hologram** (far-field pattern reconstruction) and a **Fresnel hologram** (near-field pattern reconstruction). Some holograms can be both types simultaneously, creating a desired pattern in both fields.

Fraunhofer (Fourier) hologram



Fresnel hologram



Holographic Interference

If the object O and reference R beams are produced by the same source, the complex amplitudes for both beams can be written as

$$\begin{cases} R(x, y, z) = r(x, y, z)e^{i\phi(x, y, z)} = A_R e^{ikz} \\ O(x, y, z) = o(x, y, z)e^{i\phi(x, y, z)} = A_0 e^{ikr} \end{cases} \quad \text{where } r = \sqrt{x^2 + y^2 + z^2}$$

Thus, the intensity pattern arising from the **interference** between both beams is expressed as

$$I(x, y) = |O + R|^2 = OO^* + RR^* + OR^* + O^*R$$

The resulting transmittance function T (which is related to the refractive index modulation in a volume holographic emulsion or a surface-relief modulation in a photoresist layer) becomes

$$T = C + \zeta(|O|^2 + O^*R + OR^*)$$

where C is related to the background amplitude, and ζ is a parameter of the holographic and development process (ζ can be a complex number).

When the hologram is illuminated by a beam R' , the reconstructed wavefront assumes the following form:

$$R'T = CR' + \zeta(OO^*R' + O^*RR' + OR^*R')$$

When the hologram is illuminated by the same reference beam R as the one used for the recoding process, the reconstructed wavefront becomes

$$RT = R(C + \zeta OO^*) + \zeta R^2 O^* + \zeta |R|^2 O$$

Note that the intensity term of the object wavefront in the last equation gives rise to the image of the object that was recorded.

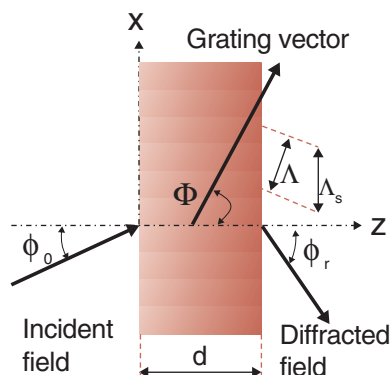
There is usually more than one reference-beam position and/or reference-beam wavelength that satisfies the Bragg condition and produces the same object image. (See Floquet's Theorem and the Bragg Conditions for how the various Bragg conditions can be calculated by Floquet's theorem.)

The Grating Vector

A **Bragg grating** (or, more generally, a Bragg hologram) is a volume hologram that has been recorded as an index-modulation transmittance function in an emulsion, such as silver halides, DCG, photopolymers, H-PDLC, or even photorefractives.

Although a surface-relief grating can also be a true volume Bragg grating, this is usually difficult to achieve because of the complexity of fabricating tilted, high-aspect-ratio structures.

Consider the following grating geometry and illumination, where α is the incidence angle, Φ is the diffracted angle, Λ_s is the projected period normal to the surface, and Λ is the real period of the grating.



The **grating vector** is then defined as

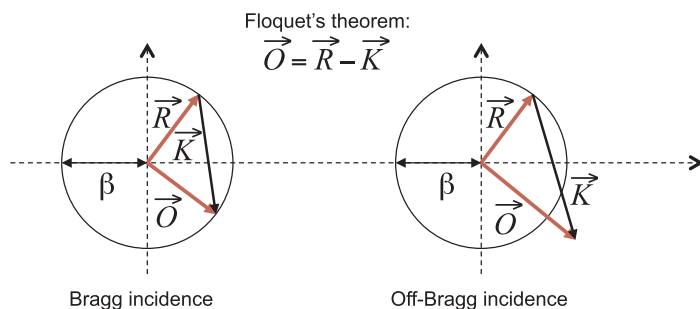
$$\begin{cases} \vec{K} = K(\cos(\Phi)\vec{z} + \sin(\Phi)\vec{x}) \\ K = \frac{2\pi}{\Lambda} \\ n(x, z) = n_0 + \Delta n(x, z) \end{cases}$$

The grating-fringe slant angle, the real period, and the projected surface period can be expressed as

$$\begin{cases} \Phi = \pi/2 + (\theta_r - \theta_0)/2 \\ \Lambda = \lambda_0 / (2n_0 |\cos(\Phi - \theta_r)|) \\ \Lambda_s = \Lambda / \sin(\Phi) \end{cases}$$

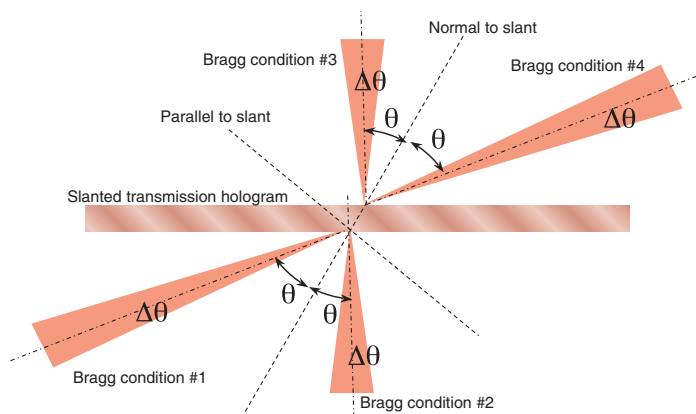
Floquet's Theorem and the Bragg Conditions

The **Bragg condition** sets the reconstruction geometry yielding maximum efficiency. **Floquet's theorem** is expressed as a function of the grating vector \vec{K} , where \vec{O} is the object vector, and \vec{R} is the reference vector.



“On-Bragg” means that the reconstruction wavelength and angle are set to the exact optimal conditions.

The following figure shows the various Bragg conditions for a same volume grating (or volume hologram) with various wavelengths and various incidence angles.



Grating Strength and Detuning Parameter

The parameter ν_s , known as the “**grating strength**,” defines the “strength” of the physical grating as a function of the index modulation (larger is better) and thickness (thicker is better) for *s*-polarization. It is a parameter linked directly to the type of holographic recording material used:

$$\nu_s = \frac{\pi \Delta n d}{\lambda \sqrt{c_r c_s}}$$

where c_s and c_r are the obliquity factors defined as

$$\begin{cases} c_s = \cos(\alpha_i) - \left(\frac{\lambda}{n_0 \Lambda}\right) \cos(\Phi) \\ c_r = \cos(\alpha_i) \end{cases}$$

where α_i is the incidence angle, and Φ is the grating angle. The **detuning parameter** ζ (also called the dephasing parameter) is a function of the recording geometry as well as the illumination geometry and is a useful parameter describing how far one is from a Bragg condition (i.e., “on-Bragg”):

$$\zeta = \left(\frac{Kd}{2c_s}\right) \left(|\cos(\Phi - \alpha_i)| - \frac{K\lambda}{4\pi n_0}\right)$$

where K is the grating vector, d is the emulsion thickness, Φ is the diffraction angle, α_i is the incident angle, and n_0 is the base index of the emulsion.

For example, when the detuning parameter becomes zero, the Bragg condition is present (or on-Bragg). When **Floquet's theorem** is satisfied, the detuning parameter also becomes zero. The theorem can be satisfied for multiple angle/wavelength conditions (multiple Bragg conditions).

The grating strength, obliquity factors, and the detuning factor are key parameters for the Kogelnik two-wave, coupled-mode-theory model for volume holograms (see next page).

Kogelnik Theory for Volume Holograms

Herwig Kogelnik derived a two-wave coupled theory in 1969 at Bell Labs. His model gives the best results in the Bragg incidence angle and for a single diffraction order. Any order other than 0 or 1 in reflection or transmission is considered as evanescent. Kogelnik's model is only valid for sinusoidal index modulations for slanted Bragg planes (ideal for volume holograms). The model is also valid for both transmission- and reflection-mode holograms.

The limitations of Kogelnik's model are that it is only valid for small index variations and near-Bragg incidence. Boundary reflections are also not considered. The diffraction efficiency in the fundamental order in transmission mode is given by

$$\eta_T = \frac{\sin\left(\sqrt{\nu_s^2 + \zeta^2}\right)^2}{1 + \frac{\zeta^2}{\nu_s^2}}$$

where ν_s is the grating strength for s-polarized light, and ζ is the detuning (or dephasing) parameter.

Similarly, the diffraction efficiency in the fundamental order in reflection mode is given by

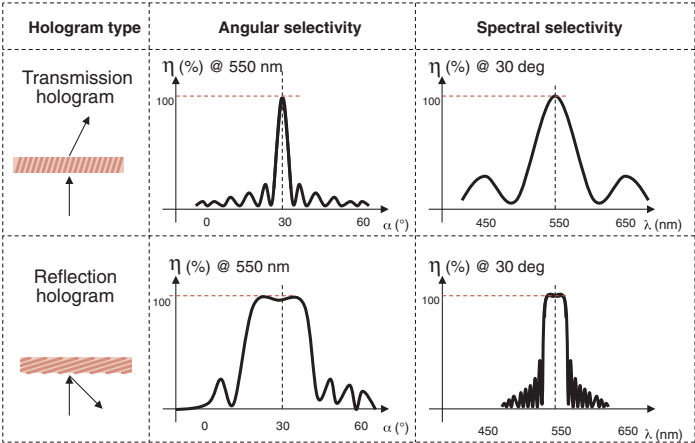
$$\eta_R = \frac{1}{1 + \frac{\left(\frac{\zeta}{\nu_s}\right)^2}{\sinh\left(\sqrt{\nu_s^2 - \zeta^2}\right)^2}}$$

The spectral and angular bandwidths, i.e., range of operation within the Bragg regime, is quite different when considering a reflection or a transmission volume hologram. Kogelnik's theory predicts the diffraction efficiency but does not provide information about the behavior of the hologram as an optical element; if the latter is important (e.g., with an HOE lens), ray tracing or physical-optics propagation might be useful.

Rigorous coupled-wave analysis (RCWA) is also a coupled-wave model, but it gives more-accurate results by considering more modes. Whereas the Kogelnik model provides simple analytical expressions for efficiencies, RCWA usually requires numerical solving algorithms.

Angular and Spectral Bandwidths in Holograms

The **angular** and **spectral bandwidths** of volume holograms can be calculated by Kogelnik’s theory and are summarized in the following table.

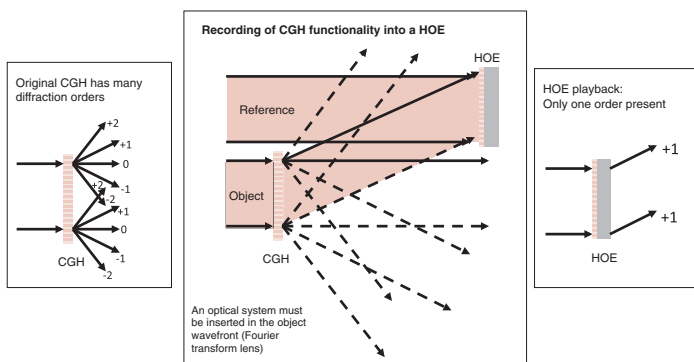


The angular bandwidth of a transmission hologram is typically narrower than that of a reflection version, but its spectral bandwidth is wider, which is why a reflective hologram is preferred for fine spectral filtering.

Two-Step Holographic Recording

In many cases, an optical functionality, such as a lensing or beam-shaping effect, is desired over the classic 3D display recording. It is therefore essential to produce the optical functionality to be recorded in the holographic media. It is often impossible to produce such a functionality from classical optics, but it is possible with diffractive optics that have been designed by a computer and fabricated by lithography (such as CGHs and DOEs).

The following figure shows the recording process of a volume hologram by using a single diffraction order produced by an intermediate digital hologram or CGH.

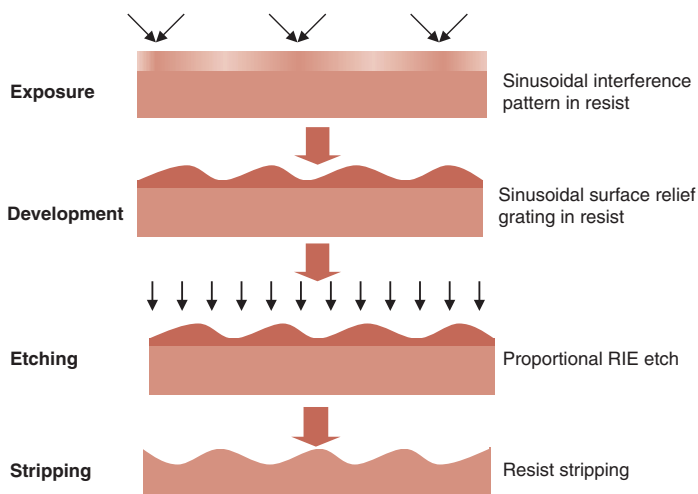


A DOE or CGH is usually fabricated as a binary or multi-level element via microlithography, and because of limited levels and fab errors, they produce a zero order and various higher and/or conjugate orders. In many applications, it is very desirable to have only a single order, in addition to an additional Bragg selectivity. When recording a single diffraction order from a CGH producing a complex optical functionality—such as a spot array generator, a beam shaper, a beam homogenizer, or an aspheric/off-axis lens from a CGH—it is possible to produce a single-order volume hologram with such a functionality.

Surface-Relief Holograms

In many applications, it is desirable to produce a thin hologram with surface-relief modulation rather than index modulation (thick volume hologram), e.g., mass-production constraints of plastic embossing, injection molding, or roll-to-roll embossing. In this case, the Bragg selectivity is usually partially lost, and the element will not function as a reflective hologram (Bragg planes parallel to the substrate).

The following figure shows the exposure process of a **surface-relief hologram** in a photoresist and the subsequent transfer into the underlying substrate via proportional, reactive ion-beam etching.



This is a sinusoidal surface-relief grating (in transmission or in reflection, with a reflective coating). A sinusoidal grating will not produce a single order but rather two conjugates and a zero order with similar efficiencies. Although the holographic exposure always produces a sinusoidal intensity profile, it is possible to etch a binary grating in the substrate by over-developing the resist layer and using a hard etch-stop layer, such as a metal (Cr, Al, etc.) that can be wet etched before RIE.

Holographic Recording Media: Applications

There are two main application categories for holograms:

- art (3D display), using DCG or silver halides, and
- security holograms and HOEs integrated in consumer electronics (such as optical disk readers, optical scanners, and data-storage media) that rely mostly on photopolymers—such as Dupont, Bayer, or DNP materials (for thick reflection or transmission holograms)—and surface-relief elements (for thin holograms), similar to DOEs, embossed in plastic or etched into fused silica after recording into photoresist.

Material	Type	Hologram Type	Application
Photo-resist	Thin resist (+ or −)	Thin (structures normal to substrate surface)	Diffraction optics/lithographic patterning
	SU-8 resist	Slanted structures, replicated by UV casting / nano-imprint	HUD, solar, LCD diffusers, phase masks, etc.
Films	Silver halides	Volume	First-gen holograms
	DCG	Thick volume	High-selectivity applications (optical storage, DWDM)
Photo-polymer	Passive (Dupont)	Thin	Anti-counterfeiting
	PDLC	Volume	Displays, telecom, datacom, storage
Crystals	Photo-refractive	Very thick volume	Various
	AO modules	Volume Bragg grating (Raman–Nath regime)	Beam-intensity modulation and beam steering
Bacteria	Rhodopsin	Thin (surface relief)	Gratings

Holographic Recording Media: Advantages and Drawbacks

Material	Type	Advantages	Drawbacks
Photo-resist	Thin resist (+ or -)	Simple process; resist pattern can be etched by RIE in substrate	Low efficiency due to resist modulation
	SU-8 resist	Bragg planes from air to plastic (highest Δn of 0.5)	Difficult to replicate; uses complex fringe writers
Films	Silver halides	Inexpensive	Thin; low selectivity; low efficiency
	DCG	Inexpensive; strong angular and spectral selectivity	Long-term stability (animal gelatin – pork or chicken)
Photo-polymer	Passive (Dupont)	Mass replication	Low resolution; unavailable outside Dupont
	PDLc	High index; high Δn ; switchable through grey levels; fast	Long-term stability (polarization issues)
Crystals	Photo-refractive	Erasable / rewritable	Expensive; polarization issues
	AO modules	Fast re-configurable grating angle	Only linear gratings; needs piezotransducers
Bacteria	Rhodopsin	High efficiency	Complex formulation

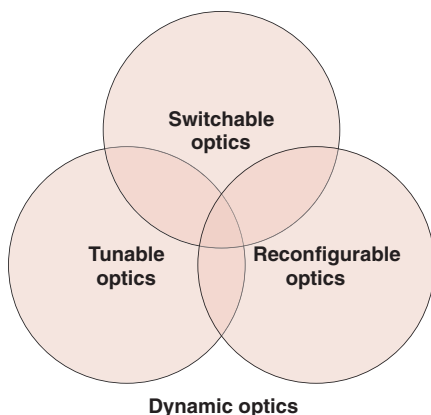
Other holographic materials include switchable H-PDLc materials, which are discussed in the next pages. These holograms can operate in either Bragg or Raman-Nath regimes.

Dynamic Micro-Optics

Dynamic optical elements are versatile components that enable new types of consumer electronics. They can be grouped into three categories:

1. **Switchable optics**, where the optical functionality can be switched from one state (e.g., transparent window) to a specific but unique functionality (a lens or a grating). Only the efficiency can be tuned in a switchable optic.
2. **Tunable optics**, where the optical functionality can be tuned, for example, by varying the focus of a lens, the deflection angle of a prism, the period, and/or the orientation of a grating.
3. **Reconfigurable optics**, where the optical element can be arbitrarily reconfigured to any optical functionality, e.g., from a lens to a grating function: MEMS, phase LCOS, etc.

Such elements were first used in optical telecom applications (tunable gratings), then in digital projection displays (reconfigurable CGHs, despecklers), and more recently in digital imaging products (tunable lenses and computational optics).

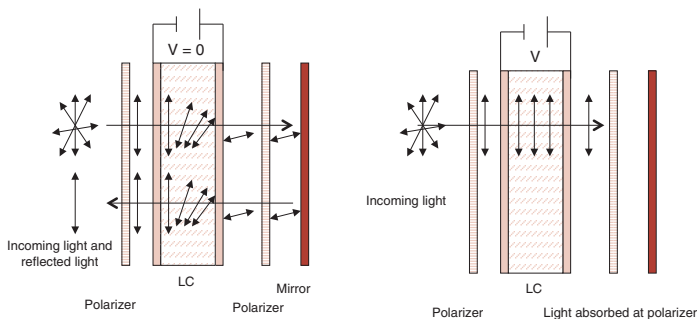


A special case of tunable optics involves **computational optics** in digital imaging systems, in which the desired image is computed rather than directly sensed (see the pages on Aperture and Wavefront Coding and on Light-Field Imaging). Computational optics (or imaging) can be used in plenoptic cameras, single-pixel cameras, or even lensless cameras.

Liquid-Crystal Optics

Liquid crystals, both ferroelectric and twisted-nematic, can be implemented in a variety of microdisplay architectures—from transmission displays (TFT LCD) to reflection displays [LCOS or ferroelectric liquid crystal on silicon (FLCOS)]. Whereas ferroelectric LCs switch within 100 μs , nematic LCs switch within 10 ms. PDLCs can be used for faster switching ($<50 \mu\text{s}$).

The following figure shows a typical LCOS pixel used as an optical valve. Without an analyzer, the LC pixel can be used as a phase modulator, thereby producing phase pixels that can implement phase maps, such as in CGHs or reconfigurable diffractives.



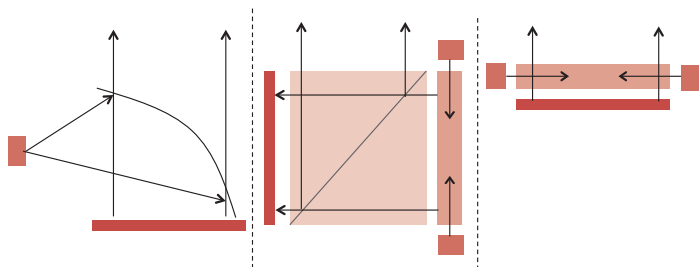
When the (ITO-coated) electrode plates constituting the inner surfaces of the LC plane are not parallel but rather tilted or etched in such a way to produce diffractive or refractive microstructures (in a 1D or 2D array), it is possible to tune the refraction angle or the diffraction efficiency by modulating the effective index of the LC material. For example, if the LC material is incorporated in a prism array structure, an analog beam steerer can be built, the deflection angle of which is a function of the index change.

The effective index of a PDLC material is not a bulk index modulation but rather an effective index produced by a subwavelength (nondiffracting) grating (see Effective Medium Theory).

Liquid-Crystal Microdisplays

Liquid-crystal microdisplays are currently the preferred microdisplay technology used in compact devices such as pico-projectors or HMDs. Transmission-mode TFT microdisplays (Kopin) and reflection-mode LCOS (or FLCOS) displays (Microvision, Himax, etc.) can be made thin, which suits applications where space is limited. However, the efficiency of such microdisplays is usually low (2–4%). They are both polarized displays and can be used either in color sequence mode (RGB LEDs) or with color filters and a single white LED. Although color sequence may produce color breakup when the display is moving in front of the eye (e.g., HMDs), the efficiency is higher due to the absence of color filters.

Backlight illumination engines can be used for TFT LC microdisplays (using BEF/DBEF and diffuser sheets), and **polarization beamsplitter** (PBS) cubes can be used to illuminate LCOS displays. Novel, thin frontlight (as opposed to traditional backlight) illumination engines can also be used in thin-form-factor LCOS displays.



The left-most figure uses a curved laminar PBS film that simultaneously serves as a condenser lens and a broadband (and broad-angle) PBS. The middle figure is the standard PBS-cube–LCOS version with a LED backlight on the right side. The right-most figure is the more-compact frontlight illumination architecture, which uses a transparent edge-coupled LED extractor suitable for small-footprint applications. Frontlight extractors are more complex than their backlight counterparts and have their own issues (uniformity, efficiency, ghosts, etc.).

OLED Microdisplays

An **organic light-emitting diode** (OLED) is an LED in which the emissive electroluminescent layer is an organic film that emits light in response to an electric current. This layer of organic semiconductor is located between two electrodes; one of them is typically transparent. Patterned OLED matrices are used in digital displays (TVs, computer monitors, tablets, smartphones). There are two main families of OLEDs: those based on small molecules, and those employing polymers. A major area of research is the development of white OLED devices for use in solid-state lighting. The flexible nature of OLED displays allows new screen architectures that can be curved (concave or convex) to create new viewing experiences or relax design constraints in compact, off-axis imaging systems.

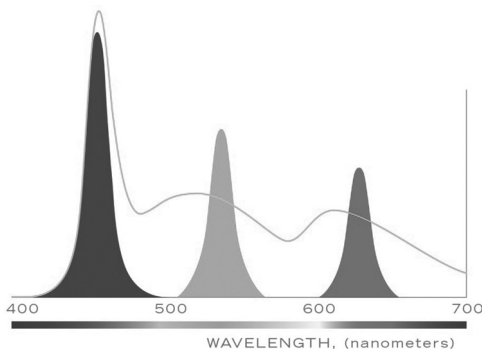
Active-matrix OLEDs (AMOLEDs) require a thin film transistor backplane to switch each individual pixel on or off, which allows for higher resolutions and larger display sizes. OLED microdisplays are built on silicon backplanes and allow for smaller pixel pitches ($<5\ \mu\text{m}$), which make them well suited for applications such as near-to-eye displays. However, it is not yet possible to directly pattern individual color OLEDs at such a high resolution—color filters are still required, which reduces the efficiency of the display. All major foundries (Microled, e-Magin, Sony) are working toward directly patterning OLED pixels at pitches below $5\ \mu\text{m}$ without color filters). Because OLED displays are emissive displays (no backlight), they provide a higher contrast.

Although the Lambertian emission cone of typical OLED pixels might have an advantage over smaller cone angles created by typical LED backlit microdisplays, a smaller cone angle might be needed to efficiently use the flux, as in HMDs. Bidirectional OLEDs have been investigated, which include emissive pixels as well as detection pixels (based on CMOS sensor technology). Such bidirectional OLED panels might be well suited for compact eye-tracking functionality in near-to-eye displays.

Quantum-Dot Displays

Most displays create an image by combining the three additive primary colors (RGB). LCD displays use either color filters or color sequencing. Plasma displays use phosphors (similar to CRT tubes). OLEDs use either color filters or phosphors. Color-filter LED LCDs use blue LEDs, coated with a yellow phosphor, to create “white” light. Although they are reasonably efficient compared with CCFL LCDs and plasmas, they waste spectral bands. For example, orange is blocked by the color filters (red and green are combined instead).

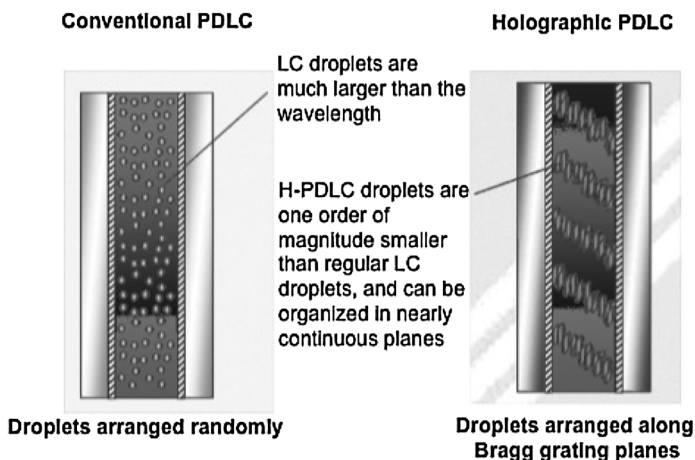
Quantum dots (QDs) have recently been introduced to produce a better color gamut and narrower spectral bandwidths in LED-backlit LCD displays (such as Amazon’s Kindle Fire). A QD is a nano-crystal made of semiconductor material. The QD excitons are confined in all three dimensions, and their electronic properties are between those of bulk semiconductors and discrete molecules. The QD band-gap determines the frequency of the light emission and is inversely related to its size. A blue LED can be used without a phosphor coating. The blue light passes through a sheet of red and green QDs inside the backlight. The blue LEDs have a double function: creating blue light and energizing red- and green-emitting QDs to produce red and green light.



Approximately two-thirds of the light created by the blue LEDs is used to excite the QDs. The rest is used to produce red and green. Companies currently developing QDs are Nanosys, QD Vision, and Nanophotonica.

H-PDLC Switchable Hologram

Holographic-polymer dispersed liquid crystals (H-PDLCs) can effectively produce a switchable optical element in either diffraction or refraction mode by holographically recording Bragg-regime volume gratings or subwavelength effective medium gratings, respectively.

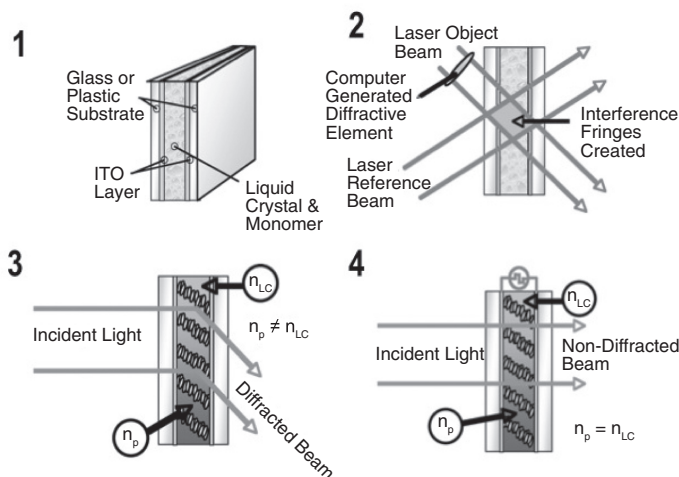


The initial monomer with dispersed LC droplets (one order smaller than traditional LC droplets, and thus faster to switch) is exposed holographically to produce a series of Bragg planes. The bright interference fringes polymerize the monomer and push the LC droplets into the dark fringes of the interference pattern, thus producing a switchable hologram by creating an index change between the fringes. The hologram can be wiped out by equalizing the indexes. The efficiency can therefore be modulated in real time, but the optical functionality cannot be changed (neither tuned nor reconfigured).

When recording a subwavelength grating, a fast bulk index modulator can be produced in order to create fast polarization rotators, tunable refractive micro-optics, or large-period diffractive elements by shaping the inner surfaces of the LC bottles. Both polarizations can be affected by using a quarter-wave plate between two sandwiched gratings.

H-PDLC Recording and Playback

The following figure shows the principle of the **recording** and **playback** of H-PDLC switchable holograms sandwiched between ITO plates.



The **Bragg planes** (fringes) are created by the polymerization of the monomer during holographic exposure. The LC microdroplet are pushed into monomer regions and depleted in polymerized regions.

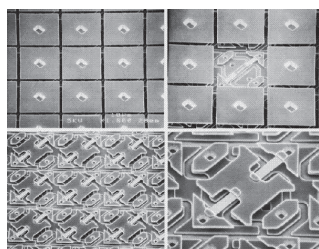
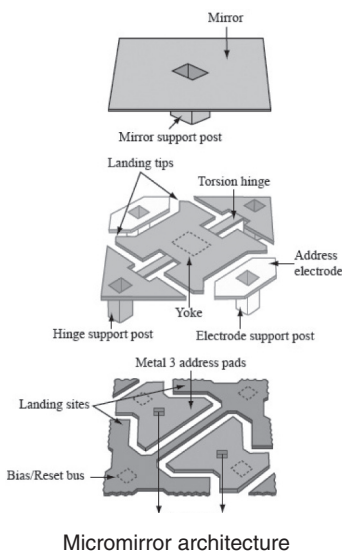
The Bragg planes are attached to the internal walls of the hologram, which are coated with indium tin oxide (ITO). Because the LC chains can be long for reflective holograms, where the Bragg planes are nearly parallel to the internal ITO surfaces, it is difficult to maintain reflective holograms in H-PDLC. Transmission H-PDLC holograms are more stable over time, but as the material properties improve, they might allow such configurations.

Note that the H-PDLC hologram is in ON (diffraction) mode when there is no voltage applied and can be turned OFF (transparent mode) by applying a voltage, thus also providing the potential of using H-PDLC material as a conventional static volume hologram.

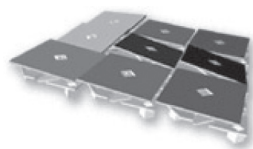
MEMS/MOEMS Micro-Optics

2D MEMS arrays have been made popular as reflective microdisplays by Texas Instruments' DLP technology, which is used in many modern front projectors (conventional and pico-projectors). Such mirrors are binary if they switch the light to a specific direction and then return to the same stable position.

3D MEMS arrays have been made popular by optical telecom applications, such as reconfigurable cross-connects or add/drop modules, whereby the mirrors can be set to a multitude of angles, sometimes in an analog way. 3D mirror arrays are more versatile but not suited for displays. The continuous monitoring of the current mirror angle in 3D mirror arrays prohibits use in consumer electronics. Such monitoring is usually done via direct torque sensing.



SEM view of micromirror arrays

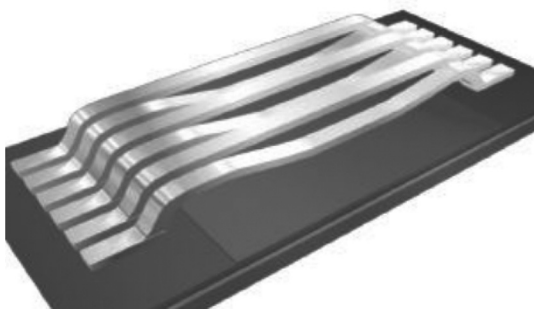


Array of 9 micromirrors

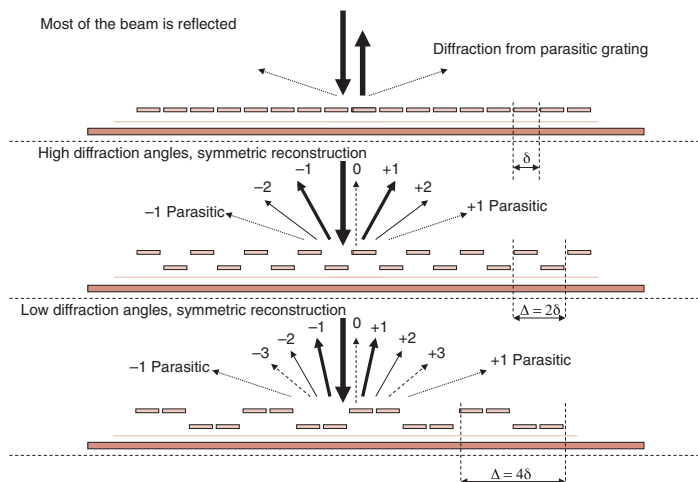
Single-mirror scanners or dual X/Y mirror scanners have been successfully used as ultra-miniature light engines for laser pico-projectors, as well as HMDs. However, they require laser light instead of LEDs due to the spatial coherence needed to deflect the light and produce a far-field image (which introduces other issues, such as potential speckle).

MEMS Gratings

Deformable-membrane **MEMS gratings** have been developed for both telecom and display applications. They usually implement a switchable optical element in which the efficiency can be tuned in greyscales from 0 to a maximum value (such as in a grating with a fixed period). The period can sometimes be switched to harmonics by producing superpixels by modulating groups of pixels collectively rather than independently.



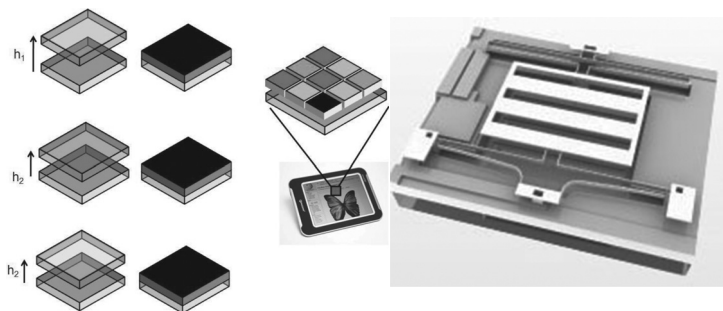
Such gratings can shape the spectral gain profile of an EDFA amplifier, and in display applications, such a grating can produce real grayscale intensity pixels in a specific direction.



MEMS Display Panels

Apart from standard DLP projection engines, MEMS have also been used as flat-screen displays in various implementations:

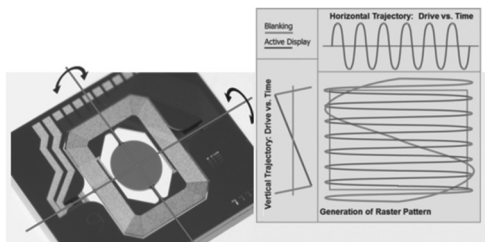
IMOD MEMS display panels, e.g., Qualcomm's Mirasol, are based on arrays of individually controllable (and bi-stable) Fabry–Pérot filters that filter the incoming ambient light. Such a panel is thus directly viewable in direct sunlight. The gap between the moving bottom mirror and the top semi-transparent film stack defines the frequency of light that is reflected through the cavity and can completely absorb light (producing high contrast). Multiple colors are created by sub-pixels, each designed to reflect a different specific color. Qualcomm's smartwatch currently uses such display technology; no larger panels are available. When no ambient light is present, a LED edge-illuminated frontlight illumination layer may be used, but it is not easy to implement.



Transmissive MEMS panels, e.g., Qualcomm's Pixtronix, are integrated as microshutter arrays based on electrostatic MEMS actuation. Unlike Mirasol displays, Pixtronix versions do not require complex frontlight illumination assemblies; they can use standard backlight technologies instead. The amount of light transmitted by such shutter arrays can be as high as ten times the light transmitted by conventional LCD panels, making them well suited for battery-operated, portable consumer electronics. This technology is currently applied to 7-in panel displays.

MEMS Laser Scanners

A single MEMS mirror and dual X/Y MEMS mirrors have been used as compact light engines in laser pico-projectors. The mirror usually vibrates in a resonance mode (Lissajous pattern), and the laser is synchronized in order to produce a pixelated image in the near or far field.

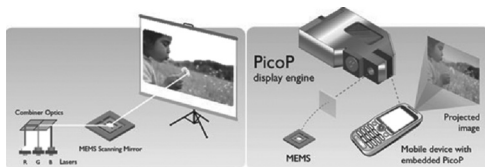


Such laser projectors have various advantages over other type of microdisplays (TFT LC or LCOS):

- no need for a backlight (or frontlight),
- small footprint of mirror(s),
- far-field image generation (no need for an objective lens),
- high color saturation due to laser color, and
- re-definition of FOV and resolution “on the fly.”

However, they lack in other areas:

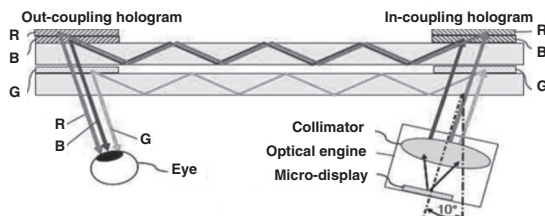
- the laser can produce speckle if the diffuser is in the optical path, and
- if full color is required, the package might be larger due to RGB laser-beam-combiner optics (bulk optics).



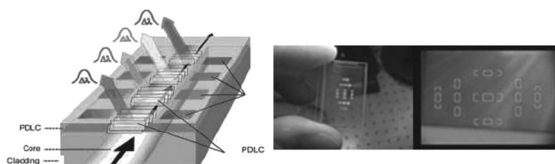
In many cases, an intermediate aerial image and a diffuser are required to form a decent eyebox for applications, such as HUDs or HMDs. This reduces the appeal of such technology because relay lenses are required, and the presence of a diffusing element in the optical path may cause speckle to appear.

Holographic Backlights and Displays

The use of holographic structures is promising for the development of efficient edge-lit systems for either laser/LED **backlight** or display applications. Surface-relief holograms, as well as index-modulation volume holograms, may be used as efficient color-specific Bragg extractors from an underlying waveguide. Multiple applications have been investigated: optical clock broadcasting in a planar waveguide, dynamic gain equalizers in EDFA fiber amplifiers, optical combiners in HMDs and viewfinders in SLR cameras, and holographic backlights for LED and laser display panels. The following figure shows an example of a holographic HMD combiner based on reflection-grating Bragg in- and out-couplers (three stacked holograms are used for RGB).



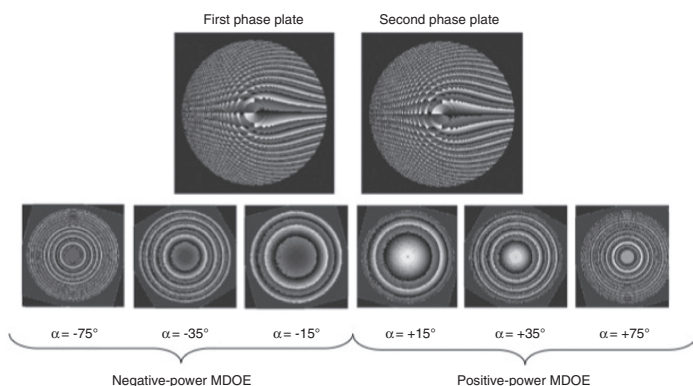
The following figure (left) shows a chirped-waveguide Bragg coupler used to spectrally equalize gain after an EDFA amp, and (right) a dual LED color holographic slab waveguide viewfinder (the holograms are recorded through a mask to pattern the light shapes to appear).



If the holograms can be switched (e.g., patterning with H-PDLC and electrodes), the spectral correction and/or viewfinder patterns may be changed at will. Holographic laser illumination backlights are ideal for applications where directivity of the light is essential. Due to their off-Bragg transparency, such holographic backlights can also be used as efficient frontlights (e.g., IMOD and LCOS panels).

Tunable Moiré Micro-Optics

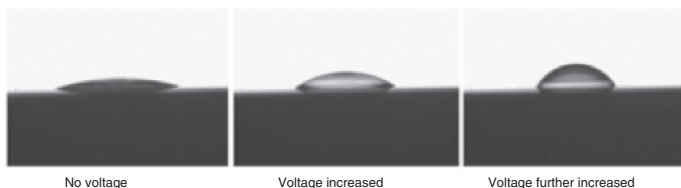
Tunable diffractive lenses can also be implemented as two sandwiched, static diffractive elements with specific phase functions, such as in a **moiré DOE** (M-DOE). The following figure shows such an M-DOE where the focal length is tuned by rotating one DOE in regard to the other.



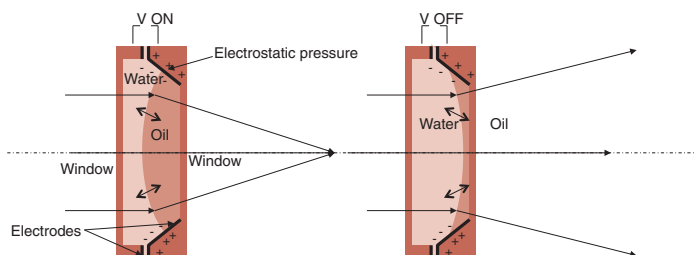
The power shift in the M-DOE presented here can vary from negative to positive (diverging to converging beam), going through zero power. However, aberrations of such mechanically tunable lenses are quite large, and thus imaging might not be the optimal application for such elements. More-appropriate applications range from optical tweezers to optical material processing (cutting, welding, surface treatment, etc.). Other implementations of mechanically tunable lenses through rotation or translation include helicoidal lenses or axicon lenses used off-axis, with the help of an aperture stop or a primary Fourier-type diffractive element (beam shaper element).

Liquid Micro-Optics

In an electro-wetting lens—or **liquid lens**—a refractive surface profile (power surface) is produced at the interface between two different, nonmixing liquids (e.g., water and oil). The surface tension can be changed by applying a voltage, thereby changing the nature of such surfaces (hydrophobic or hydrophilic) and thus the contact angle.



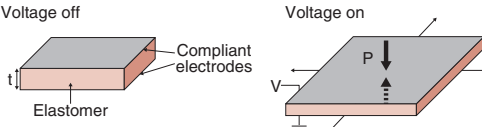
The liquid interface surface also changes, producing an optical power change. A typical electro-wetting lens architecture is shown below (Varioptic).



Such lenses may be cost effective with low power consumption and are polarization insensitive (unlike LC-based tunable or switchable lenses). Although the range of effective surface curvatures that can be produced may be wide (from negative to positive) when compared to other technologies, the surface profile at the liquid interface cannot be controlled very accurately, and the modulation speed remains slower than their LC switchable-lens counterparts, thus limiting the range of applications. Such lenses might be a best fit for integrated optical sensors and lower-resolution/low-power cameras with (relatively) fast focus-control needs.

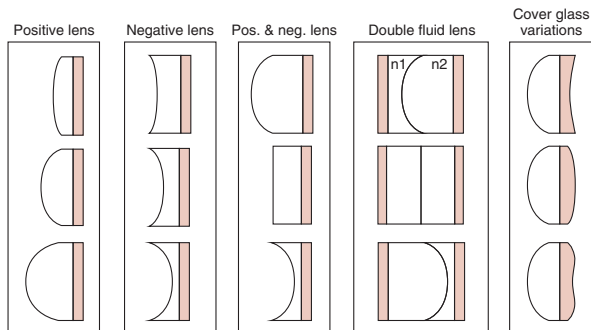
Electroactive Polymer Microlenses

Electroactive polymers (EAPs) can be used to implement various switchable or tunable micro-optics. These so-called “artificial muscles” can undergo a large amount of deformation while sustaining large forces. Whereas today’s piezoelectric actuators only deform by a fraction of a percent, EAPs can exhibit a strain of up to 380%. Dielectric EAPs (DEAPs) are driven by an electric field: when a voltage V is applied between two electrodes sandwiching a dielectric elastomer, an electro-mechanical thickness strain S is induced by electrostatic force. Assuming that the thickness compression results in an equibiaxial planar strain, the strain can be expressed as

$$S = \frac{1}{\sqrt{1 - \epsilon_r \epsilon_0 \frac{V^2}{Yt^2}}} - 1$$


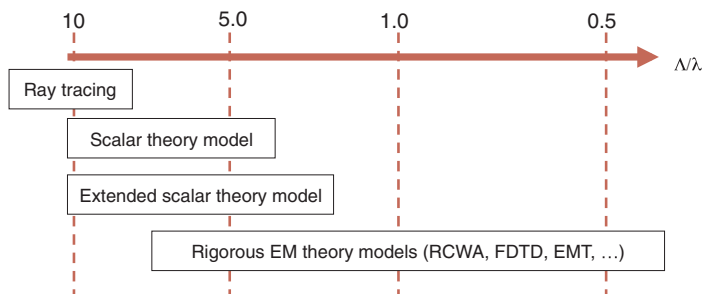
where t is the thickness, Y is the elasticity modulus, ϵ_0 is the permittivity of free space, and ϵ_r is the dielectric constant.

Optotune’s (CH) tunable lenses are shape-changing lenses based on a combination of optical fluids and a polymer membrane. The core element is a container filled with an optical liquid and sealed with a thin, elastic polymer membrane. A circular ring that pushes onto the center of the membrane shapes the tunable lens. The deflection of the membrane (and the radius of the lens) can be changed by pushing the ring toward the membrane, by exerting pressure on the outer part of the membrane, or by pumping liquid into or out of the container.



Diffraction Modeling Theories

Various theories have been proposed to predict the diffraction efficiency and diffraction pattern arising from micro- and nanostructures. The following figure includes the most prevalent theories and their corresponding ratio of the smallest period to the wavelength.



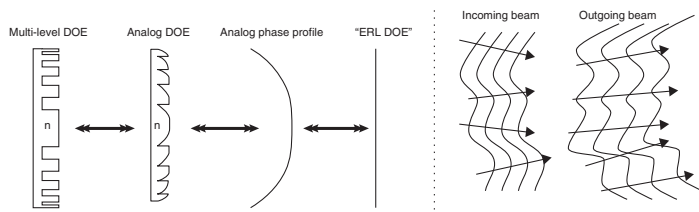
Scalar theory can provide information about both the diffraction pattern and diffraction efficiencies in various orders for periods larger than a few wavelengths. It does not provide information about polarization effects.

When the period becomes close to or smaller than the reconstruction wavelength, rigorous electromagnetic models should be used, and numerical implementations, such as finite-difference time domain (FDTD), rigorous coupled-wave analysis (RCWA), or EMT can be derived.

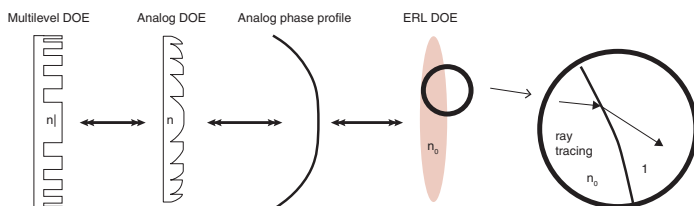
- **FDTD** can be applied to the diffraction through any pattern, not necessarily subwavelength and not necessarily repetitive. It is, however, a CPU-intensive numerical algorithm. Typical numerical window dimensions range within a few hundred wavelengths.
- **RCWA** is a coupled-wave model that requires a repetitive pattern and is well suited for gratings or holograms. Whereas FDTD gives information about both the efficiency and complex field, RCWA only provides values for efficiency.
- **EMT** may be used when attempting to create a quasi-analog phase profile from subwavelength binary structures.

Ray Tracing through Diffractives

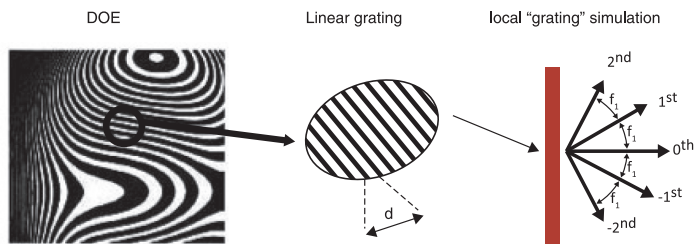
Various modeling techniques have been applied to diffractive optics. Most of them rely on **ray tracing**, such as the equivalent refractive-lens model with an infinite index:



the **Sweatt model**:



or the **local grating approximation (LGA)**:



Most current optical-design software use the LGA as their main modeling tool for diffractives. In the LGA, the diffractive is locally assimilated to a linear grating, at which point the grating equation is applied to find the various diffraction angles, and scalar diffraction theory is applied to find the efficiency in the various diffraction orders.

Fresnel and Fourier Approximations

The **Rayleigh–Sommerfeld diffraction integral** can be written as follows:

$$U'(x'_1, y'_1, z'_1) = \frac{-i}{2} \iint_{S_0} \frac{e^{ikr_{01}}}{|\vec{r}_{01}|} \cos(\vec{n}, \vec{r}_{01}) ds$$

where r_{01} is the vector from one point of the diffractive element to one point in the reconstruction space, and n is the vector normal to the diffractive surface.

The Fresnel (B) and Fourier (A) approximations of the Rayleigh–Sommerfeld formulation of diffraction can be expressed as follows:

$$\left\{ \begin{array}{l} U(u, v) = \iint_{\infty} U(x, y) e^{-i2\pi(ux+vy)} dx dy \quad (\text{A}) \\ U(x', y') = \left(\frac{e^{ikd}}{ikd} \right) \iint_{\infty} U(x, y) e^{i\frac{\pi}{\lambda d}[(x' - x)^2 + (y' - y)^2]} dx dy \quad (\text{B}) \end{array} \right.$$

The Fourier expression is thus limited to a simple 2D Fourier transform (Fraunhofer diffraction in the angular spectrum of plane waves), and the Fresnel expression (in the near field) can be written either as a direct Fresnel integral (Fourier transform of the incoming field multiplied by a spherical wavefront expression):

$$U(x', y') = \left(\frac{e^{ikd}}{ikd} \right) e^{i\frac{\pi}{\lambda d}(x'^2 + y'^2)} \iint_{\infty} U(x, y) e^{i\frac{\pi}{\lambda d}(x^2 + y^2)} e^{-i\frac{2\pi}{\lambda d}(x'x + y'y)} dx dy$$

or as a convolution:

$$U(x', y') = \left(\frac{e^{ikd}}{ikd} \right) \iint_{\infty} U(x, y) e^{i\frac{\pi}{\lambda d}((x' - x)^2 + (y' - y)^2)} dx dy$$

where d is the near-field distance, λ is the reconstruction wavelength, x' and y' is the coordinate system in the near field, x and y is the coordinate system in the plane of the diffractive element, and u and v is the frequency-dimension system in the angular spectrum.

Near- and Far-Field Regions

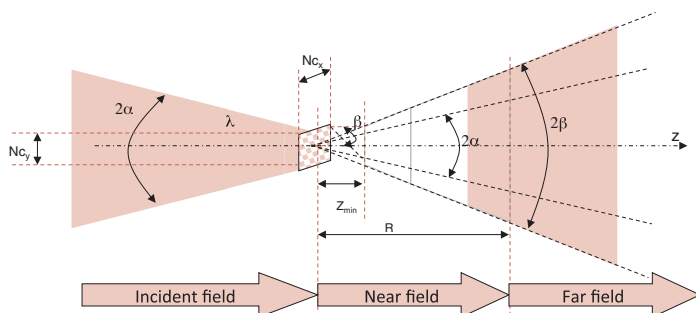
When using Fresnel (near field) and Fourier (far field) propagators to accurately model diffraction effects from diffractive elements or even refractive micro-optics, it is useful to know where the terms “**near field**” and “**far field**” can be applied. The minimum reconstruction distance from which one can use scalar propagators in the near field is usually given by

$$Z_{\min} \approx Nc \frac{1}{2(\beta - \alpha)} \propto 5Nc$$

Similarly, the minimum distance at which a region can be called far field (Fourier or Fraunhofer regime) is usually given by the Rayleigh distance:

$$R = \frac{2p^2}{\lambda} \Rightarrow \begin{cases} R_x = 8 \frac{c_x^2}{\lambda} \\ R_y = 8 \frac{c_y^2}{\lambda} \end{cases}$$

The following figure depicts the validity regions for the scalar near field and far field. Note that these regions are described by cones and not planes because of the paraxial approximation constraint of the maximum diffraction angles (scalar regime), even when the area of interest is located beyond Z_{\min} .



FFT-Based Physical Optics Propagators

In order to propagate a complex wavefront (from either analytic or numeric elements, or even from a refractive element) into the near or far field, a simple set of **FFT-based propagators** can be used:

$$\left\{ \begin{array}{l} U'(u_n, v_m) = FFT[U(x_n, y_m)] \quad (A) \\ U'(x'_{1n}, y'_{1m}) = e^{\frac{i\pi}{\lambda d}(x_{1n}^2 + y_{1n}^2)} FFT \left[U(x_n, y_m) e^{\frac{i\pi}{\lambda d}(x_n^2 + y_n^2)} \right] \quad (B) \\ U'(x'_{2n}, y'_{2m}) = FFT^{-1} \left[FFT[U(x_n, y_m)] FFT \left[e^{\frac{i\pi}{\lambda d}(x_n^2 + y_n^2)} \right] \right] \quad (C) \end{array} \right.$$

Propagator (A) is simply a 2D FFT transform that propagates the incoming complex wavefront modulated by the optical element's phase and amplitude profiles into the far field (angular spectrum of plane wavefronts).

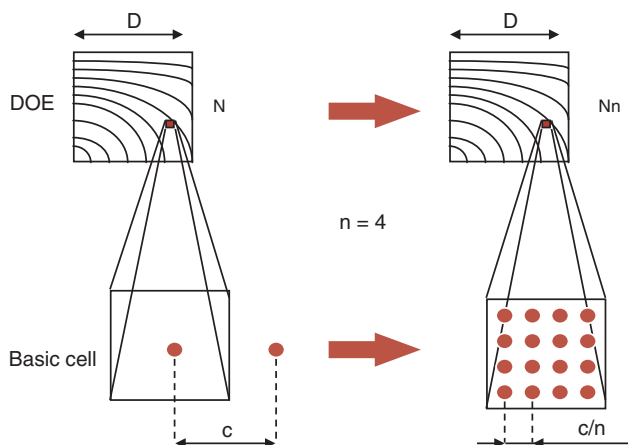
The second (B) and third (C) are both FFT-based means of propagating a complex wavefront into the near field. Propagator (B) is based on a single Fourier transform, and propagator (C) is a convolution-based process. They do not yield the same numerical results because the scaling of the reconstruction windows is different (d is the reconstruction distance).

- Oversampling the element can provide more-accurate information about the fabrication technology to be used (e.g., a square fabrication pixel defined by four design pixels organized in a square). The resulting reconstruction will thus show higher diffraction orders.
- Embedding the sampled element in a field of zeroes in amplitude (thus increasing the number of pixels without changing the sampling rate) can increase the resolution of the reconstruction (e.g., to preview speckle).

The oversampling and embedding ratios can be combined to produce very accurate numerical reconstructions that have realistic phase and intensity profiles that even depict speckle pattern.

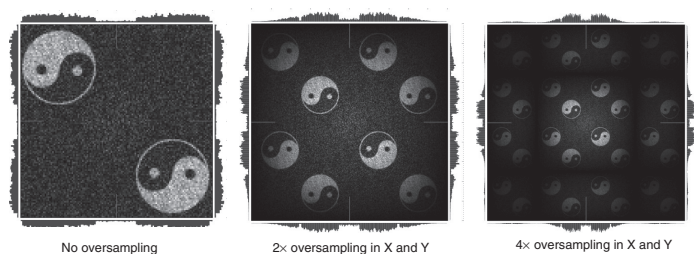
Oversampling Process in CGH Modeling

If the diffractive optical element to be modeled is fabricated by square or rectangular (or even other geometry) “pixels,” such as a CGH, it is possible to visualize the higher diffraction orders by **oversampling** the plane of the element.



By using large oversampling factors (such as 2, 4, or even 8), it is possible to reconstruct multiple higher diffraction orders and analyze how these various orders interfere if they overlap (such as in Fresnel elements).

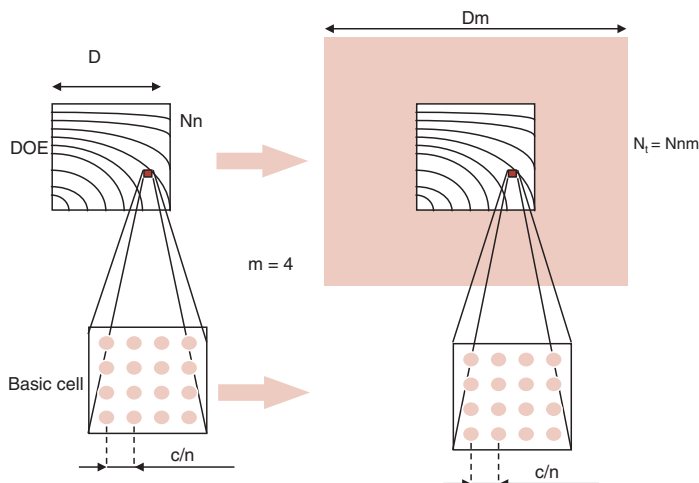
The following figure shows the oversampling process for a Fourier element (orders do not overlap).



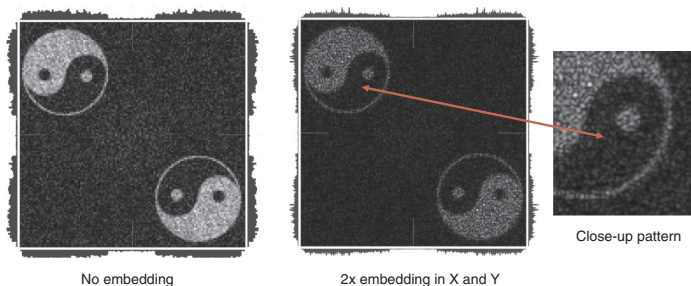
The other effect appearing in the reconstruction plane is sinc modulation over higher orders, which can dramatically reduce the intensity at the first and secondary zero locations of this function (see the right side of figure).

Physical Optics Modeling: Resolution Increase

Unlike the oversampling process, the **embedding** process does not change the sampling rate of the initial optical element; rather, it adds pixels around its aperture. Therefore, if using an FFT-based propagator, the number of pixels in the reconstruction plane is also larger, and the scaling is unchanged. Therefore, the sampling rate in the reconstruction window is synthetically increased.

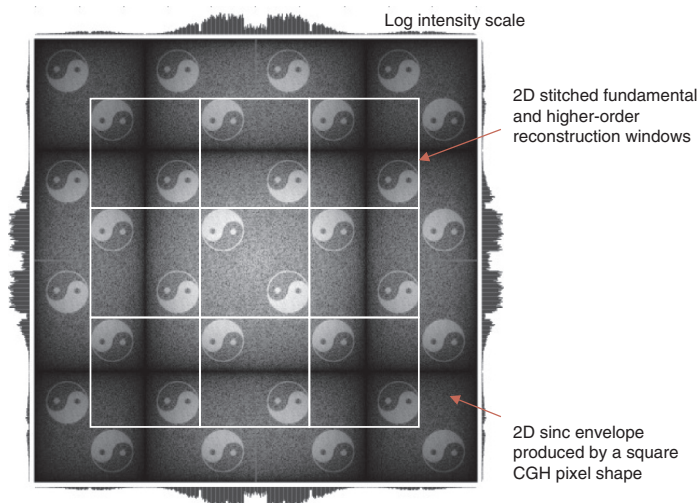


The following figure shows the results of the embedding process on the same Fourier CGH as the one used for the previous oversampling process. An embedding factor of 4 was used in each direction to accurately model the speckle over the reconstructed intensity pattern.



Physical Optics Modeling with FFT Algorithms

The following image shows the result of **physical optics modeling** of the off-axis, binary-phase Fourier CGH discussed earlier by simultaneously introducing an over-sampling factor (in order to visualize the higher diffraction orders and the sinc envelope produced by the square CGH pixels) as well as an embedding factor (to increase the resolution over the entire reconstruction window).



The various higher-order windows appear here as white lines. The first and second zeroes of the sinc envelope are clearly visible (dark lines). Fortunately, they do not intersect the patterns here (which is not always the case, depending on the element). Note that the white lines are independent of the dark lines.

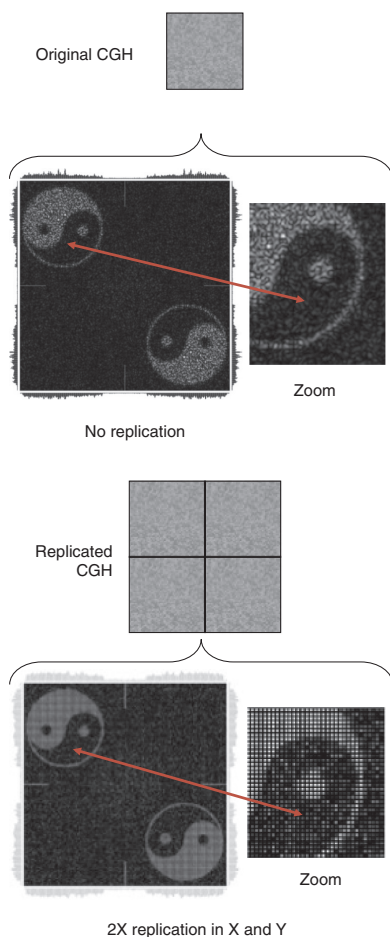
The white lines are paved, fundamental reconstruction windows, the size of which is a function of the size of the object pattern window. The dark lines are a function solely of the size of the individual pixels constituting the diffractive element (and are not related to the number of pixels defining the entire optical element area and thus also a fundamental reconstruction window).

Replication of CGHs

By replicating Fourier CGHs in the x and y directions, and by propagating the resulting enlarged pattern via FFT- or DFT-based propagators, it is possible to increase the resolution in the reconstruction window (angular spectrum) as well as in near-field windows. It is often the case that a nonreplicated CGH pattern will not show any of the parasitic sampling effects (energy going from maximum to zero) observed in the reconstruction plane.

For example, when designing a beam-shaping Fourier CGH, the numerical reconstruction can look smooth, but the actual optical reconstruction looks grainy (such as speckled). In order to increase the resolution further, an embedding factor might be used alongside the replication factor.

By replicating the sampled CGH pattern in x and y directions, it is possible to increase the dynamic range and show the sampling of the pattern in the far field (as shown here). Such sampling effects might be beneficial in some applications, such as spot array generators, but parasitic in others, such as beam shapers and pattern generators.



Numerical-Reconstruction Windows

Direct far-field reconstruction via a 2D FFT

In this case the angular spectrum is scaled by the maximum diffraction angle that can be achieved by the smallest grating possible (with a period defined by two pixels):

$$\begin{cases} U(x_n, y_m) = A(x_n, y_m)e^{\varphi(x_n, y_m)} \\ U'(u_n, v_m) = FFT[U(x_n, y_m)] = A'(u_n, v_m)e^{\varphi'(u_n, v_m)} \end{cases}$$

$$\text{where } \begin{cases} x_n = c_x \left(n - \frac{N}{2}\right) & , & y_m = c_y \left(m - \frac{M}{2}\right) \\ u_n = c_u \left(n - \frac{N}{2}\right) & , & v_m = c_v \left(m - \frac{M}{2}\right) \end{cases} \quad \text{and} \quad \begin{cases} c_u = \frac{2}{N} \arcsin\left(\frac{\lambda}{2c_x}\right) \\ c_v = \frac{2}{M} \arcsin\left(\frac{\lambda}{2c_y}\right) \end{cases}$$

Direct near-field reconstruction via a 2D FFT

This reconstruction produces scaling that can be dramatic and not include the entire reconstruction in the near field:

$$\begin{cases} U(x_n, y_m) = A(x_n, y_m)e^{\varphi(x_n, y_m)} \\ U_1(x'_{1n}, y'_{1m}) = A'_1(x'_{1n}, y'_{1m})e^{\varphi'_1(x'_{1n}, y'_{1m})} \\ \quad = Quad_2(x'_{1n}, y'_{1m})FFT[Quad_1(x_n, y_m)FFT[U(x_n, y_m)]] \end{cases}$$

$$\text{where } \begin{cases} x_n = c_x \left(n - \frac{N}{2}\right) & , & y_m = c_y \left(m - \frac{M}{2}\right) \\ x'_{1n} = c'_{1x} \left(n - \frac{N}{2}\right) & , & y'_{1m} = c'_{1y} \left(m - \frac{M}{2}\right) \end{cases} \quad \text{and} \quad \begin{cases} c'_{1x} = \frac{\lambda d}{c_x} \\ c'_{1y} = \frac{\lambda d}{c_y} \end{cases}$$

Convolution-based near-field reconstruction

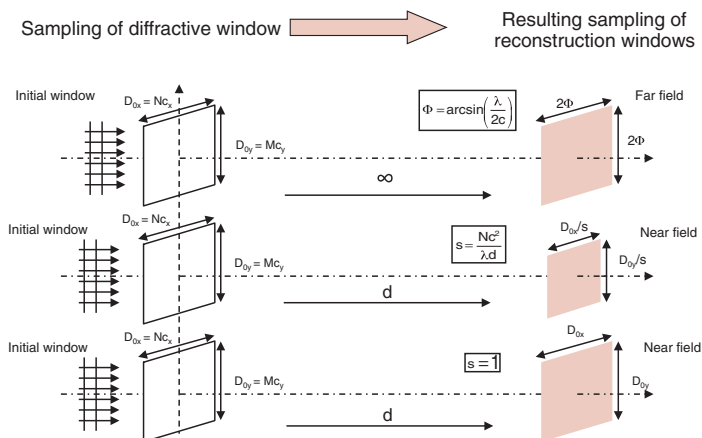
Unlike the previous direct near-field propagator, the convolution near-field propagator does not change the size of the reconstruction window; its size is the size of the element:

$$\begin{cases} U(x_n, y_m) = A(x_n, y_m)e^{\varphi(x_n, y_m)} \\ U_2(x'_{2n}, y'_{2m}) = A'_2(x'_{2n}, y'_{2m})e^{\varphi'_2(x'_{2n}, y'_{2m})} \\ \quad = FFT^{-1}[FFT[Quad_1(x_n, y_m)]FFT[U(x_n, y_m)]] \end{cases}$$

$$\text{where } \begin{cases} x_n = c_x \left(n - \frac{N}{2}\right) & , & y_m = c_y \left(m - \frac{M}{2}\right) \\ x'_{2n} = c'_{2x} \left(n - \frac{N}{2}\right) & , & y'_{2m} = c'_{2y} \left(m - \frac{M}{2}\right) \end{cases} \quad \text{and} \quad \begin{cases} c'_{2x} = c_x \\ c'_{2y} = c_y \end{cases}$$

Numerical-Reconstruction Window Scaling

The following figure summarizes the scaling of **numerical reconstruction windows** when using FFT-based propagators in the near and far fields.



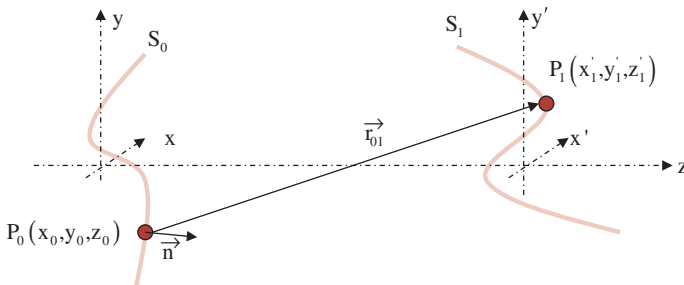
FFT-based propagators are very fast, even for arrays over several million pixels. However, the rigid scaling of such numerically reconstructed planes is a severe constraint that often prevents the optical designer from accurately modeling local or global effects because it is impossible to define arbitrary-reconstruction windows with arbitrary sampling rates.

FFT-based propagators are especially well suited for use in iterative optimization algorithms, such as IFTA and simulated annealing, due to their speed. However, they are not well suited for accurate modeling of a diffractive or general micro-optical element. **DFT-based propagators** are better suited for such a task.

DFT-Based Propagators

Previous pages illustrate that the FFT-based scalar propagators produce various constraints, especially when scaling the reconstruction plane. In many cases, it is preferable to arbitrarily define the size and location of the reconstruction plane, as well as its sampling rate.

DFT-based scalar propagators are directly based on the Rayleigh–Sommerfeld diffraction integral and not on the Fresnel or Fourier approximations leading to the constrained and rigid FFT-based propagators:



$$U'(x'_1, y'_1, z'_1) = \frac{-i}{2} \iint_{S_0} \frac{e^{ikr_{01}}}{|\vec{r}_{01}|} \cos(\vec{n}, \vec{r}_{01}) ds$$

in which the obliquity factor and r_{01} vector are defined as

$$\cos(\vec{n}, \vec{r}_{01}) = \frac{\vec{n} \cdot \vec{r}_{01}}{|\vec{n}| |\vec{r}_{01}|} \approx \frac{1}{\sqrt{1 + \frac{x_r^2 + y_r^2}{z_r^2}}} \quad \text{where} \quad \begin{cases} x_r = x'_k - x_n \\ y_r = y'_l - y_m \\ z_r = z'_{k,l} - z_{n,m} \end{cases}$$

$$|\vec{r}_{01}| = \sqrt{(z'_1 - z_0)^2 + (x'_1 - x_0)^2 + (y'_1 - y_0)^2} \cong z_1 \left(1 + \frac{1}{2} \left(\frac{x'_1 - x_0}{z_1} \right)^2 + \frac{1}{2} \left(\frac{y'_1 - y_0}{z_1} \right)^2 \right)$$

Thus, the expression of a generic DFT-based propagator in the near field can be written as

$$U'(x'_k, y'_l, z'_{k,l}) = \sum_{n=0}^N \sum_{m=0}^M \left(\frac{z_r}{x_r^2 + y_r^2 + z_r^2} \right) U(x_n, y_m, z_{n,m}) e^{i \frac{\pi}{\lambda} (\sqrt{x_r^2 + y_r^2 + z_r^2})}$$

Such a propagator is not limited to 2D planes parallel to the optical element and can reconstruct 3D volumes or planes tilted to the element (e.g., reconstruction planes parallel to a lens' optical axis).

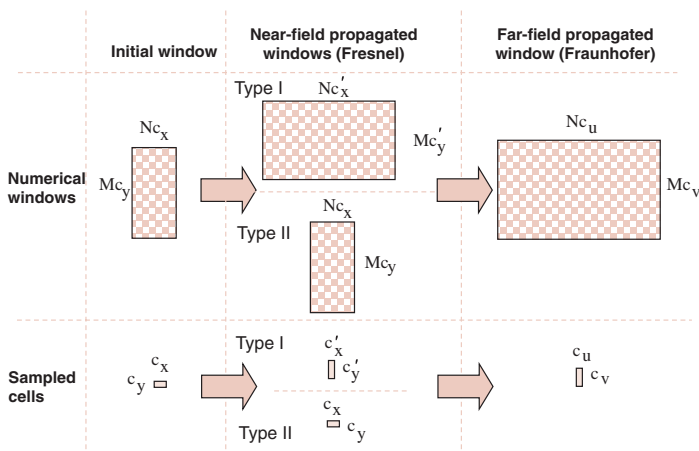
Fresnel Propagator Using a DFT

DFT propagators are especially useful for near-field reconstructions, such as phase and intensity maps along the optical axis of lenses. The following equations describe numerical DFT propagators:

$$\begin{aligned}
 U'(x_k, x_l) &= e^{\frac{i\pi}{\lambda d}(x_k'^2 + y_l'^2)} \text{DFT} \left[U(x_n, y_m) e^{\frac{i\pi}{\lambda f}(x_n^2 + y_n^2)} \right] \\
 &= e^{\frac{i\pi}{\lambda d}(x_k'^2 + y_l'^2)} \sum_{n=-N/2}^{N/2} \sum_{m=-M/2}^{M/2} U(x_n, y_m) e^{\frac{i\pi}{\lambda f}(x_n^2 + y_n^2)} e^{-i2\pi(x_n(u_n - u_0) + y_n(v_m - v_0))}
 \end{aligned}$$

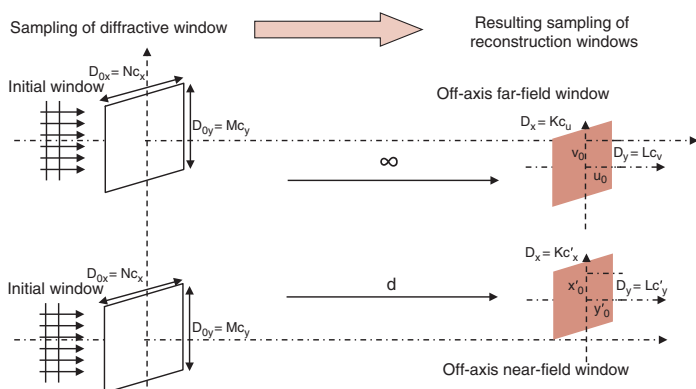
with $\begin{cases} x_n = c_x \left(n - \frac{N}{2} \right) \\ y_n = c_y \left(m - \frac{M}{2} \right) \end{cases}$ and $\begin{cases} x'_k = c'_x \left(k - \frac{K}{2} \right) - x_0 \\ x'_l = c'_y \left(l - \frac{L}{2} \right) - y_0 \end{cases}$

The following figure compares the reconstruction window of a FFT-based near-field propagator (both cases of direct and convolution-based Fresnel transform) and the arbitrary size and sampling of a DFT-based propagator window.

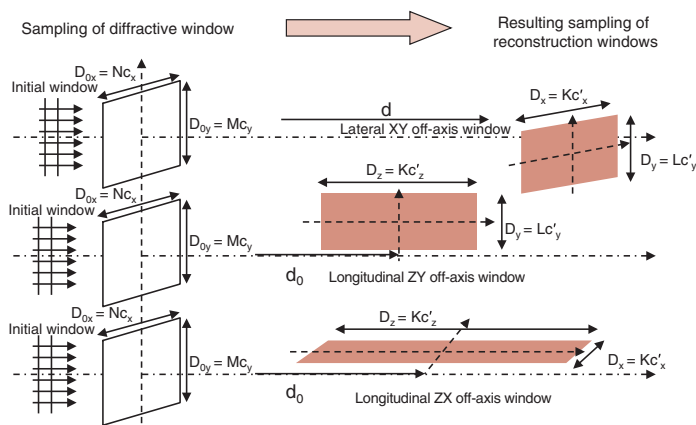


Arbitrary-Reconstruction Windows

As seen in the previous page, when using DFT propagators, the reconstruction window location, its size, and its resolution are not constrained as they are with FFT-based propagators. In fact, the reconstruction window can be placed virtually anywhere in the near or far field. Moreover, the window does not need to be planar, nor does it have to be parallel to the diffractive window. The following figure shows the various orientations of far-field windows computed by a DFT propagator (Fraunhofer regime).

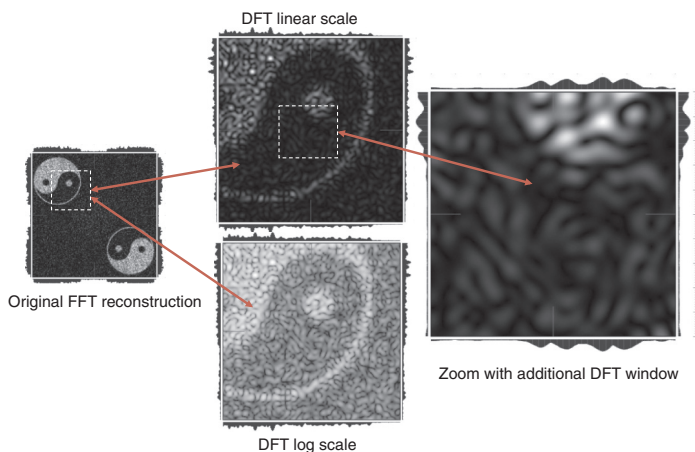


The next figure shows some of the potential orientations of such DFT-based propagator windows in the near field (Fresnel regime).



DFT-Based Numerical Propagator

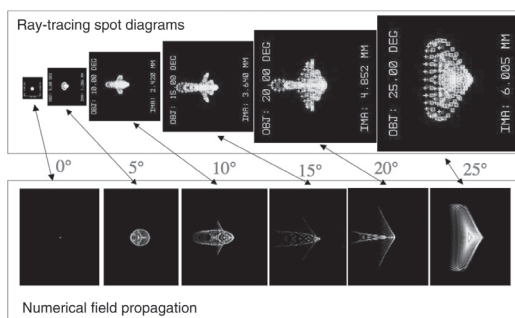
The following reconstruction shows how a **DFT-based propagator** can arbitrarily increase the resolution of a reconstruction plane in order to focus on certain details (e.g., focusing on a speckle pattern). The figure shows the far-field reconstruction of a binary CGH representing a logo, with a standard FFT-based algorithm (left side) and then the same reconstruction using a DFT algorithm in which the numerical window and the number of pixels (resolution) have been arbitrarily set (both for intensity and phase windows). It is possible to “zoom in” even more with a higher resolution (sampling) in order to depict the speckle pattern inherent to such a reconstruction.



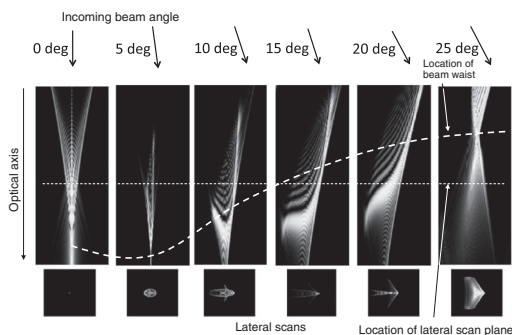
In FFT-based reconstructions, the numerical window has the same number of pixels as the diffracting plane and is centered in the optical axis. In a DFT-based reconstruction, both the window orientation (in 3D) and the number of pixels can be arbitrary. It is, therefore, theoretically possible to reconstruct a very precise near- or far-field pattern (large number of reconstruction pixels) from a CGH sampled over only a few pixels.

Physical Optics versus Ray Tracing

The following is a comparison of a FOV modeling for a hybrid refractive/diffractive lens, performed in ZemaxTM through standard ray tracing (spot diagram) and a DFT propagator in the near field.



The different aberrations of the focused spot for various tilts are very similar when using ray tracing or DFT propagation. However, DFT propagation shows many more details, as well as the interferences between higher orders and noise due to fabrication errors (systematic and random). These images show longitudinal reconstructions along the optical axis, which is nearly impossible to perform via ray tracing.



Here, again, one can distinguish local interference patterns and potential multiple orders that overlap, as well as effects due to fabrication errors (systematic and random). One can also distinguish the field curvature of such a hybrid lens, which is very difficult to display when using ray tracing in standard optical-design software.

Fabrication Timeline of Micro-Optics

The following figure summarizes in chronological order the various techniques used in research and industry to fabricate digital micro-optics.

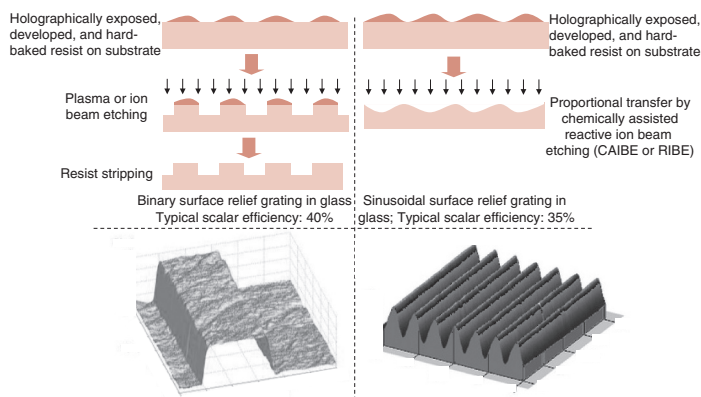
	BC	Scratch-o-grams	
	1785	Rittenhouse	Gratings made of hair
	1882	Rowland	} Ruling engines
	1910	Wood	
	1948	Gabor	In-line holography (phase objects)
Holography infancy	1962	Leith/Upatnieks	Off-axis holography and HOEs
	1969	Lohmann/Brown	Synthetic holography (CGHs)
	1972	D'Auria/Huignard	Optical lithography
	1975		CNC precision diamond ruling/turning
Lithography boom	1983	Gale/Knop	Direct analog laser write in resist
	1985	Arnold	Direct binary e-beam write
	1989	Swanson/Weldkamp	Multi-level optical lithography
	1994	Lee/Daschner	Direct analog e-beam write
	1995	Potomac	Direct analog excimer laser ablation
Greyscale	1998	Canyon materials	Greyscale masking lithography
	2002	DOC	Stacked wafer scale (backside alignment)
	2004	UCSD	LAF greyscale masking
Nano-boom	2005		Nano-imprint / soft lithography
	2008		Direct nano-write (fringe writer, two photon, ...)

- **Scratch-o-grams** were the first implementation of synthetic diffractive structures (arrays of scratches in glassy rocks). Ruling engines were used since the 19th century to carve out up to a few hundred periods per millimeter.
- **Analog holography** was the precursor for digital holography and diffractive fabrication, first by Denis Gabor (on-axis) and then by Leith and Upatnieks (off-axis).
- **Binary optical lithography** and, later, **multilevel lithography** were developed thanks to developments in the IC fab industry during the 1980s. **Greyscale lithography** benefited from a further leap in the performance of high-efficiency, quasi-analog surface-relief elements (diffractives, refractives, and MLA arrays).

More recently, advances in nano-replication (soft lithography) have made it possible to produce subwavelength structures at large scale, as well as interference lithography.

Holographic Exposure and Etching

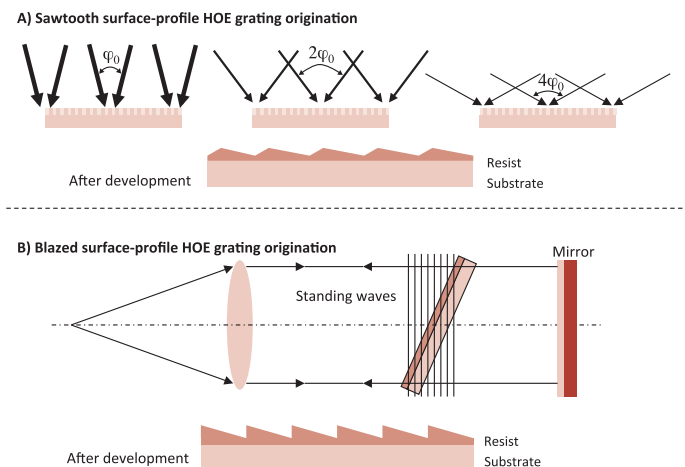
As discussed earlier, **holographic exposure** over photoresist can produce sinusoidal surface-relief elements. It is also possible to produce binary gratings through holographic exposure by overexposure or use of a metal hard stop below the resist layer (metal wet etch followed by dry oxide RIE etch), as depicted in the following figure. Binary gratings have several advantages over surface-relief sinusoidal gratings (efficiency, zero-order gratings, etc.).



Holographically exposed binary grating structures can overcome some of the issues encountered in traditional lithography technologies, such as the element-size limitation (produced by the stepper field in i-line or DUV steppers) or the wafer-size and low-resolution limitation in contact/proximity mask aligners. Although a stepper can step and repeat gratings to cover an entire 8- or 12-in wafer, the typical field-to-field alignment errors prohibit such gratings from use in demanding applications where very small field-stitching errors may produce adverse phase shifting effects, such as large-area binary phase gratings for the exposure of volume Bragg gratings in doped waveguides or fibers.

Multiple Holographic Exposures

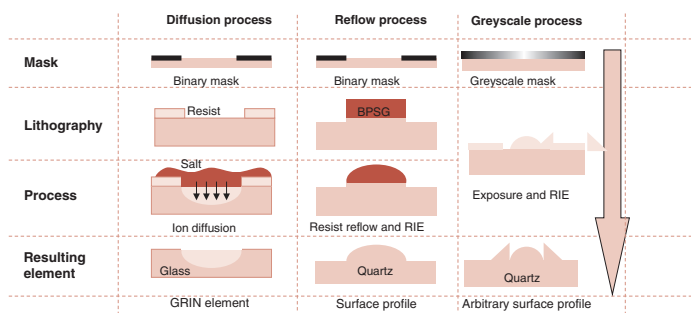
Holographic exposure usually produces sinusoidal profiles in photoresist, normal to the substrate or tilted. However, more-complex structures are often desired, such as binary-blazed structures (see previous page) or double-blazed structures (echelette gratings). They can be produced by **multiple holographic exposures**. The resist is developed only after the last exposure, followed by proportional RIE etch.



Such multibeam holographic exposure techniques are also referred to as “interference lithography.” They are commonly used to produce periodic structures with critical dimensions not constrained by the resolution limit of projection optics (such as with mask aligners and steppers). One-dimensional structures (such as linear gratings), curved gratings, and 2D structures (such as crossed gratings or hexagonal patterns of dots) have been developed that implement photonic crystal structures via such techniques. This is usually done on a wafer that is then further processed as if it were exposed via a traditional lithography tool.

Refractive Micro-Optics Fabrication

Due to the continuous surface profile of refractive and/or reflective micro-optics, their fabrication via lithographic techniques can be quite challenging. Microlithography has been optimized for IC fabrication where structures are binary (binary multilevel fabrication approximates continuous surfaces). However, there are a few fabrication techniques that rely on binary masks to fabricate micro-refractive elements, such as MLA: ion diffusion, reflow, and grayscale lithography.



Ion diffusion using molten salt has been used to produce index-modulated waveguides (with an added field to draw the ions further inside the substrate) without needing surface-relief modulation. Such cores usually lie very close to the surface. Similarly, index-modulated refractive lenses or even diffractives have been fabricated this way.

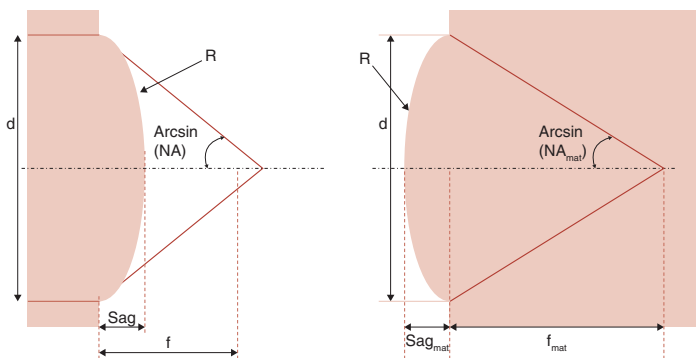
Resist reflow is the most popular process to produce refractive lenses from a single binary lithographic step. Instead of resist reflow, one can also use another material, such as BPSG (boron-phosphorous-silica glass), that has a specific dialed-in index and melts at a lower temperature than the substrate (fused silica). BPSG is a standard glass-growth process in IC fabrication to protect CMOS structures. When using resist reflow, a proportional dry-etch transfer may be used to produce MLAs in the substrate (or negative nickel mold electroforming). When using BPSG reflow, the lens (or lens array) can be used as is.

Sag Calculations for Microlenses

Microrefractive lenses, such as MLAs, may be fabricated to operate in air or in the underlying substrate. The key figure for a microlens (or MLA) fabricated lithographically is usually the lens sag (i.e., the maximum etch depth required in the substrate).

Although etch depths of more than 100 μm have been achieved via wet etching (e.g., HF etch), 30 μm can be achieved via dry etching (CHF_3/CF_4 for fused-silica etching). Deep etching usually produces a poor surface figure, such as roughness. Proportional etching rates of approximately 1 to 3 (etching depth up to three times the resist depth) can yield very good roughness figures.

The following figures show both in-wafer and in-air operation of a refractive microlens and the corresponding sag calculation expressions for a given focal length and index.



$$\begin{cases} f\# = \frac{f}{d} = \frac{1}{2NA} \\ R = f(n - 1) \\ \text{Sag} = R - \sqrt{R^2 - \left(\frac{d}{2}\right)^2} \end{cases}$$

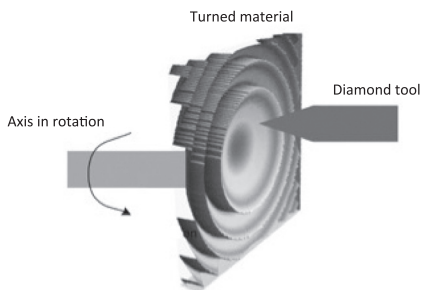
$$\begin{cases} f\# = \frac{f_{\text{mat}}}{d} = \frac{1}{2NA_{\text{mat}}} \\ R = \frac{n - 1}{n} f_{\text{mat}} \\ \text{Sag}_{\text{mat}} = R - \sqrt{R^2 - \left(\frac{d}{2}\right)^2} \end{cases}$$

Diamond Ruling/Turning

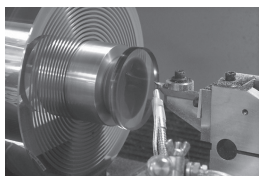
Diamond ruling is the *de facto* fabrication technique for large-dimension and/or deep gratings, especially reflection gratings (such as for spectroscopic applications).

Diamond turning machines

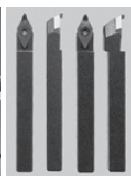
(DTMs) are well suited to produce circularly symmetric grooves, e.g., refractive and diffractive Fresnel lenses and circular gratings, as well as micro-refractive lenses with sags deeper than the ones achievable by dry-etch lithography (see previous page).



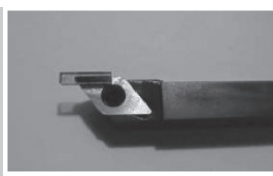
For more-complex surfaces, four- or five-axes-of-freedom DTMs can be used to produce astigmatic lenses and other noncircularly symmetric elements (five-axes-of-freedom DTMs are usually also freeform-surface capable, e.g., Precitech or Moore DTMs). The geometry of the diamond tool's tip is very important and must be carefully chosen to cut the desired structures.



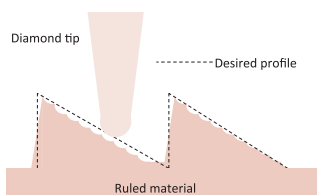
Diamond turning lathe and plastic substrate



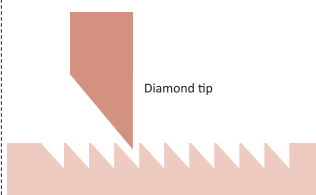
Various diamond tool tips



2 x 10 mm synthetic diamond tool on 55-deg insert



Diamond tip not adapted to grating geometry

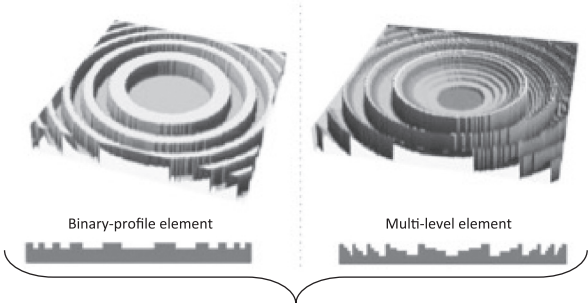


Diamond tip adapted to grating geometry

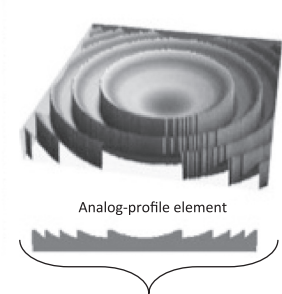
Metal molds can also be directly ruled or turned and used as shim inserts in plastic embossing or injection molding.

Binary Lithography

In many cases, multilevel fabrication is preferred over binary (two-level) fabrication, producing a higher diffraction efficiency and smoother profiles. Although multilevel fabrication produces theoretically better performances, its complexity also compounds many systematic and random fabrication errors that can affect the optical functionality of the resulting element. Binary fabrication is sometimes preferred over multilevel (see, for example, EMT subwavelength optical elements).



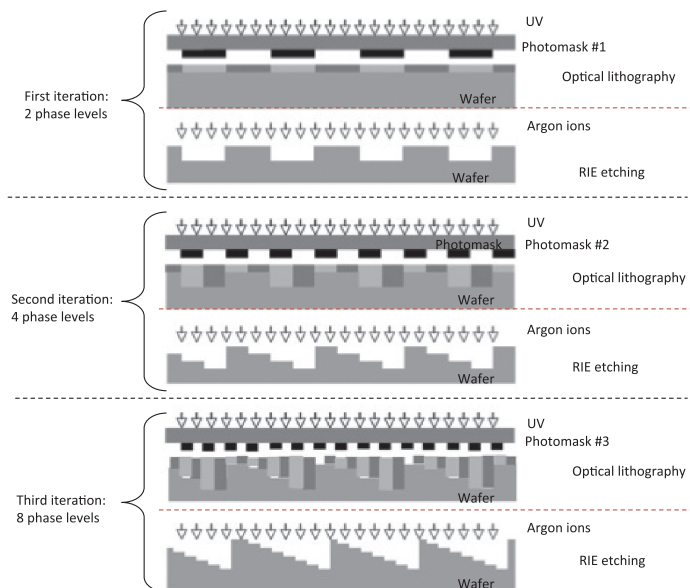
Fabrication	Conventional lithography
Efficiency (theoretical)	40–98%
Efficiency (real)	30–85%



Fabrication	Greyscale lithography
Efficiency (theoretical)	99–100%
Efficiency (real)	80–90%

Multilevel Optical Lithography

Binary and **multilevel optical lithography**, followed by dry RIE etching into fused silica or silicon substrates, is a common technique used to produce high-quality micro-optics. The following figure shows the fabrication process of an eight-phase-level element by using three consecutive binary masking layers followed by three dry etchings.



In general, n masking layers are required for the production of 2^n phase levels, which is why optical microstructures seldom have an odd number of phase levels. Systematic and random process errors in multilevel lithography include field-to-field misalignments and cascaded etch-depth errors in successive fields. These process errors yield high-spatial-frequency structures (both negative and positive) and periodic duty-cycle fluctuations, which will affect efficiency and signal contrast. However, such process errors do not produce any periodicity fluctuations if the original element (sets of masks) is periodic, so absolute diffraction angles are unaffected. Greyscale and direct-write techniques overcome both the field-to-field alignment errors and successive etch-depth errors.

Etch Depth: Critical Dimension and Groove Depth

In order to get the maximum efficiency for any phase profile (binary, multilevel, or analog), the depth of the structures must be designed to yield the optimal phase shift that, in turn, will produce the highest local-interference contrast. The fundamental diffraction order is considered.

The efficiencies in reflection or transmission modes are identical if the elements are fabricated with the correct groove depth. However, because depths in reflection modes are shallower than in transmission modes, the depth tolerances in fabrication are more difficult to achieve for reflection-mode elements.

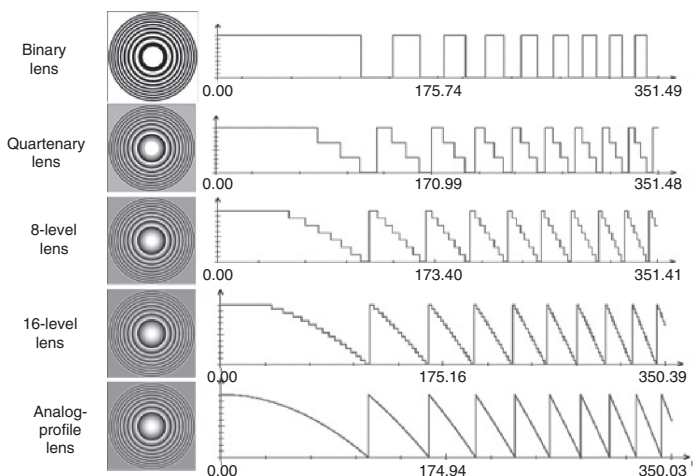
Number of Phase Levels	Critical Dimension	Total Groove Depth (transmissive / reflective)
2 (amplitude)	$\Delta_{\min} / 2$	NA
2	$\Delta_{\min} / 2$	$\frac{\lambda}{2(n-1)} / \frac{\lambda}{4}$
4	$\Delta_{\min} / 4$	$\frac{3\lambda}{2(n-1)} / \frac{3\lambda}{8}$
8	$\Delta_{\min} / 8$	$\frac{7\lambda}{8(n-1)} / \frac{7\lambda}{16}$
16	$\Delta_{\min} / 16$	$\frac{15\lambda}{16(n-1)} / \frac{15\lambda}{32}$
Continuous surface	Δ_{\min}	$\frac{\lambda}{(n-1)} / \frac{\lambda}{2}$

Etch Depth: Single-Step Height and Diffraction Efficiency

Number of Phase Levels	Single-Step Height (transmissive / reflective)	Diffraction Efficiency
2 (amplitude)	NA	10%
2	$\frac{\lambda}{2(n-1)} / \frac{\lambda}{4}$	40.5%
4	$\frac{\lambda}{4(n-1)} / \frac{\lambda}{8}$	81%
8	$\frac{\lambda}{8(n-1)} / \frac{\lambda}{16}$	95%
16	$\frac{\lambda}{16(n-1)} / \frac{\lambda}{32}$	99%
Continuous surface	NA	100%

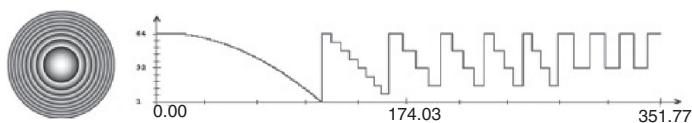
Multilevel Lithographic Fabrication

The diffraction efficiency in the fundamental diffraction order increases as the number of phase levels increase. When fabricating a diffractive element, such as the lens described here, the output tool usually has a limited resolution that allows only a specific number of phase levels to be fabricated in each groove. However, in a Fresnel diffractive lens, the groove periods are large in the center and smaller on the edges of the lens. It is therefore possible to modulate the number of phase levels over the entire lens, as follows:



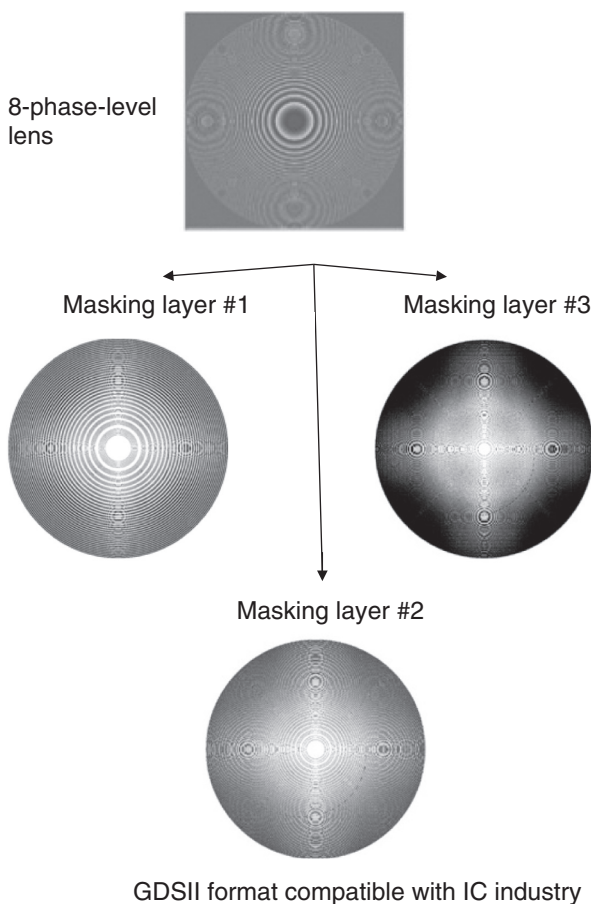
This behavior has the advantage of using the full capability of the chosen fabrication tool to produce the highest efficiency.

In many cases, the goal is to modulate the number of phase levels in each groove—not to meet a fabrication-tool resolution constraint but rather to apodize the lens transmission in order to produce specific imaging properties, e.g., suppression side lobes on the focused spot by apodizing the lens in a Gaussian way.



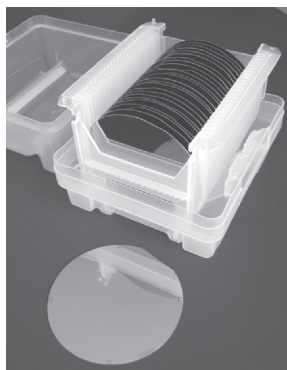
GDSII Mask Layouts

When using microlithography techniques developed for the microelectronics fabrication industry, one must also use the layout formats developed for the same IC industry to represent the shapes to be patterned on the photomask. Many formats are used: Graphical Data Structure II (GDSII), Caltech Intermediate Format (CIF), Gerber, DXF, etc. These are vector image formats, not raster image formats. The following figure shows how an eight-phase-level diffractive lens is fractured into three consecutive vector masks, each in the GDSII format.

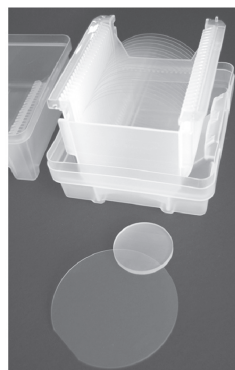


Wafers for Micro-Optics

- **Fused-silica (synthetic quartz) wafers** are often used to produce digital optics, either through multilevel lithography, resist reflow, or greyscale lithography.
- Although cheaper to produce, **glass wafers** (borosilicate, etc.) cannot be dry etched as well as fused-silica wafers due to their anisotropy. Fused-silica wafers can easily be dry RIE etched with CHF_3 and/or CF_4 reactive gases.
- **Silicon wafers** can also be used to produce micro-optics, either in transmission mode for infrared or in reflection mode with or without added metal coating.

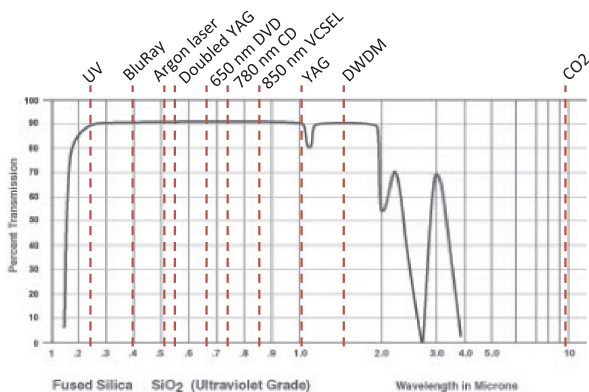


Silicon wafers



Fused-silica wafers

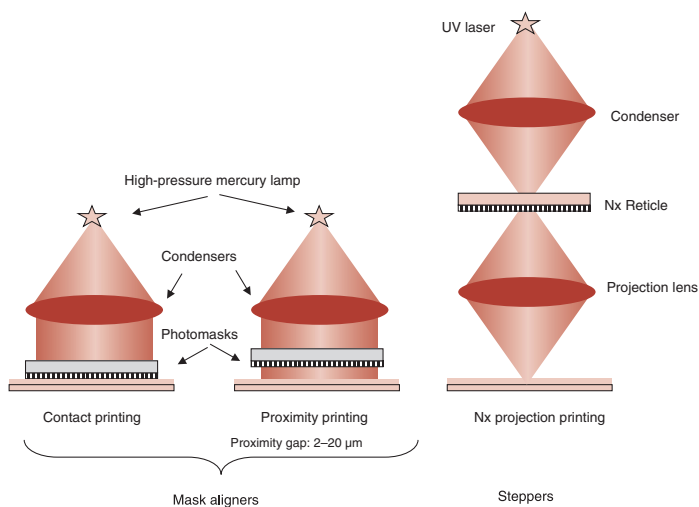
The transmission curve of common fused-silica wafers is shown below.



Optical Lithography

Optical lithography consists of transferring a pattern from a mask onto a wafer. A mask aligner can work in either contact, proximity, or projection mode.

- In **contact mode**, the mask and the wafer are in soft or hard (vacuum) contact, which provides high resolution (down to $0.5\ \mu\text{m}$) but deteriorates the mask.
- In **proximity mode**, the resolution is limited to a few microns, but the tooling does not deteriorate. Proximity mode is also used for binary greyscale masking and Talbot self-imaging.
- **Projection mode** can be performed at $1\times$ with a mask aligner or with a demagnification ratio (usually $5\times$ or $4\times$) in a stepper, where the mask (reticle) field is reduced and stepped across the wafer.

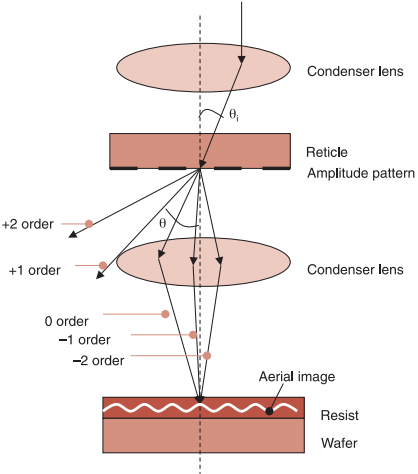


When the device to be printed is larger than the maximum stepper field size (typically $20\ \text{mm}$), the only solution is to use a mask aligner. Mask aligners are retrofitted to be used as nano-imprint equipment, such as the Karl Suss MA6. Backside alignment is also a desirable feature in mask aligners, which is difficult to implement in steppers (such as the MA6BA, in either visible or IR backside-alignment configurations).

Step-and-Repeat Lithography

Steppers are high-resolution tools that use reticles at 10×, 5×, or 4× magnification, but they can only print small fields, such as 20 × 20 mm, typically. When the elements to be printed are larger than that field, a mask-aligning lithography tool (1× system) must be used.

Various stepper systems currently exist with increasingly smaller illumination wavelengths. A stepper can be one to two orders more expensive than a mask aligner, but it can produce much-smaller features, though on a smaller field. Yesterday’s I-line steppers can go below 0.5 μm, today’s deep UV (DUV) steppers can go below 100 nm, and tomorrow’s extreme UV (EUV) steppers go below 10 nm.



Year	Source	Type	λ (nm)	NA	k_1	δx (μm)
1980	Mercury arc lamp	G-line	436	0.28	0.96	1.50
1983				0.35	0.96	1.20
1986		H-line	405	0.45	1.00	1.00
1989		I-line	365	0.45	0.86	0.70
1992				0.54	0.74	0.50
1995				0.60	0.57	0.35
1997	UV laser	KrF	248	0.93	0.50	0.25
1999				1.00	0.43	0.18
2001				0.75	0.37	0.11
2003	DUV laser	ArF	193	0.85	0.45	0.09
2005		F ₂	157	0.90	0.45	0.06
2008	EUV	X ray (R&D)	13	0.20	0.50	0.03

Useful Lithography Parameters

The following parameters are useful when assessing the quality of a given optical lithography process.

- The **diffraction through a reticle** in mask aligners (proximity mode) and steppers obeys the same grating equation as standard diffractives (where m is the diffraction order, and Δ is the period): $\sin(\theta) - \sin(\theta_i) = (m\lambda)/\Delta$. Therefore, the **reconstructed aerial image** through a stepper lens with a finite aperture can be expressed as the recombination of multiple diffraction orders:

$$I(x) = I_0 \left[\frac{1}{2} - \frac{2}{\pi} \sum_{m=1}^{\infty} \frac{(-1)^m}{m} \sin\left(\frac{m\pi}{2}\right) \cos\left(\frac{m\pi x}{d}\right) \right]^2$$

- The **minimum feature size** resolved in the aerial image is

$$\delta x = \left(\frac{1}{2}\right) \frac{\lambda}{\sin(\theta_0)}$$

- The **point spread function** (PSF) of the lithography tool through a circular aperture is

$$I(x) = I_0 \left(2 \frac{J_1(x)}{x} \right)^2$$

- The **Rayleigh resolution criterion** is

$$\delta x = 0.61 \frac{\lambda}{NA} = k_1 \frac{\lambda}{NA}$$

where k_1 is the resolution factor dependent on the optics and process (typically from 0.25 to 1.0).

- Because the illumination for many lithography tools is usually partially coherent, the **resolution** becomes

$$\delta x = k_1 \frac{\lambda}{(\sigma + 1)NA}$$

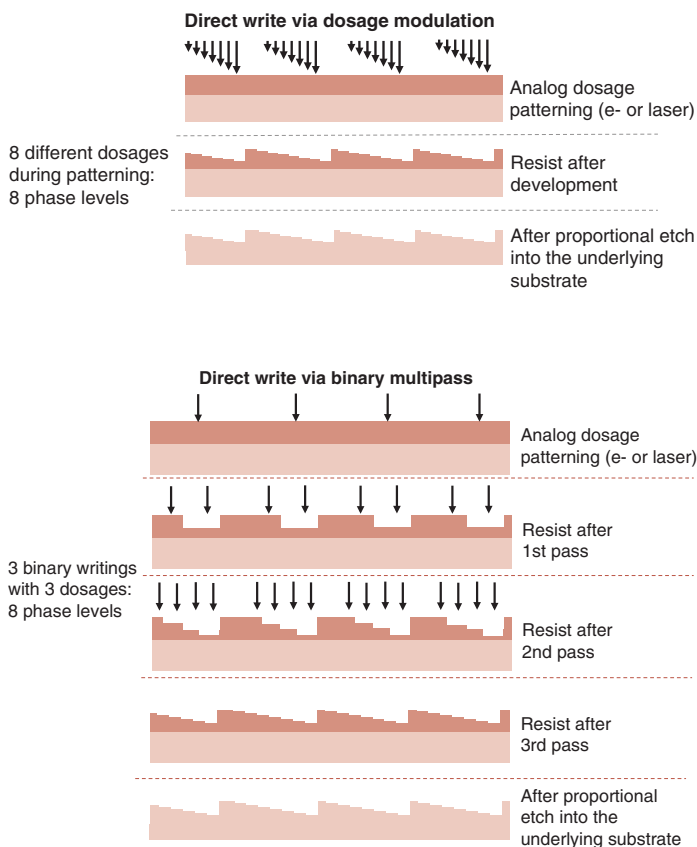
- The **depth of focus** of projection optics is

$$\delta z = \pm 0.5 \frac{\lambda}{NA^2} = k_2 \frac{\lambda}{NA^2}$$

where k_2 is a parameter with a value between 0.5 and 1.0, depending on the technology used.

Direct-Write Lithography

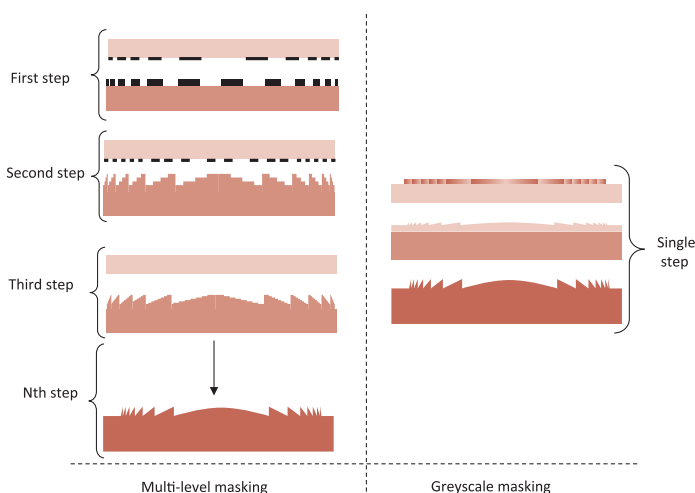
Direct write (via e-beam or laser beam), both binary and analog, is a good alternative to costly multilevel lithography to produce high-quality masters (after proportional RIE transfer), which are used as masters for replication (nano-imprint, embossing, molding) rather than tooling for lithography (masks, reticle).



Greyscale Masking Techniques

Greyscale masking uses a single optical-lithography step to produce a multilevel or quasi-analog surface-relief profile in the resist spun on the wafer. There are two primary techniques:

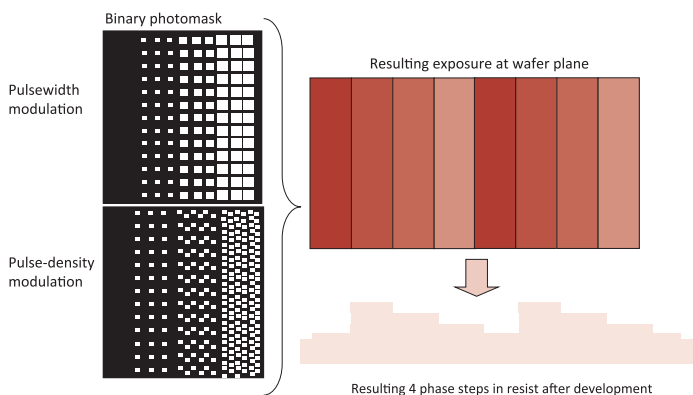
- **Analog masking** requires a mask that has real greyscale transmission, such as **high-energy beam-sensitive (HEBS) glass**, and a contact mask alignment or high-resolution stepper projection.
- **Binary masking** uses traditional chromium-on-glass masks, in which the greyscale function is encoded as a binary pulsewidth or pulse-density modulation. The quasi-analog illumination is produced in the vicinity of the mask by using the mask aligner in proximity mode (from a distance of 30–100 μm).



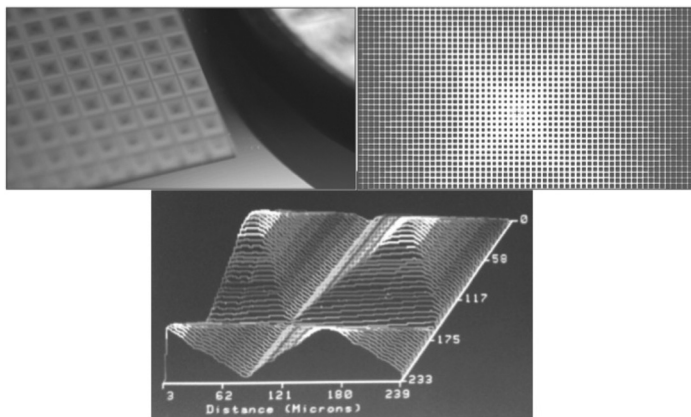
In many cases, binary masking is preferred over analog because of the simplicity of the process and the costs of a standard mask. However, the resolution of the features produced by binary masking are large—ill-suited to diffractive optics but ideal for refractive micro-optics, such as MLAs, lenticular lens arrays, and refractive beam shapers.

Greyscale Lithography (Binary)

Binary greyscale masking is similar to the greyscale image coding used by traditional laser printers. Many greyscale encoding schemes have been developed, such as PWM, PDM, and error diffusion. The following figure shows a four-phase-level grating period encoded as PWM or PDM in a conventional, binary Cr mask. The resolution of the mask is much higher than the resolution of the lithography tool (intentionally reduced in proximity lithography, e.g., a 30- μm gap in contact aligners).

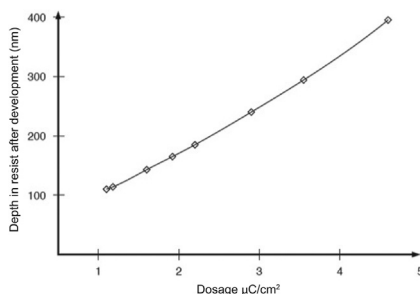


The following example shows the greyscale pattern used to produce an analog pyramid array in fused silica.

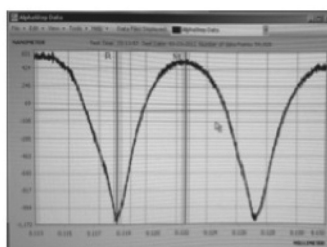
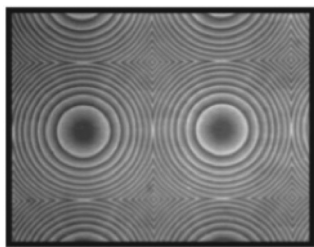


Greyscale Lithography (HEBS)

Analog greyscale lithography uses a true analog amplitude mask in which the absorption coefficient can be varied from 0 to 1. Various materials have been tested with mixed success. Inorganic resists, such as SeGe, silver halides, and, more recently, **HEBS glass**, have been used. HEBS glass is sensitive to both electron-beam and laser-beam exposure. The figure on the right shows the depth in the resist achieved after analog two-beam exposure/development. The HEBS-glass process is a good alternative to multiple binary-mask exposures, especially when producing thin microstructures, such as analog surface-relief diffractives. Microrefractives have also been produced by HEBS glass, as well as hybrid structures, with limited sag depths of around 50 μm after RIE transfer. The resolution of the HEBS glass is reduced by the diffusion process in the glass. Analog greyscale glass with smaller diffusion cones has been developed, such as the **light-absorbing film (LAF)** material.

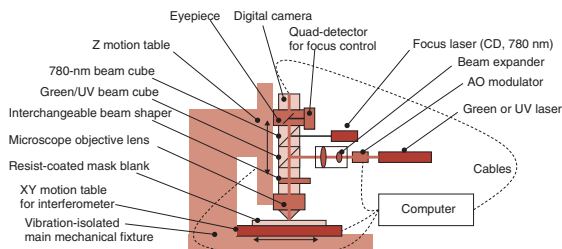


The following figures show an analog surface-relief diffractive lens produced by a HEBS-glass greyscale masking (left) and a refractive MLA (right) in fused silica.

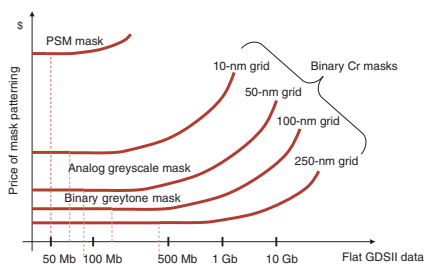
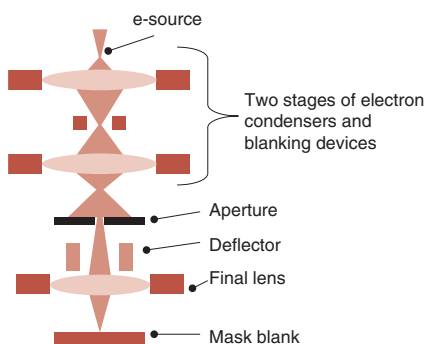


Photomask Patterning

Photomask patterning (or reticle patterning) is the first step for a lithographic fabrication process. After the GDSII layout is generated, the job deck and the layouts (tape-out) are sent to the mask shop. The **critical dimension** (CD), as well as the tolerance, will dictate which tool is most suitable for the patterning process (laser beam or e-beam).



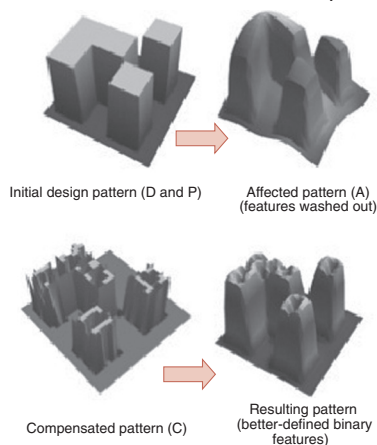
The price of a mask is related not only to the desired resolution and target CD dimension at $1\times$ (mask aligner) or $4\text{--}5\times$ (stepper) but also to the amount of data in the layout. For micro-optics, the layout is usually flat (not a hierarchy or replication, as in IC patterns, unless the optics are set in an array); therefore, the layout can be quite large (a few gigabytes of flat GDSII data). The following chart shows typical prices for standard and greyscale masks as a function of the flat-layout data file size in GDSII.



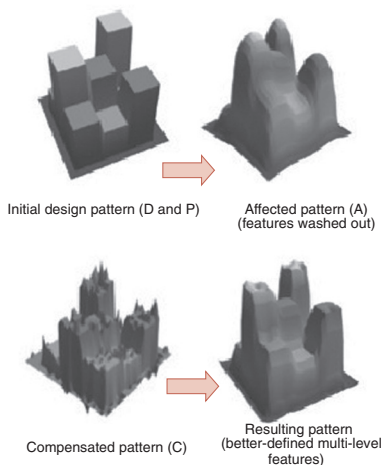
Optical Proximity Correction

Similar to the **optical proximity correction** (OPC) used in traditional IC mask layouts, correction is often required when patterning micro-optics in resist, either by e-beam lithography or by optical lithography. The following figure shows OPC applied to binary structures and multilevel structures typical for a CGH optical element.

2D EPE effects in e-beam resist and numeric compensation

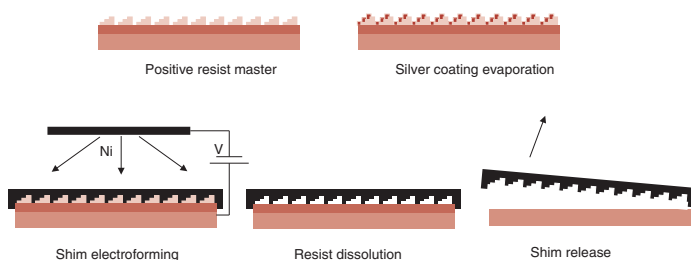


3D EPE effects in e-beam resist and numeric compensation



Replication Shim

For cost-effective mass production of wafer-scale micro-optics, a plastic **replication** process often provides the best results. The first step is the production of a negative mold that can be used in either embossing, casting, or molding. A positive master can be fabricated by traditional lithography/etching or by diamond turning/milling. This master is then placed in an electrolytic bath that will grow a thin metallic layer (usually nickel), which will form the negative mold (or **shim**).



This shim is then replicated and used in the final replication tool (roll embossing, plate embossing, hot or UV embossing, UV casting, injection molding, CD-type injection molding, etc.).

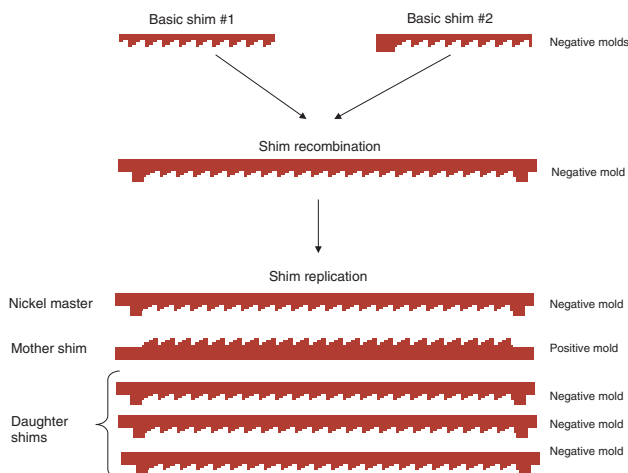
To compensate for mold wear-out, a set of similar molds are produced from the initial mold. Several positive shims are then grown (mother shims), and subsequent similar negative shims are created for the actual replication process (daughter shims).

When diamond-turning fabrication is used, the shim is directly turned in a metal and inserted in the final mold cavity. Turning metal usually provides better surface-roughness figures than turning plastic or glass. However, the waviness (peak-to-valley) of the embossed or injected part is usually worse than the mold itself.

Shrinkage during embossing must be accounted for, especially in the vertical direction for planar microstructures. A shrinkage of 5% is common.

Shim Recombination

Shim recombination is an important process in the generation of the final embossing/injection mold insert because it allows the use of larger embossing or molding widths than the original wafer, thereby reducing the cost.



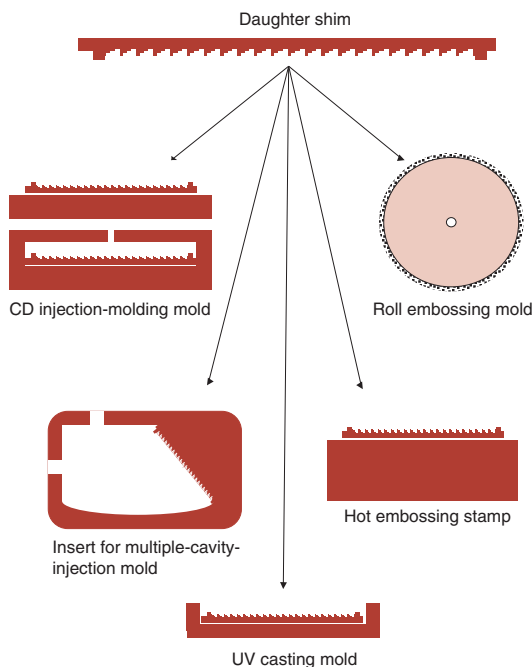
Such recombination processes are mastered by traditional holographic film replicators via roll-to-roll embossing, such as specialized holographic packaging paper. However, the CD can be as small as a few hundred nanometers with a standard replication process and a few tens of nanometers with UV embossing.

When stitching the shims together, it is important to understand that no matter how precise the stitching may be, it will never be as precise as the structure's alignment during lithography. For example, if the main pattern is a high-resolution grating, it might be best to stitch shims along the grooves rather than along the periods in order to prevent a moiré effect from appearing.

The recombination process is a very effective way to produce large shims for use with large-format roll-to-roll embossing equipment from a small initial master. However, stitching errors in shim recombination can be large.

Plastic Replication Technologies

After the shim is produced (through nickel electro-forming or diamond turning/milling), it can be used in various different **plastic replication techniques**, such as the ones shown below.

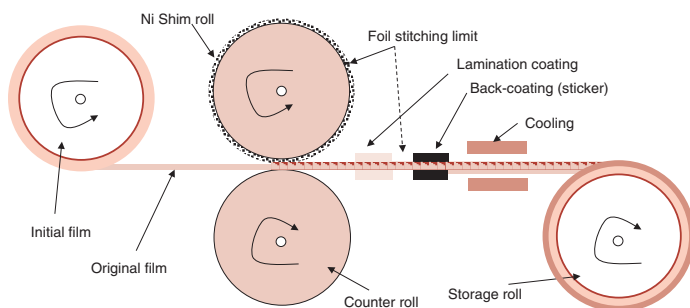


In addition to a shrinkage factor, one must account for various other artifacts that might appear after un-molding, including index gradients near injection ports.

For replication tasks, such as injection molding, the mold inserts can be directly produced by diamond turning of metal instead of nickel electroforming of shims (see previous page). Today, diamond turning machines (DTMs) can directly turn metal molds for simple surfaces (planar, spherical, or cylindrical), aspherics (toroids, even or odd aspheres, or off-axis surfaces), or even freeform surfaces [such as with the Moore 350FG (freeform generator) 5-axis DTM machine with a slow servo].

Roll-to-Roll UV Embossing

The **roll-to-roll embossing** process is a very cost-effective microstructure-replication process that can incorporate processes such as coating (reflective-metal AR coatings or custom dichroic coatings, backside-sticking layers, top lamination, etc.). The following figure shows a typical roll-to-roll embossing system.



The shim produced here is usually recombined to form a full width of the roll (a few feet). Typical roll materials can be PET or Mylar, and thicknesses can range from a few tens of microns to a few millimeters.

The depth of the structures that can be embossed via roll-to-roll vary from a few tens of nanometers to a few hundreds of microns (microrefractive). The lateral structures may vary in size from millimeters to sub-micron.

UV roll-to-roll embossing can also be used if the structures are sub-micron. It is possible to emboss structures that are tilted to the substrate, such as subwavelength slanted gratings, which can yield very interesting diffraction effects similar to the Bragg selectivity of traditional volume holograms.

Roll-to-roll has been used to produce analog-profile refractive MLAs, subwavelength gratings, nano-metric moth-eye structures, AR pyramid arrays, prism arrays (BEF films), binary diffractive structures, all manner of diffractive and refractive diffusers, and large-area refractive Fresnel lenses.

Plastics: Acrylic and Polycarbonate

The following tables list the various plastics currently used in the micro-optics replication industry, some as low-birefringence optical clear materials. These plastics can also be used as blanks for direct diamond turning or as plates for thermal embossing (roll-to-roll or plate).

Properties	Acrylic (PMMA)	Polycarbonate (PC)
Refractive index:	1.497	1.599
N_F (486.1 nm)	1.491	1.585
N_D (589.3 nm)	1.489	1.579
N_C (656.3 nm)		
Abbe value	57.2	34.0
Transmission [%] (visible spectrum, 3.174-mm thickness)	92	85–91
Detection temp: 3.6 F/min @ 66 psi 3.6 F/min @ 264 psi	214F/101C 198F/92C	295F/146C 288F/142C
Max. continuous service temp.	198F/92C	255F/124C
Water absorption [%] (in 73 F water for 24 h)	0.3	0.15
Specific gravity	1.19	1.20
Hardness	M97	M70
Haze [%]	1–2	1–2
Coeff. of linear exp. [cm $\times 10^{-5}$ /cm/C]	6.74	6.6–7.0
$dN/dT \times 10^{-5}/C$	–8.5	–11.8 to –14.3
Impact strength [ft·lb/in] (Izod notch)	0.3–0.5	12–17
Key advantages	Scratch resistance, chemical resistance, high Abbe, low dispersion	Impact strength, temperature resistance

Plastics: Polystyrene and Cyclic Olefin Copolymer

Properties	Polystyrene (PS)	Cyclic olefin copolymer
Refractive index:	1.604	1.540
N_F (486.1 nm)	1.590	1.530
N_D (589.3 nm)	1.584	1.526
N_C (656.3 nm)		
Abbe value	30.8	58.0
Transmission [%] (visible spectrum, 3.174-mm thickness)	87–92	92
Detection temp: 3.6 F/min @ 66 psi 3.6 F/min @ 264 psi	230F/110C 180F/82C	266F/130C 253F/123C
Max. continuous service temp.	180F/82C	266F/130C
Water absorption [%] (in 73 F water for 24 h)	0.2	<0.01
Specific gravity	1.06	1.03
Hardness	M90	M89
Haze [%]	2–3	1–2
Coeff. of linear exp. [cm $\times 10^{-5}$ /cm/C]	6.0–8.0	6.0–7.0
$dN/dT \times 10^{-5}/C$	–12.0	–10.1
Impact strength [ft-lb/in] (Izod notch)	0.35	0.5
Key advantages	Clarity, lowest cost	High moisture barrier, high modulus, good electrical properties

Plastics: Cyclic Olefin Polymer and Ultem 1010

Properties	Cyclic olefin polymer	Ultem 1010 (PEI)
Refractive index: N_F (486.1 nm) N_D (589.3 nm) N_C (656.3 nm)	1.537 1.530 1.527	1.689 1.682 1.653
Abbe value	55.8	18.94
Transmission [%] (visible spectrum, 3.174-mm thickness)	92	36–82
Detection temp: 3.6 F/min @ 66 psi 3.6 F/min @ 264 psi	266F/130C 263F/123C	410F/210C 394F/201C
Max. continuous service temp.	266F/130C	338F/170C
Water absorption [%] (in 73 F water for 24 h)	<0.01	0.25
Specific gravity	1.01	1.27
Hardness	M89	M109
Haze [%]	1–2	–
Coeff. of linear exp. [$\text{cm} \times 10^{-5}/\text{cm}/\text{C}$]	6.0–7.0	4.7–5.6
$dN/dT \times 10^{-5}/\text{C}$	–8.0	–
Impact strength [ft·lb/in] (Izod notch)	0.5	0.6
Key advantages	Low birefringence, chemical resistance, completely amorphous	Impact resistance, thermal & chemical resistance, high index

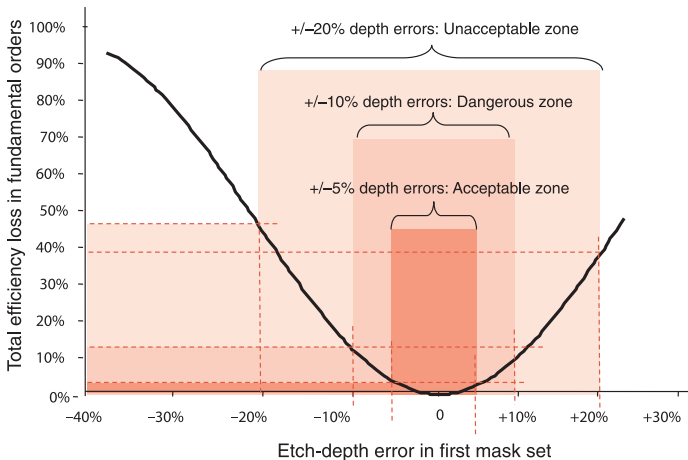
Effects of Fabrication Errors

There are two types of **fabrication errors** that can affect the efficiency of the micro-optics fabricated by lithography and/or plastic replication: random errors and systematic errors.

- **Random errors** are usually field-alignment errors that differ from wafer to wafer, as well as etch-depth errors.
- **Systematic errors** are linked to the optics used for lithography and are, for example, optical proximity errors.

For microrefractive optics, the results are usually a deterioration of the imaging qualities of the lens and an increase in surface roughness.

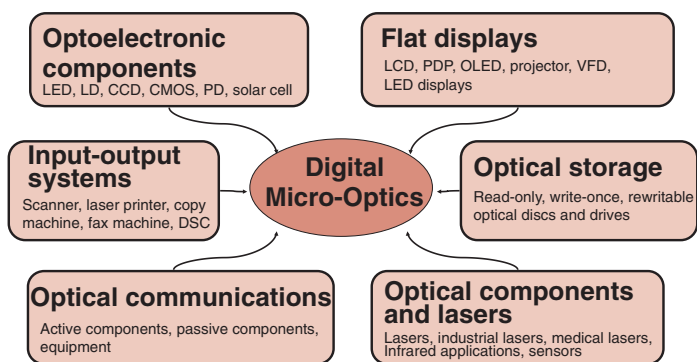
For diffractive optics, the main result is usually the reduction of the diffraction efficiency due to etch-depth errors and the propagation of parasitic orders due to field misalignments.



Efficiency loss (i.e., an increase in zero-order light) in diffractives is especially harmful to the application if the zero order falls into a region that consists of or is close to the order used in this application. Thus, it is often desirable to design the element as an off-axis element to prevent zero-order contamination.

Micro-Optics in Industry

The **micro-optics industry** (foundries and product integrators) has shown solid growth in the past decade, with a compound annual growth rate (CAGR) well into the double digits. Although wafer-level micro-optic fabrication (etched, fused silica or silicon in refractives or diffractives) are best suited for demanding applications in prototypes and low volumes (optical telecom, high-energy flux, or environmentally challenging applications), polymer micro-optics replicated by either injection molding or embossing (roll-to-roll) are best suited for high-volume consumer electronic devices (display, imaging, sensing) or disposable medical devices (sensors). Such devices should last through typical consumer electronics lifecycles of no more than 2–3 years.



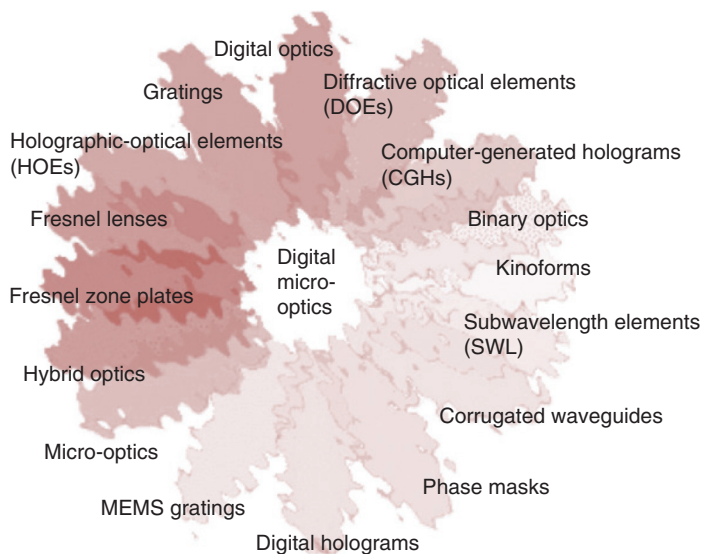
Although the consumer market quickly adopted polymer optics—such as MLAs in digital imaging/projection and OPU, and diffractives (optical scanners, depth-map sensors), it has been slower to adopt volume holograms, primarily due to environmental stability concerns (DCG, silver halides, etc.). However, recent developments in environmentally stable photopolymers [by Bayer (Germany), Dupont (US), and DNP (Japan)] have proven that such materials may be ready. More-specific metamaterials, nano-antenna optics, surface plasmonics, and photonic crystals are poised to handle tomorrow's challenging applications, and specific nano-replication technologies are already showing progress towards this goal.

Applications of Micro-Optics

Digital-optics **applications** have been relatively slow to emerge, primarily limited to R&D applications, with some exceptions being optical security tags, spectroscopy, optical data storage, and optical telecom.

However, thanks to optical needs for new consumer electronics (gaming, displays, pico-projectors, and, more generally, mobile or wearable computing), digital micro-optics are emerging as an important tool in today's optical engineer's toolbox. Low costs and mass replication make them a perfect candidate for various mobile computing needs. According to Intel, digital optics is one of the ten technologies that will meet tomorrow's constantly evolving computing needs.

A few applications worth noting include Canon's hybrid zoom; Microsoft Kinect's structured-light pattern generator; wafer-scale-camera objective lenses; and LCD micro-optics films, such as BEFs, DBEFs, and diffusers.



The industry has come a long way from the first applications of gratings in spectroscopy a few decades ago.

Equation Summary

Snell's law and grating equation:

$$\begin{cases} \sin(\alpha + \gamma) = n \sin(\gamma) & \text{(A)} \\ \sin(\beta) = \frac{\lambda}{\Delta} & \text{(B)} \end{cases}$$

Equating refractive and diffractive angles:

$$\alpha = \beta \Rightarrow h_{\text{opt}} = \frac{\lambda}{n - \sqrt{1 - \left(\frac{\lambda}{\Delta}\right)^2}} \rightarrow \approx \frac{\lambda}{n - 1} \quad \text{for } \lambda \ll \Delta$$

TIR angle (critical angle):

$$\alpha_t = \arcsin\left(\frac{n_2}{n_1}\right)$$

Numerical aperture of a fiber:

$$NA = \sin(\varphi) = \sqrt{n_1^2 - n_2^2}$$

Normalized frequency for a step-index fiber:

$$w = 2a \left(0.65 + \frac{1.619}{V^{3/2}} + \frac{2.879}{V^6} \right)$$

Insertion losses from fiber butt-coupling:

$$\left\{ \begin{array}{l} \text{offset loss} = \left(\frac{2w_1w_2}{w_1^2 + w_2^2} \right)^2 e^{-2 \frac{d^2}{w_1^2 + w_2^2}} \\ \text{tilt loss} = \left(\frac{2w_1w_2}{w_1^2 + w_2^2} \right)^2 e^{-2 \frac{(\pi n_2 w_1 w_2 \varphi)^2}{\lambda^2 (w_1^2 + w_2^2)}} \\ \text{gap loss} = \frac{4 \left(4Z^2 + \frac{w_1^2}{w_2^2} \right)}{4Z^2 \left(1 + \frac{w_1^2}{w_2^2} \right) + \frac{w_1^2 + w_2^2}{w_2^2}}, \text{ where } Z = \frac{g\lambda}{2\pi n_2 w_1 w_2} \end{array} \right.$$

Equation Summary

Spectral resolving power of a prism:

$$R_{\text{prism}} = \frac{\lambda_0}{\delta\lambda} = b \frac{\partial}{\partial\lambda}(n)$$

Spectral resolving power of a grating:

$$R_{\text{grating}} = \frac{\lambda_0}{\delta\lambda} = mN_0$$

Beam-steering angle from lateral MLA displacement:

$$\varphi = -\arctan\left(\frac{\Delta x}{df\#}\right)$$

Angular dispersion of a reflective grating:

$$D = \frac{\partial\beta}{\partial\lambda} = \frac{m}{\Lambda\cos\beta} = \frac{\sin\alpha + \sin\beta}{\lambda\cos\beta}$$

Spectral resolution of a reflective grating:

$$R = \frac{\lambda}{\delta\lambda} = mN_0 = \frac{N_0\Delta(\sin\alpha + \sin\beta)}{\lambda}$$

Maximum resolving power of a reflective grating:

$$R_{\text{max}} = \frac{2W}{\lambda}$$

Free spectral range of a reflective grating:

$$\begin{cases} F_\lambda = \Delta\lambda = \frac{\lambda_1}{m} \\ \lambda_1 + \Delta\lambda = \frac{m+1}{m}\lambda_1 \end{cases}$$

Fourier expansion of a binary amplitude grating:

$$a(x, y) = \begin{cases} 1 & \text{if } m\Lambda \leq x \leq c + m\Lambda \\ 0 & \text{elsewhere} \end{cases} \Rightarrow$$

$$a(x, y) = \frac{c}{\Lambda} \sum_{m=-\infty}^{+\infty} e^{-i\pi\left(\frac{mc}{\Lambda}\right)} \frac{\sin\left(m\pi\frac{c}{\Lambda}\right)}{m\pi\frac{c}{\Lambda}} e^{2i\pi\frac{x}{\Lambda}}$$

Equation Summary

Diffraction efficiency of binary amplitude gratings:

Duty cycle c	Symmetric
$\eta_m = \left \frac{\sin\left(m\pi \frac{c}{\Lambda}\right)}{m\pi} \right ^2$	$\eta_m = \left \frac{\sin\left(\frac{m\pi}{2}\right)}{m\pi} \right ^2$

Phase profile of a diffractive spherical lens in successive zones:

$$\begin{cases} \phi(r, \lambda) = 2\pi\alpha \left(i - \frac{\sqrt{r^2 + f^2} - f}{\lambda_0} \right), r_i \leq r \leq r_{i+1} \\ \alpha = \frac{\lambda_0}{\lambda} \left[\frac{n(\lambda) - 1}{n(\lambda_0) - 1} \right] \end{cases}$$

Sag equation describing aspheric phase profiles:

$$\theta(r) = \frac{2\pi}{\lambda} \left(\frac{Cr^2}{1 + \sqrt{1 - (A+1)r^2C^2}} \right) + \sum_{i=1}^N C_i r^{2i}$$

Circularly symmetric phase profile description:

$$\theta(r) = \sum_{i=2}^n C_i r^i$$

General xy aspheric phase profile:

$$\theta(x, y) = \sum_{j=1}^m \sum_{i=1}^n C_i x^i \cdot C_j y^j$$

f -number of a lens:

$$f\# = \frac{f}{D}$$

Numerical aperture of a diffractive lens:

$$NA = \sin(\alpha_{\max}) = \frac{\lambda}{\Lambda_{\min}} = \sin\left(\arctan\left(\frac{D}{2f}\right)\right) = \frac{D}{2f}$$

Smallest feature size in a diffractive lens:

$$\delta = \frac{\lambda}{pNA} = \frac{\Lambda_{\min}}{p}$$

Equation Summary

Depth of focus of a spherical lens:

$$DOF = 2\lambda f\#^2$$

Shift in focal length in a diffractive lens as a function of wavelength drift:

$$\begin{cases} \phi(x) = \exp\left(-i\pi \frac{x^2}{\lambda_0 f_0}\right) \Rightarrow f(\lambda) = \frac{\lambda_0 f_0}{\lambda} \\ \lambda_0 f_0 = \text{constant} \end{cases}$$

Abbe V numbers for diffractive and refractive lenses:

$$\begin{cases} V_{\text{ref}} = \frac{n_{\lambda_2} - 1}{n_{\lambda_1} - n_{\lambda_3}} \\ V_{\text{dif}} = \frac{\lambda_2}{\lambda_1 - \lambda_3} \end{cases}$$

Effective focal length of a hybrid diffractive/refractive singlet:

$$\frac{1}{f_{\text{doublet}}} = \frac{1}{f_{\text{ref}}} + \frac{1}{f_{\text{dif}}}$$

Zernike wavefront description polynomial:

$$\phi(r, \varphi) = \sum a_{m,n} Z_{m,n}(r, \varphi)$$

Zernike orthogonal phase states:

$$\begin{cases} Z_{0,0} = 1 & \rightarrow \text{piston} \\ Z_{1,-1} = 2r\sin(\varphi) & \rightarrow \text{tip} \\ Z_{1,1} = 2r\cos(\varphi) & \rightarrow \text{tilt} \\ Z_{2,-2} = \sqrt{6}r^2\sin(2\varphi) & \rightarrow \text{astigmatism} \\ Z_{2,0} = \sqrt{3}(2r^2 - 1) & \rightarrow \text{focus} \\ Z_{2,2} = \sqrt{6}r^2\cos(2\varphi) & \rightarrow \text{astigmatism} \end{cases}$$

Space-bandwidth product of a CGH:

$$SBWP = \frac{NM}{c_x c_y} P$$

Equation Summary

Zero-order grating condition (no orders diffracted):

$$\frac{\Lambda}{\lambda} < \frac{1}{\max\{\sqrt{\epsilon_{\text{I}}}, \sqrt{\epsilon_{\text{III}}}\} + \sqrt{\epsilon_{\text{II}} \sin^2 \theta_{\text{max}}}}$$

Maxwell's time harmonic equations:

$$\begin{cases} \text{curl}(\vec{E}) = -\mu \frac{\partial \vec{H}}{\partial t} \\ \text{curl}(\vec{H}) = \epsilon \frac{\partial \vec{E}}{\partial t} \\ \text{div}(\epsilon \vec{E}) = 0 \\ \text{div}(\mu \vec{H}) = 0 \end{cases}$$

Quality factor of volume holograms:

$$Q = \frac{2\pi\lambda d}{n\Delta^2 \cos\alpha}$$

Interference pattern from the interference between reference and object waves:

$$I(x, y) = |O + R|^2 = OO^* + RR^* + OR^* + O^*R$$

Transmittance function from holographic interference pattern:

$$T = C + \zeta(|O|^2 + O^*R + OR^*)$$

Grating vector:

$$\begin{cases} \vec{K} = K(\cos(\Phi)\vec{z} + \sin(\Phi)\vec{x}) \\ K = \frac{2\pi}{\Lambda} \\ n(x, z) = n_0 + \Delta n(x, z) \end{cases}$$

Grating strength of a Bragg grating:

$$\nu_s = \frac{\pi \Delta n d}{\lambda \sqrt{c_r c_s}}$$

Equation Summary

Strain expression in an active EAP:

$$S = \frac{1}{\sqrt{1 - \epsilon_r \epsilon_0 \frac{V^2}{Yl^2}}} - 1$$

Rayleigh–Sommerfeld diffraction integral:

$$U'(x'_1, y'_1, z'_1) = \frac{-i}{2} \iint_{S_0} \frac{e^{ikr_{01}}}{|\vec{r}_{01}|} \cos(\vec{n}, \vec{r}_{01}) ds$$

Direct Fresnel integral:

$$U(x', y') = \left(\frac{e^{ikd}}{ikd} \right) e^{i\frac{\pi}{\lambda d}(x'^2 + y'^2)} \iint_{\infty} U(x, y) e^{i\frac{\pi}{\lambda d}(x^2 + y^2)} e^{-i\frac{2\pi}{\lambda d}(x'x + y'y)} dx dy$$

Convolution-based Fresnel integral:

$$U(x', y') = \left(\frac{e^{ikd}}{ikd} \right) \iint_{\infty} U(x, y) e^{i\frac{\pi}{\lambda d}((x'-x)^2 + (y'-y)^2)} dx dy$$

Minimum distance for scalar near-field description:

$$Z_{\min} \approx Nc \frac{1}{2(\beta - \alpha)} \propto 5Nc$$

Rayleigh distance (far-field limit):

$$R = \frac{2p^2}{\lambda} \Rightarrow \begin{cases} R_x = 8 \frac{c_x^2}{\lambda} \\ R_y = 8 \frac{c_y^2}{\lambda} \end{cases}$$

Rayleigh–Sommerfeld integral showing the obliquity factor:

$$U'(x'_1, y'_1, z'_1) = \frac{-i}{2} \iint_{S_0} \frac{e^{ikr_{01}}}{|\vec{r}_{01}|} \cos(\vec{n}, \vec{r}_{01}) ds$$

Equation Summary

Obliquity factor in the Rayleigh–Sommerfeld integral:

$$\cos(\vec{n}, \vec{r}_{01}) = \frac{\vec{n} \cdot \vec{r}_{01}}{|\vec{n}| |\vec{r}_{01}|} \approx \frac{1}{\sqrt{1 + \frac{x_r^2 + y_r^2}{z_r^2}}} \quad \text{where} \quad \begin{cases} x_r = x'_k - x_n \\ y_r = y'_l - y_m \\ z_r = z'_{k,l} - z_{n,m} \end{cases}$$

Point spread function of a lithography tool:

$$I(x) = I_0 \left(2 \frac{J_1(x)}{x} \right)^2$$

Resolution due to the partial coherence of an illumination system:

$$\delta x = k_1 \frac{\lambda}{(\sigma + 1)NA}$$

Depth of focus for a lithographic projection lens:

$$\delta z = \pm 0.5 \frac{\lambda}{NA^2} = k_2 \frac{\lambda}{NA^2}$$

Bibliography

J. P. Allebach, "Representation related errors in binary digital holograms: a unified analysis," *Appl. Opt.* **20**(2), 290–299, (1981).

H. Andersson et al., "Single photomask multilevel kinoforms in quartz and photoresist: manufacture and evaluation," *Appl. Opt.* **29**(28), 4259–4267 (1990).

G. P. Behrmann et al., "Color correction in athermalized hybrid lenses," *OSA Tech. Digest* **9**, 67–70 (1993).

B. E. Bernacki et al., "Hybrid optics for the visible produced by bulk casting of sol-gel glass using diamond turned molds," *Proc. SPIE* **2536**, 463–474 (1995) [doi: 10.1117/12.218453].

S. Biehl, R. Danzebrink, P. Oliveira, and M. A. Aegerter, "Refractive microlens fabrication by ink-jet process," *J. Sol-Gel Sci. Technol.* **13**(1/3), 177–182 (1998).

M. Born and E. Wolf, *Principles of Optics*, 6th Ed., Pergamon Press, London (1980).

J. Braat, "Effects of lens distortion in optical step-and-scan lithography," *Appl. Opt.* **35**(4), 690–700 (1996).

B. R. Brown and A. W. Lohmann, "Computer-generated Binary Holograms," *IBM J. Res. Dev.* **13**, 160–168 (1969).

K.-H. Brenner et al., "Application of three-dimensional micro-optical components formed by lithography, electroforming and plastic molding," *Appl. Opt.* **32**(32), 6464–6469 (1993).

T. Brunner, "Impact of lens aberrations on optical lithography," *IBM J. Res. Develop.* **41**(1), 57–67 (1997).

S. Y. Chou, P. R. Krauss, and W. Zhang, "Sub-10 nm imprint lithography and applications," *J. Vac. Sci. Tech. B.* **15**(6), 2897–2904 (1997).

P. Clarck, "Ray-tracing models for Diffractive Optical Elements," *OSA Tech. Digest* **8**, 2–3 (1993).

Bibliography

- N. Cobb and A. Zakhor, "Fast sparse aerial-image calculation for OPC," *Proc. SPIE* **2621**, 534–545 (1995) [doi: 10.1117/12.228208].
- L. G. Commander, S. E. Day, and D. R. Selviah, "Variable focal length microlenses," *Opt. Comm.* **177**(1–6), 157–170 (2000).
- J. A. Cox, B. S. Fritz, and T. R. Werner, "Process-dependant kinoform performances," *Proc. SPIE* **1507**, 100–109 (1991) [doi: 10.1117/12.47032].
- X.-Y. Da, "Talbot effect and the array illuminators that are based on it," *Appl. Opt.* **31**(16), 2983–2986 (1992).
- W. Däschner, P. Long, R. Stein, C. Wu, and S. Lee, "One step lithography for mass production of multilevel diffractive optical elements using high energy beam sensitive (HEBS) grey-level masks," *Proc. SPIE* **2689**, 153–155 (1996) [doi: 10.1117/12.239618].
- W. Däschner, P. Long, R. Stein, C. Wu, and S. Lee, "General aspheric refractive Micro Optics fabricated by optical lithography using a high energy beam sensitive (HEBS) glass grey level mask," *Vac. Sci. Technol. B* **14**, 3730–3733 (1996).
- D. Daly, *Microlens Arrays*, Taylor & Francis, London (2001).
- D. Daly, R. F. Stevens, M. C. Hutley, and N. Davies, "The manufacture of microlenses by melting photoresist," *Meas. Sci. Technol.* **1**(8), 759–766 (1990).
- H. Dammann, "Blazed synthetic phase-only holograms," *Optik* **31**, 95–104 (1970).
- H. Dammann and K. Görtler, "High-efficiency in-line multiple imaging by means of multiple phase holograms," *Opt. Commun.* **3**, 312–315 (1971).
- P. Dannberg et al., "Wafer scale integration of micro-optic and optoelectronic elements by polymer UV reaction moulding," *Proc. SPIE* **3631**, 244–251 (1999) [doi: 10.1117/12.348319].

Bibliography

- L. d'Auria, J.-P. Huignard, and A. M. Roy, "Photolithographic fabrication of thin film lenses," *Opt. Commun.* **5**(4), 232–235 (1972).
- L. H. Domash et al., "Switchable-focus lenses in holographic polymer-dispersed liquid crystal," *Proc. SPIE* **2689**, 188–194 (1995) [doi: 10.1117/12.239623].
- M. Duparré, "Investigations of computer-generated diffractive beam shapers for flattening of single-modal CO₂ laser beams," *Appl. Opt.* **34**(14), 2489–2497 (1995).
- R. Eschbach, "Comparison of error diffusion methods for computer generated holograms," *Appl. Optics* **30**(26), 3702–3710 (1991).
- M. Fally, M. Ellabban, and I. Drevensek-Olenik, "Out-of-phase mixed holographic gratings: a quantitative analysis," *Opt. Express* **16**(9), 6528–6536 (2008).
- M. W. Farn, "Design and Fabrication of Binary Diffractive Optics," Doctoral thesis, Stanford University, Stanford, CA (1990).
- M. W. Farn, "Effects of VLSI fabrication errors on kinoform efficiency," *Proc. SPIE* **1211**, 125–136 (1991) [doi: 10.1117/12.17929].
- M. W. Farn and J. W. Goodman, "Diffractive doublets corrected at two wavelengths," *J. Opt. Soc. Am. A* **8**(6), 860 (1991).
- J. R. Fienup, "Iterative method applied to image reconstruction and to computer generated holograms," *Opt. Eng.* **19**(3), 297–305, (1980) [doi: 10.1117/12.7972513].
- T. Fujita, H. Nishihara and J. Koyama, "Blazed gratings and Fresnel lenses fabricated by electron-beam lithography," *Opt. Lett.* **7**(12), 578–580 (1982).
- D. Gabor, "A new microscopic principle," *Nature* **161** (4098), 777–778 (1948).

Bibliography

M. T. Gale, "Continuous relief diffractive optical elements for two-dimensional array generations," *Appl. Opt.* **32**(14), 2526–2533 (1993).

M. T. Gale et al., "Fabrication of micro-optical elements by laser beam writing in photoresist," *Proc. SPIE* **1506**, 65–70 (1991) [doi: 10.1117/12.45959].

M. T. Gale, M. Rossi, J. Pedersen, and H. Schütz, "Fabrication of continuous-relief micro-optical elements by direct laser writing in photoresist," *Opt. Eng.* **33**, 3556–3566 (1994) [doi: 10.1117/12.179892].

T. K. Gaylor and M. G. Moharam, "Thin and thick gratings: terminology clarification," *Appl. Opt.* **20**(19), 3271–3273 (1981).

R. W. Gerchberg and W. O. Saxton: "A practical algorithm for the determination of phase from image and diffraction plane pictures," *Optik* **35**(2), 237–246 (1972).

M. Goel and D. L. Naylor, "Analysis of design strategies for Dammann gratings," *Proc. SPIE* **2689**, 35–45 (1996) [doi: 10.1117/12.239636].

J. W. Goodman, *Introduction to Fourier Optics*, McGraw Hill, New York (1968).

R. Gruhlke, "Diffractive optics for industrial lasers: Effects of fabrication error," *Proc. SPIE* **1751**, 118–127, (1992) [doi: 10.1117/12.138873].

C. W. Haggans et al., "Effective-medium theory of zeroth-order lamellar gratings in conical mounting," *J. Opt. Soc. Am. A* **10**(10), 2217–2225 (1993).

P. Hariharan, *Optical Holography*, Cambridge University Press, Cambridge (1984).

H.-P. Herzig, *Micro-Optics: Elements, Systems and Applications*, Taylor and Francis, London (1997).

M. C. Hutley, *Diffraction Gratings*, Academic Press, London (1982).

Bibliography

K. Iga, Y. Kokubun, and M. Oikawa, *Fundamentals of Micro-Optics*, Academic Press, New York (1984).

J. Jahns, “Two-dimensional array of diffractive microlenses fabricated by thin film deposition,” *Appl. Opt.* **29**(7), 931–936 (1990).

T. R. Jay, M. B. Stern, and R. E. Knowlden, “Effect of refractive microlens array fabrication parameters on optical quality,” *Proc. SPIE* **1751**, 236–245 (1992) [doi: 10.1117/12.138886].

B. K. Jennisson, “Analysis of the leakage from computer-generated holograms synthesized by direct binary search,” *J. Opt. Soc. Am. A* **6**(2), 234–243 (1989).

A. Kathman, “Phase grating optimization using genetic algorithms,” *OSA Tech. Digest* **9**, 71–73 (1993).

E.-B. Kley, H.-J. Fuchs, and A. Kilian, “Fabrication of glass lenses by melting technology,” *Proc. SPIE* **4440**, 85–92 (2001) [doi: 10.1117/12.448027].

E.-B. Kley, F. Thomas, U. D. Zeitner, L. Wittl, and H. Aagedal, “Fabrication of micro optical surface profiles by using grayscale masks,” *Proc. SPIE* **3276**, 254–262 (1997) [doi: 10.1117/12.302404].

H. Kogelnik, “Coupled-wave theory for thick hologram gratings,” *Bell Syst. Tech. J.* **48**(9), 2909–2947 (1969).

U. Kohler et al., “Fabrication of microlenses by combining silicon technology, mechanical micromachining and plastic molding,” *Proc. SPIE* **2687**, 18–22 (1996) [doi: 10.1117/12.234632].

R. K. Kostuk, “Hybrid diffractive elements for planar optics,” *OSA Tech. Digest* **9**, 38–41 (1993).

M. Kulishov et al., “Nonreciprocal waveguide Bragg gratings,” *Opt. Express* **13**(8), 3068–3078 (2005).

G. N. Laurence, “Using rules of thumb in the design of physical optics systems,” *OSA Tech. Digest* **9**, 12–13 (1993).

Bibliography

B. Layet, I. G. Cormack, and M. R. Taghizadeh, "Stripe color separation with diffractive optics," *Appl. Opt.* **38**, 7193–7201 (1999).

W.-H. Lee, "Method for converting a Gaussian laser beam into a uniform beam," *Opt. Commun.* **36**(6), 469–471 (1981).

D. Leseberg, "Computer-generated holograms: cylindrical, conical and helical waves," *Appl. Opt.* **26**(20), 4385–4390 (1987).

B. Lesem, P. M. Hirsch and J. Jordan, "The kinoform: a new wavefront reconstruction device," *IBM J. Res. Dev.* **13**, 150–155 (1969).

M. D. Levenson et al., "The phase-shifting mask II: imaging simulations and submicrometer resist exposures," *IEEE Trans. Electron Devices* **31**(6), 753–763 (1984).

B. J. Lin, "Where is the lost resolution?" *Proc. SPIE* **0633**, 44–40 (1986) [doi: 10.1117/12.963701].

A. W. Lohman and D. P. Paris, "Binary Fraunhofer holograms generated by computer," *Appl. Opt.* **6**, 1739–1748 (1967).

C. W. Londoño, W. T. Plummer, and P. P. Clark, "Athermalization of a single-component lens with diffractive optics," *Appl. Opt.* **32**(13), 2295–2302 (1993).

C. W. Londoño, "Hybrid diffractive/refractive lenses and achromats," *Appl. Opt.* **27**(14), 2960–2971 (1988).

C. Y. Luo, S. G. Johnson, J. D. Joannopoulos, and J. B. Pendry, "Sub-wavelength imaging in photonic crystals," *Phys. Rev. B*, **68**, 045115 (2003).

U. Mahlab, "Genetic algorithm for optical pattern recognition" *Opt. Lett.* **16**(9), 648–650 (1991).

E. W. Marchand and E. Wolf, "Boundary diffraction wave in the domain of the Rayleigh–Kirchhoff diffraction theory," *J. Opt. Soc. Am.* **52**(7), 761–767 (1962).

Bibliography

- S. Masuda, T. Nose, and S. Sato, "Optical properties of a polymer-stabilized liquid crystal microlens," *Japan J. Appl. Phys.* **37**, L1251–L1253 (1998).
- J. M. Miller, "Multilevel-grating array generators: fabrication error analysis and experiments," *Appl. Opt.* **32**(14), 2519–2525 (1993).
- S. E. Miller, "Integrated optics: an introduction," *Bell Sys. Tech. J.* **48**, 2059–2068 (1969).
- K. Miyamoto, "The phase Fresnel lens," *J. Opt. Soc. Am.* **17**, 17–21 (1961).
- M. G. Moharam and T. K. Gaylord, "Rigorous coupled-wave analysis of planar grating diffraction," *J. Opt. Soc. Am.* **71** (7), 811–818 (July 1981).
- D. T. Moore, ed., *Selected Papers on Gradient-Index Optics*, SPIE Press, Bellingham, WA (1993).
- M. E. Motamedi, W. H. Southwell, and W. J. Gunning, "Antireflection surfaces in silicon using binary optic technology," *Appl. Opt.* **31**(22), 4371–4376 (1992).
- M. E. Motamedi et al., "Micro-optic integration with focal plane arrays," *Opt. Eng.* **36**(5), 1374–1381 (1997) [doi: 10.1117/1.601347].
- C. Neipp, I. Pascual, and A. Belendez, "Experimental evidence of mixed gratings with a phase difference between the phase and amplitude grating in volume holograms," *Opt. Express* **10**(23), 1374–1383 (2002).
- A. R. Nelson et al., "Computer-generated electrically switchable holographic composites," *Proc. SPIE* **2404**, 132–143, (1995) [doi: 10.1117/12.207469].
- E. Noponen, "Complex amplitude modulation by high-carrier-frequency diffractive elements," *J. Opt. Soc. Am. A* **13**(7), 1422–1428 (1996).
- D. O'Shea, "Gray scale masks for diffractive optics fabrication: II. Spatially filtered halftone screens," *Appl. Opt.* **34**(32), 7518–7526 (1995).

Bibliography

- R. Petit et al., *Electromagnetic Theory of Gratings*, Springer-Verlag, Berlin (1980).
- R. D. Rallison, "Wavelength compensation by time-reverse ray tracing," in *Diffraction and Holographic Optics Technology II*, I. Cindrich and S. H. Lee, eds., 217–226 (1995).
- D. W. Ricks, "Scattering from diffractive optics," *Diffraction and Miniaturized Optics*, S. Lee, ed., SPIE Critical Reviews, 187–1211, SPIE Press, Bellingham, WA (1993).
- D. Schurig et al., "Metamaterial electromagnetic cloak at microwave frequencies," *Science* **314**(5801), 977–980 (2006).
- F. P. Shvartsman, "Holographic optical elements by dry photopolymer embossing," *Proc. SPIE* **1461**, 313–320 (1991) [doi: 10.1117/12.44742].
- F. P. Shvartsman, "SURPHEXTM: new dry photopolymers for replication of surface relief diffractive optics," *Proc. SPIE* **1732**, 121–130 (1993) [doi: 10.1117/12.140390].
- W. Singer, "Gradient index microlenses: numerical investigations of different spherical index profiles with the wave propagation method," *Appl. Opt.* **34**(13), 2165–2171 (1995).
- S. Sinzinger, "Transition between diffractive and refractive micro-optical components," *Appl. Opt.* **34**(26), 5970–5976 (1995).
- S. Sinzinger and J. Jahns, *Microoptics*, VCH, Weinheim, Germany (1999).
- D. R. Smith, J. B. Pendry, and M. C. K. Wiltshire, "Metamaterials and negative refractive index," *Science* **305**(5685), 788–792 (2004).
- S. Somekh, "Introduction to ion and plasma etching," *J. Vac. Sci. Technol.* **13**(5), 1003–1007 (1976).
- W. H. Southwell, "Ray-tracing kinoform lens surfaces," *Appl. Opt.* **31**(13), 2244–2247 (1992).
- G. H. Spencer and M. V. R. K. Murty, "General ray-tracing procedure," *J. Opt. Soc. Am.* **52**(6), 650 (1951).

Bibliography

M. B. Stern, "Fabricating binary optics: Process variables critical to optical efficiency," *J. Vac. Sci. Technol. B* **9**, 3117–3121 (1991).

T. J. Suleski, "Gray scale masks for diffractive optics fabrication: I. Commercial slide imagers," *Appl. Opt.* **34** (32), 7507–7517 (1995).

T. J. Suleski, B. Baggett, and W. F. Delaney, "Fabrication of high spatial frequency gratings through computer generated near-field holography," *Opt. Lett.* **24**(9), 602–604 (1999).

T. J. Suleski and R. D. TeKolste, "Roadmap for micro-optics fabrication," *Proc. SPIE* **4440**, 1–15 (2001) [doi: 10.1117/12.448025].

G. J. Swanson, *Binary Optics Technology: The theory and design of multi-level diffractive optical elements*, MIT/Lincoln Lab Tech. Report **854**, Lexington, MA (1989).

G. J. Swanson and W. B. Veldkamp, "Diffractive optical elements for use in infrared systems," *Opt Eng.* **28**, 605–608 (1989) [doi: 10.1117/12.7977008].

W. C. Sweatt et al., "Mass-producible microholographic tags," *Proc. SPIE* **2689**, 170–175 (1995) [doi: 10.1117/12.239621].

W. C. Sweatt, "Mathematical equivalence between a holographic optical element and an ultra-high index lens," *J. Opt. Soc. Am. A* **69**, 486–487 (1979).

M. Tanigami, "Low-wavefront aberration and high temperature stability molded micro-Fresnel lenses," *IEEE Photon. Technol. Lett.* **1**(11), 384–385 (1989).

R. D. TeKolste, W. H. Welch, and M. R. Feldman, "Injection molding for diffractive optics," *Proc. SPIE* **2404**, 129–131 (1995) [doi: 10.1117/12.207463].

J. Turunen and F. Wyrowsky, *Diffractive Optics for Industrial and Commercial Applications*, Akademie Verlag, Berlin (1997).

Bibliography

H.-G. Unger, *Planar Optical Waveguides and Fibers*, Clarendon Press, Oxford (1977).

K. S. Urquhart, R. Stein, and S. H. Lee, "Computer-generated holograms fabricated by direct write of positive electron-beam resist," *Opt. Lett.* **18**(4), 308–310 (1993).

M. V. Vasnetsov, "Oscillations conditions in a gain grating in the Bragg diffraction regime," *Opt. Commun.* **282**(10), 2028–2031 (2009).

W. B. Veldkamp, "Binary Optics: the Optics Technology of the Decade," *37th Int. Symp. Electron, Ion and Photon Beams*, San Diego, CA (1993).

W. B. Veldkamp and T. J. McHugh, *Binary Optics*, Scientific American **5**, 50–55 (1992).

E. A. Wilson, D. T. Miller, and K. J. Bernard, "Fill factor improvement using microlens arrays," *Proc. SPIE* **3276**, 123–133 (1998) [doi: 10.1117/12.302390].

A. Wong, *Optical Imaging in Projection Microlithography*, SPIE Press, Bellingham, WA (2005) [doi: 10.1117/3.612961].

F. Wyrowski, "Design theory of diffractive elements in the paraxial domain," *J. Opt. Soc. Am. A* **10**(7), 1553–1561 (1993).

F. Wyrowski, "Digital phase holograms: coding and quantization with an error diffusion concept," *Opt. Commun.* **72**(2), 37–41 (1989).

F. Wyrowski, "Iterative quantization of digital amplitude holograms," *Appl. Opt.* **28**(18), 3864–3870 (1989).

E. Yablonovitch, "Inhibited spontaneous emission in solid-state physics and electronics," *Phys. Rev. Lett.* **58**(20), 2059–2062 (1987).

E. Yablonovitch, "Photonic band-gap structures," *J. Opt. Soc., Am. B* **10**, 283–295 (1993).

Bibliography

G. Yang, “Iterative optimization approach for the design of diffractive phase elements simultaneously implementing several optical functions,” *J. Opt. Soc. Am. A* **11**(5), 1632–1640 (1994).

N. Yu and F. Capasso, “Flat optics with designer metasurfaces,” *Nature Mater.* **13**(2), 139–150 (2014).

H. Zappe, “Novel components for tunable micro-optics,” *Optoelectronics Lett.* **4**(2), 86–88 (2008).

F. Zolla, S. Guennea, A. Nicolet, and J. B. Pendry, “Electromagnetic analysis of cylindrical invisibility cloaks and the mirage effect,” *Opt. Lett.* **32**(9), 1069–1071 (2007).

Index

- 2D MEMS arrays, 99
- 3D MEMS arrays, 99

- Abbe V number, 33
- active-matrix OLED (AMOLED), 95
- amplitude grating, 26
- analytic diffractive element, 20
- analytic element, 21, 24
- andom errors, 152
- angular bandwidth, 87
- antireflection (AR), 12, 69
- applications, 154
- athermalization, 37

- backlight, 103
- beam-shaping CGH, 57
- beam steering, 18
- binary greyscale masking, 141
- binary phase grating, 27
- Bragg condition, 84
- Bragg grating, 83
- Bragg plane, 98

- cladding, 7
- computational optics, 92
- contact mode, 136
- core, 7
- critical dimension (CD), 143

- Dammann grating, 60
- depth of focus (DOF), 33, 138
- detuning parameter, 85
- DFT-based propagators, 117, 121
- DFT-based scalar propagators, 118
- diamond ruling, 128
- diamond turning machine (DTM), 128
- diffraction asymmetry, 72
- diffraction efficiency, 28, 30
- diffraction through a reticle, 138
- diffractive analytic beam shapers, 42
- diffractive Fresnel lens, 31
- diffractive lens, 32
- diffractive null lens, 47
- diffractive phase depth, 4
- digital electronics, 1
- digital micro-optics, 1
- direct binary search (DBS), 55
- direct write, 139
- dynamic diffractive element, 20

- effective medium theory (EMT), 67, 107
- efficiency loss, 152
- electroactive polymer (EAP), 106
- extended depth of focus (EDOF), 44

- f-number, 33
- fabrication errors, 152
- far field, 110
- FFT-based propagators, 111
- finite-difference time domain (FDTD), 107

Index

- Floquet, 84–85
- Fourier diffractive
 - element, 22
- Fraunhofer hologram, 81
- free-space micro-optics, 3, 11
- Fresnel diffractive optical
 - element, 22
- Fresnel hologram, 81
- Fresnel lens, 4

- Gabor, Denis, 78
- Gerchberg_x2013Saxton
 - algorithm, 54
- glass wafer, 135
- graded-index (GRIN)
 - micro-optics, 8, 12
- grating strength, 85
- grating vector, 83
- grating-assisted coupler, 71
- greyscale masking, 140
- GRIN lens, 12–13
- GRIN rod, 13
- guided-wave micro-optics, 3

- head-mounted display (HMD), 17
- high-energy beam-sensitive (HEBS)
 - glass, 140, 142
- holographic exposure, 124
- holographic optical
 - element (HOE), 20
- holographic-polymer
 - dispersed liquid crystal (H-PDLC), 97
- hybrid refractive/diffractive singlet, 39
- embedding, 113
- IMOD MEMS display
 - panels, 101
- insertion losses (ILs), 10
- interference, 82
- interferogram lens, 48
- ion diffusion, 126
- iterative Fourier transform
 - algorithm (IFTA), 54

- Kogelnik, Herwig, 86

- large-period grating, 63
- Leith, Emmett, 78
- light-absorbing film (LAF), 142
- light-field camera, 16
- light-field display, 17
- liquid-crystal micro-display, 94
- light pipe, 8
- liquid crystal, 93
- liquid lens, 105
- local grating
 - approximation (LGA), 108

- MEMS gratings, 100
- merit function, 53
- metamaterials, 75
- metasurfaces, 76
- microlens array (MLA), 1, 19, 59
- micro-optics industry, 153
- microrefractive lens, 127

Index

- minimum feature size, 138
- moiré DOE (M-DOE), 104
- multifocus lens, 59
- multilevel lithography, 123
- multilevel optical lithography, 130
- multiple holographic exposures, 125

- narrow-band diffractive, 34
- near field, 110
- numeric diffractive element, 20, 21, 51
- numerical aperture (NA), 7, 33
- numerical reconstruction windows, 117

- optical lithography, 136
- optical pick-up unit (OPU), 46
- optical proximity correction (OPC), 144
- optical waveguide, 7–8
- optothermal expansion coefficient, 37
- organic light-emitting diode (OLED), 95
- oversampling, 112

- parameters, 9
- parity time (PT), 70
- periodicity condition, 4
- photomask patterning, 143
- photonic crystal (PC), 74
- physical optics modeling, 114

- planar waveguides, 8
- plastic replication techniques, 147
- playback, 77, 98
- point spread function (PSF), 138
- polarization beamsplitter (PBS), 94
- projection mode, 136
- proximity mode, 136
- pulse-density-modulation (PDM), 66
- pulsewidth modulation (PWM), 66

- quantum dot (QD), 96

- ray tracing, 108
- Rayleigh resolution criterion, 138
- Rayleigh–Sommerfeld diffraction integral, 109
- reconfigurable optics, 92
- reconstructed aerial image, 138
- recording, 77, 98
- reflective grating, 25
- reflow, 126
- refractive effect, 4
- refractive microlens arrays, 15
- replication, 145
- resist, 126
- resolution, 138
- rigorous coupled-wave analysis (RCWA), 86, 107
- roll-to-roll embossing, 148

Index

- scalar diffraction theory, 5
- scratch-o-grams, 123
- shift in focal length, 33
- shim, 145
- shim recombination, 146
- silicon wafer, 135
- simulated annealing (SA), 56
- smallest feature, 33
- small-period grating, 63
- space–bandwidth product (SBWP), 50
- spatial multiplexing, 46
- spectral bandwidth, 87
- spectral dispersion, 14
- spot array generator, 58
- step-index waveguide, 8
- steppers, 137
- subwavelength diffractive element, 20
- subwavelength micro-optics, 62
- successive-order modes, 9
- surface, 69
- surface plasmon polariton (SPP), 73
- surface-relief hologram, 89
- Sweatt model, 108
- switchable optics, 92
- systematic errors, 152
- Talbot effect, 61
- thick hologram, 79
- thin hologram, 79
- total internal reflection (TIR), 6–7
- transmissive MEMS panels, 101
- tunable optics, 92
- Upatnieks, Juris, 78
- vortex lens, 43
- wafer-scale micro-optics, 3
- wide-band diffractive, 34
- zero-order grating, 63–64



The author with a
Google Glass headset

For over 20 years, **Bernard Kress** has made significant scientific contributions as a researcher, professor, consultant, advisor, instructor, and author, making major contributions to digital micro-optical systems for consumer electronics, generating IP, and teaching and transferring technological solutions to industry. Many of the world's largest producers

of optics and photonics products have consulted with him on a wide range of applications, including laser-material processing, optical security, optical telecom/datacom, optical data storage, optical computing, optical motion sensors, optical gesture sensing, depth mapping, heads-up displays, head-mounted displays, virtual-reality headsets and smart glasses, pico-projectors, micro-displays, digital imaging processing, and biotechnology sensors.

Kress has more than 30 international patents. He has published four books, a book chapter, 102 refereed publications and proceedings, and numerous technical publications. He has also been involved in European research in micro-optics, including the Eureka Flat Optical Technology and Applications (FOTA) project and the Network for Excellence in Micro-Optics (NEMO) project. He is currently the Optics Lead of the Advanced Prototypes Lab at Google[X] Labs in Mountain View, California.

Digital Micro-Optics

Bernard C. Kress

Traditional macro-optics can be designed without complex design software tools. However, digital optics, especially wafer-scale micro-optics, require specific software and tools. There is often no analytical solution, and thus complex iterative optimization algorithms may be required. This book covers refractive and diffractive micro-optics, the iterative optimization process, and modeling and fabrication techniques crucial to this field. The ability to create hybrid systems capable of producing analog and digital functionality is also addressed.

SPIE Field Guides

The aim of each *SPIE Field Guide* is to distill a major field of optical science or technology into a handy desk or briefcase reference that provides basic, essential information about optical principles, techniques, or phenomena.

Written for you—the practicing engineer or scientist—each field guide includes the key definitions, equations, illustrations, application examples, design considerations, methods, and tips that you need in the lab and in the field.

John E. Greivenkamp
Series Editor

SPIE.

P.O. Box 10
Bellingham, WA 98227-0010
ISBN: 978081628411836
SPIE Vol. No.: FG33

ISBN 9781628411836



9 0 0 0 0



9 781628 411836

www.spie.org/press/fieldguides